UNIVERSITY OF OKLAHOMA

GRADUATE COLLEGE

STRATIGRAPHIC AND PETROPHYSICAL CONTROLS ON RESERVOIR PAY AND ITS SPATIAL VARIABILITY, WILLIAMS FORK FORMATION, MAMM CREEK FIELD, COLORADO

A THESIS

SUBMITTED TO THE GRADUATE FACULTY

in partial fulfillment of the requirements for the
Degree of

MASTER OF SCIENCE

By

GRACE SHANNON BARBER

Norman, Oklahoma

2024

STRATIGRAPHIC AND PETROPHYSICAL CONTROLS ON RESERVOIR PAY AND ITS SPATIAL VARIABILITY, WILLIAMS FORK FORMATION, MAMM CREEK FIELD, COLORADO

A THESIS APPROVED FOR THE

SCHOOL OF GEOSCIENCES

BY THE COMMITTEE CONSISTING OF

Dr. Matthew Pranter, Chair

Dr. Heather Bedle

Dr. Fnu “Ming” Suriamin

© Copyright by GRACE SHANNON BARBER 2024

All Rights Reserved.

DEDICATION

This thesis is dedicated to my family. Thank you to my mom and dad for always encouraging me and believing in me. You taught me how to take on challenges and chase my dreams with tenacity and purpose. This thesis is only the beginning. Thank you also to each one of my sisters. To my older sisters, thank you for paving the way before me. Watching you do life with excellence despite difficulties faced along the way instilled a fire in me to do the same. To my little sisters, thank you for cracking me up and inspiring me to be the best example for you that I can be. This thesis is the result of the love and support each of you have shown me.

ACKNOWLEDGEMENTS

This research was funded by the Reservoir Characterization and Modeling Laboratory, the School of Geosciences, and the Graduate College at the University of Oklahoma. The primary dataset (well logs, formation tops, seismic data, and core porosity and permeability data) used in this study (and in previous work this study builds upon) was provided by Bill Barrett Corporation. Software was provided by Schlumberger (Petrel). I am very thankful for the many resources and research opportunities that have been provided through this school and associated partners. Thank you for extending your time and money to pour into students like me.

I would also like to thank my advisor, Dr. Matthew Pranter, for not only helping me grow as a geoscientist and 3D modeler, but also for his mentorship and advice along the way. In addition to Dr. Pranter, thank you to my other committee members, Dr. Heather Bedle and Dr. FNU "Ming" Suriamin for your helpful guidance and encouragement throughout my time here. Thank you to all my friends, fellow student peers, office mates, and mentors that helped me along the way as well. Whether I had technical questions, was seeking workflow advice, or simply needed a good laugh or word of encouragement, the people surrounding me throughout my graduate school journey made it all worthwhile. I feel incredibly blessed to have met and shared life with each one of you.

My journey throughout graduate school did not follow a common path. Although I was met with many unforeseen challenges along the way, one thing always rang true. I was not doing this journey alone; God was with me each step of the way. The completion of this thesis is a testament to His perfect plan, His perfect timing, and His grace over my life. Jesus is my best friend, and He wrote this thesis with me. Thank you, God, for patiently taking care of my heart and for showing me the joys of life you have to offer while allowing me to study your awesome geologic creations. I love and trust you, God! Thank you for showing me what I am capable of.

“You will keep in perfect peace those whose minds are steadfast, because they trust in You (God)”- Isaiah 26:3

Thank you to my family for supporting me, encouraging me, and most of all, believing in me. Although they were far away, whether it was a phone call, text of encouragement, sweet handwritten letter, homecooked meal, or (my favorite) a surprise visit and quick hug, they always found ways to put a smile on my face. Finally, thank you to my close friends that became my home away from home. I am forever grateful for the memories and laughs we shared together during my time spent in Norman. Each one of you helped me grow into the person I am today.

TABLE OF CONTENTS

Dedication……..iv

Acknowledgements……..……..v

Abstract……xix

Keywords…….…….....xx

Introduction……..……..1

Geologic Setting……..7

Basin History…….....….7

Local Stratigraphy……...…….……...……8

Data……...…….……..…….11

Core…….…….…….……11

Well logs…….……...11

Seismic……...12

Methods……12

Petrophysical-Property Calculations……...……...……..13

Stratigraphic Correlation and Mapping……..……15

Seismically Constrained Lithology Thickness Probability Map Generation……....21

3D Geological Modeling……..…….21

Results……...……...……32

Lithologies and Petrophysical Properties..……..…….32

Stratigraphic Framework…….…….34

Lithology Thickness Probability Maps/ Lateral Lithology Distribution……..….41

3D Lithology Model……..43

Spatial Distribution of Reservoir Properties and Reservoir Pay Sandstone…….……...47

Discussion……...……..61

Lithologies and Petrophysical Properties…….……..…..61

Williams Fork Formation Sandstones……...62

Williams Fork Formation Shales……...…63

Williams Fork Formation Coals……63

Depositional Environment Implications…….……...……65

Spatial Distribution of Reservoir Properties and Reservoir Pay Sandstone…….65

Fault-Enhanced Permeability……66

Limitations…….70

Conclusion…….……...71

References……..…...74

Appendices……....78

Appendix A: *3D Seismic Volume*……...78

Appendix B: *Establishing a Relationship Between Lithology, Total porosity, and Sweetness*……...79

Appendix C: *Cross-Plot Generation*……..79

Appendix D: *3D Sweetness Attribute Volume*……81

Appendix E: *Total Porosity Logs (upscaled)*…….82

Appendix F: *3D Total Porosity Model (not constrained or biased to lithology)*……83

Appendix G: *Lithology Thickness Probability Map Constraints (Zone 1)*……..84

Appendix H: *Selection of Lithology Thickness Probability Maps Produced Per Zone*…..85

Appendix I: *Histograms Displaying Lithologic (upscaled lithology log) Distribution Per Zone*……86

Appendix J: *Table of Variogram Parameters*……87 & 88

Appendix K: *Core and Cloud Transform Cross Plot*…….89

Appendix L: *Faults Applied in this Study (select vs. all)*……...90 & 91

Appendix M: *Fault-Enhanced Permeability (all faults) along A-A'*……..92

Appendix N: *Permeability Models with and without Faulting*……..93 & 94

Appendix O: *Table of Bulk and Pore Volume Per Zone of Reservoir Pay and Non-pay*….95

LIST OF FIGURES

Figure 1: Regional basemap of the Piceance Basin showing exposed Mesaverde Group outcrops along the margins of the basin and major Mesaverde Group gas fields within the basin. The study area is outlined in black. Modified from Hoak and Klawitter (1997), Pranter et al. (2009), and Baytok (2010)……..…….2

Figure 2: Study area basemap. The green line represents the area in which seismic data is available. The black line outlines the extent of the study area. Core (Appendix K(a)), gas wells, and type log (Figure 4) locations are also shown. Because multiple wells exist at each pad location, the individual gas well symbols represent the location of multiple wells. Modified from Baytok (2010)……...6

Figure 3: Stratigraphic nomenclature of the Upper Cretaceous strata of the southern Piceance Basin. The Williams Fork Formation is subdivided into lower, middle, and upper intervals in this portion of the basin. Approximate location of transect is shown in map inset. The interval of interest associated with this study runs from the top of the Rollins Sandstone Member (also known as the top of the Iles Formation), to the top of the Upper Williams Fork. Modified from Johnson and May (1980), Johnson and Flores (2003), Hettinger and Kirschbaum (2002, 2003), Patterson et al. (2003), Carroll et al. (2004), Burger (2007), Cole and Pranter (2008), and Baytok (2010)..…..9

Figure 4: Type log (Specialty 41A-28-692 (see Figure 2 for location)) associated with the modeling interval labeled with abbreviated stratigraphic nomenclature. The modeling interval vertically extends approximately 2,800 ft from the lowermost purple line (top of Rollins Sandstone) to the upper blue line (top of Price Coal). The modeling interval includes: 1) Cameo-Wheeler Coal Zone (CWCZ), 2) Middle Sandstone/ South Canyon Coal Zone (MSs./SCCZ), 3)

Upper Sandstone, 4) Paonia Shale, 5) Middle Williams Fork (Middle WFK), and 6) Upper Williams Fork (Upper WFK)…….10

Figure 5: **a)** Vertical proportion curve associated with the initial grid and upscaled lithology logs. Lithologies are depicted such that shale is gray, sandstone is yellow, and coal is black. **b)** The six main depositional events visible within the vertical proportion curve are denoted via brackets, and **c)** the associated formation tops that were picked as a result are denoted by dashed lines. **d)** For visual comparison, the resulting zones used in the final 3D grid associated with the study are partitioned via color.……...……17

Figure 6: NW-SE structural cross section along A-A' (approximate location of cross section also displayed in Figure 8b) depicting the conformance between well-top and seismic-horizon interpretations for the seven formation tops used as stratigraphic framework to define six zones……..……18

Figure 7: NE-SW structural cross section along B-B' depicting the conformance between well-top and seismic-horizon interpretations for the seven formation tops used as stratigraphic framework to define six zones.…….…..19

Figure 8: a) Structure contour maps of the 7 main formation tops associated with this study. Well density coverage of the 234 well penetrations are depicted. b) Displayed are the 6 zones associated with the modeling interval of this study. The transparent plane denotes the location of cross-section A-A' that will be referenced throughout this study…….20

Figure 9: Depiction of the 3D grid generated and used throughout this study. The uppermost image displays the 3D grid dimensions at a vertical exaggeration of 1 while the image beneath depicts the same 3D grid at a vertical exaggeration of 5 to accentuate the stratigraphic framework. This

grid covers approximately 12 mi^2 (31 km^2) with aerial cell dimensions of 100 ft x 100 ft (30.5 m x 30.5 m) and a cell layer thickness of about 2 ft (0.6 m). It consists of 115 x 297 x 1386 cells in the I, J, and K directions, totaling 47,338,830 cells arranged with a proportional layering scheme. The number of layers per zone was calculated by dividing the average thickness of each zone by the vertical cell height…….23

Figure 10: Depiction of the workflow used in this study to generate a seismically constrained 3D lithology model……..25

Figure 11: Visual depiction of the workflow used to generate 3D fault-enhanced permeability models. The select group of faults (interpreted by Baytok (2010) and quality checked) represented in **a)** were used as inputs to calculate and generate **b)** a 3D "distance from faults" model. To create a model representing the highest values along the faults that decrease to zero with distance, calculations were applied to generate **c)** an "inverse distance from faults" 3D model (an inverse of the 3D "distance from fault" model). Qualitatively, the resulting "inverse distance from fault" 3D model was then analyzed numerically and partitioned into different regions based on proximity to faulting. Numerically, these regions were used to create a separate **d)** "permeability multiplier" model, assigning values as follows: areas along the faults (≥ 1) were assigned a multiplier of 5, areas near the faults (1-0.2) a multiplier of 2, and areas beyond the faults (≤ 0.2) a multiplier of 1. Once the permeability multiplier model was generated, it was multiplied by the existing **e)** permeability model to yield a **f)** fault-enhanced 3D permeability model. This process was applied a second time (using all faults interpreted by Baytok (2010) (Appendix L(b))) to generate a separate fault-enhanced permeability model that incorporates all faults (Appendix N(c)).……...……..28 & 29

Figure 12: A generalized summary of the various workflows used throughout this study to generate 3D total porosity, effective porosity, permeability, water saturation, bulk volume water, and reservoir pay models.……...……31

Figure 13: Typical log and petrophysical responses present in Williams Fork Formation sandstone, shale, and coal within the study area. Williams Fork Formation sandstones typically exhibit: 1) GR 60-70 API, 2) gas-effect depicted by NPHI/DPHI crossover, 3) moderate resistivity readings of 40-50 ohmm, 4) a volume of shale (Vsh) of 17-20%, 5) effective porosity of 1-8%, 6) water saturation range in value of 50-90% averaging ~87%, and 5) BVW ranging from 0.03-0.06. Williams Fork Formation shales exhibit: 1) significantly higher NPHI values in comparison to DPHI values (shale effect), 2) resistivity readings of 25-50 ohmm, 3) a higher Vsh of 60-80%, 4) effective porosity of 0.2-3%, 5) water saturation of 60-100%, and 6) BVW values of 0.4-0.6. Williams Fork Formation coals exhibit: 1) high NPHI and DPHI readings, 2) very high effective porosity and resistivity readings, and 3) extremely low readings of Vsh, water saturation, and BVW.……...……..33

Figure 14: Draped by the structure contour map associated with the top of the Price Coal, the 3D grid of the Williams Fork Formation displays a northwest dipping trend within the study area. All 6 zones within the model follow this structural northwest-dipping trend. Positively correlated to the structure map displayed, a thickness map of the Williams Fork Formation reveals that the formation is thinner to the northwest and thickens towards the southeast. The Williams Fork Formation ranges in thickness from approximately 2670-2880 ft (813-877 m), with an average thickness of 2780 ft (847 m)……...35

Figure 15: a) Upper Williams Fork (Zone 6) structure vs. thickness. Draped by the Upper Williams Fork top structure-contour map, the Upper Williams Fork displays a northwest dipping

trend and has a range in thickness of ~880-1090 ft (268-332 m), averaging 990 ft (301 m). Thinner areas present to the north and east, thicker towards the central southwest. **b)** Middle Williams Fork (Zone 5) structure vs. thickness. Draped by the Middle Williams Fork top structure-contour map, the Middle Williams Fork displays a northwest dipping trend and has a thickness range of 370-680 ft (112-207 m), averaging ~553 ft (168 m) thick. Apart from a few thicker areas in the center and to the east and west of the study area, the Middle Williams Fork generally maintains uniform thickness. **c)** Lower Williams Fork Formation (zone 1-4) structure vs. thickness. Draped by the Paonia Shale Member top structure-contour map, the Lower Williams Fork Formation has a thickness range of 1130-1380 ft (344-420 m), an average thickness of 1230 ft (374 m), and is thin to the west, and thickest in the southeastern portion of the study area.…….....36 & 37

Figure 16: Formation thickness vs sandstone thickness vs pay thickness comparisons within each zone of the Williams Fork Formation. The left column **(a, d, g, j, m,** and **p)** depicts formation thickness maps associated with each of the 6 zones within the Williams Fork Formation. The middle column **(b, e, h, k, n,** and **q)** depicts the probability sandstone thickness maps (*see methods section*) used to constrain the lateral distribution of sandstone per zone in the 3D lithology model. The column on the right, **(c, f, i, l, o,** and **r)**, depicts the reservoir pay thickness within each zone. Within all 6 zones of the Williams Fork Formation, there is a positive correlation between the thickest regions of each zone and the thickest sandstone and reservoir pay deposits……39 & 40

Figure 17: Visual comparison of the sandstone and coal thickness probability maps associated with zone 1 and zone 2. Within the Cameo-Wheeler Coal Zone (zone 1), the thickness probability maps of **c)** sandstone and **d)** coal coincide such that high sandstone presence to the northwest, southeast, and central edges of the study area corresponds with low coal presence. Conversely, areas to the southwest, northeast, and central interior are predominantly coal rich **(d)**. Within the

Middle Sandstone/South Canyon Coal Zone (zone 2), the lateral distribution of sandstones and coals displayed by the lithology thickness probability maps showcase similar conformance. Areas of higher **b)** coal presence in the northwest and southwest correspond to lower **a)** sandstone presence, while higher sandstone presence in the east is associated with lower coal presence.……...……..42

Figure 18: a) Seismically constrained 3D lithology model of the Williams Fork Formation. Within the study area, the Williams Fork Formation is composed of ~54% shale, 42% sandstone, and 4% coal. Brown lines denote the 6 different zones within the entire formation. **b)** Comparison of the upscaled wells' vertical proportion curve and lithology model's vertical proportion curve displays how the model honors the stratigraphic trends in lithology…….44

Figure 19: Model and fence diagram depictions of Williams Fork Formation lithology within the study area. **a)** 3D lithology model of the Williams Fork Formation. **b)** The Upper Williams Fork (zone 6) is composed of ~74% shale, ~26% sandstone, and ~0.3% coal, representative of an alluvial plane depositional environment. **c)** The Middle Williams Fork (zone 5) is composed of 51% shale, 49% sandstone, and 0% coal, representative of a depositional transition from coastal to alluvial plain. **d)** Grouped together based on depositional environment, the upper 2 zones of the Lower Williams Fork Formation (zones 3&4), are composed of 50% shale, 47% sandstone, and 3% coal, representing a depositional transition from swamp to coastal plain. **e)** Grouped together based on representing swamp depositional environments, the lower 2 zones of the Lower Williams Fork Formation are composed of 31% shale, 54% sandstone, and 15% coal……....45 & 46

Figure 20: Model and fence diagram depictions of total porosity within Williams Fork Formation sandstone within the study area. **a)** 3D total porosity model of the Williams Fork Formation. **b-e)**

On average, total porosity consistently reflects a range in value of 5-15% regardless of zone/ stratigraphy……48

Figure 21: Model and fence diagram depictions of effective porosity within Williams Fork Formation sandstone within the study area. **a)** 3D effective porosity model of the Williams Fork Formation. **b-e)** On average, effective porosity consistently reflects a range in value of 1-8% regardless of zone/ stratigraphy……..49

Figure 22: Model and fence diagram depictions of permeability within Williams Fork Formation sandstone within the study area. **a)** 3D permeability model of the Williams Fork Formation. **b-e)** On average, permeability consistently reflects a range in value of 0.7-10 µD regardless of zone/ stratigraphy……..……...50

Figure 23: Model and fence diagram depictions of water saturation within Williams Fork Formation sandstone within the study area. **a)** 3D water saturation model of the Williams Fork Formation. **b-e)** Water saturation consistently reflects a range in value of ~50-90%, and on average ~87% regardless of zone/ stratigraphy……...…….51

Figure 24: Model and fence diagram depictions of bulk volume water within Williams Fork Formation sandstone within the study area. **a)** 3D bulk volume water model of the Williams Fork Formation. **b-e)** On average, bulk volume water consistently reflects a range in value of 0.03-0.06 regardless of zone/ stratigraphy.…….…...….52

Figure 25: Model and fence diagram depictions of reservoir pay sandstone within the Williams Fork Formation within the study area. **a)** 3D reservoir pay sandstone model of the Williams Fork Formation. **b-e)** Depicted in the pie charts and fence diagrams, the Lower Williams Fork

Formation (zones 1-4) and Middle Williams Fork (zone 5) are composed of a higher percentage of reservoir pay sandstone than the Upper Williams Fork (zone 6)…….53

Figure 26: 3D reservoir pay sandstone model of the Williams Fork Formation. On average, 40 % of the entire Williams Fork Formation within the study area is composed of reservoir pay sandstone, while the thickest reservoir pay deposits are located to the central southeast of the study area. Throughout the Williams Fork Formation, reservoir pay sandstone deposits vary in thickness from ~700-1100 ft (213-335 m), averaging around 1000 ft (304 m)……...56

Figure 27: Model zones and associated reservoir pay thickness maps depicting the distribution of reservoir pay sandstone within the Williams Fork Formation within the study area. **a)** 3D reservoir pay sandstone of the Williams Fork Formation. On average, 40 % of the entire Williams Fork Formation within the study area is composed of reservoir pay sandstone. **b)** The Upper Williams Fork (zone 6) is composed of 22% reservoir pay deposits, evenly dispersed, that range in thickness from ~ (300-375 ft) (91-114 m). **c)** The Middle Williams Fork (zone 5) is composed of 42% reservoir pay deposits, evenly dispersed, that range in thickness from ~ (300-400 ft) (91-121 m). **d)** The Lower Williams Fork Formation (zones 1-4) is composed of 38% reservoir pay deposits, focused in the central-southeast, that range in thickness from ~ (350-550 ft) (106-167 m)..…….57

Figure 28: Model zones and associated reservoir pay thickness maps depicting the distribution of reservoir pay sandstone within the Lower Williams Fork Formation within the study area. **a)** The Paonia Shale Member (zone 4) is composed of 32% reservoir pay sandstone, thickening from the northeast to the south and southwest, that range in thickness from ~ (20-240 ft) (6-73 m), averaging 120 ft (36 m) thick. **b)** The Upper Sandstone (zone 3) is composed of 49% reservoir pay sandstone, focused in the central-southeast, that range in thickness from ~ (10-210 ft) (3-64 m), averaging 100 ft (30 m) thick. **c)** The Middle Sandstone/ South Canyon Coal Zone (zone 2) is composed of

44% reservoir pay sandstone, focused in the central-southeast, that range in thickness from ~ (60-330 ft) (18-100 m), averaging 180 ft (54 m) thick. **d)** The Cameo-Wheeler Coal Zone (zone 1) is composed of 33% reservoir pay sandstone, thickening radially to the northwest and southeast from the thinner centralized region of the study area, that range in thickness from ~ (2-225 ft) (0.5-68 m), averaging 80 ft (24 m) thick.……...……...…..58 & 59

Figure 29: Per **a)** each zone within the stratigraphic modeling interval, a visual comparison between the **b)** vertical proportion curve of lithology (within the 3D lithology model), **c)** vertical proportion curve of reservoir pay sandstone (within the 3D reservoir pay model), and **d)** pore volume of pay depicts several stratigraphic trends. The strong conformance between sandstone (yellow) within the **b)** 3D lithology model's vertical proportion curve and reservoir pay sandstone (red) within the **c)** 3D reservoir pay model's vertical proportion curve demonstrates that most of the Williams Fork Formation sandstone in the study area consists of reservoir pay. In addition, throughout the modeling interval, the variation in magnitude of those trends varies stratigraphically such that the majority of reservoir pay sandstone exists in the lower three zones of the Lower Williams Fork Formation, followed by the Middle Williams Fork, while the Upper Williams Fork is the lowest pay contributor. The **d)** pore volume of pay also displays a higher cumulative pore volume contribution from the Lower Williams Fork Formation and Middle Williams Fork compared to the Upper Williams Fork...……64

Figure 30: Cross-sectional slices along A-A' (approximate location of cross section displayed in (Figure 8b)) depicting 3D **a)** lithology, **b)** zones within the model grid, **c)** total porosity, **d)** water saturation, **e)** effective porosity, **f)** bulk volume water, **g)** permeability, and **h)** reservoir pay modeling results for comparison purposes. The 3D permeability model derived from core data suggests matrix permeability is positively correlated with total and effective porosity. Although

the range and mean values of petrophysical properties do not vary significantly stratigraphically, the magnitude of lithology, reservoir pay, and associated petrophysical properties are highly variable stratigraphically. ……..……....67 & 68

Figure 31: A comparison of the **a)** original Williams Fork Formation 3D permeability model (no faults incorporated) and **b)** fault-enhanced 3D permeability model (incorporating a select group of quality-checked faults interpreted by Baytok (2010)) in cross-sectional view along A-A'. (See Figure 8b for approximate location of A-A'). Increasing permeability along faults, in some cases as high as ~550 µD, faults within the study area positively correlate with areas of highest reservoir quality. See Appendix M for an additional comparison between the original Williams Fork Formation 3D permeability model and fault-enhanced 3D permeability model (incorporating all faults interpreted by Baytok (2010)). …..……...69

ABSTRACT

The Upper Cretaceous Williams Fork Formation of the Mesaverde Group within the Piceance Basin of northwestern Colorado is a significant producer of natural gas from low permeability reservoirs (tight-gas sandstones). The Williams Fork Formation consists of six stratigraphic intervals. From base to top, these zones include the Lower Williams Fork Formation including 1) Cameo-Wheeler Coal Zone, 2) Middle Sandstone/South Canyon Coal Zone, 3) Upper Sandstone, and 4) Paonia Shale Member, and the 5) Middle Williams Fork, and 6) Upper Williams Fork. The two lowermost zones of the Lower Williams Fork Formation consist of fluvial sandstones, shales, and laterally extensive coal zones. The upper two zones of the Lower Williams Fork Formation record a transition from lower coastal plain and swamp to coastal plain deposits represented by fewer coals and a higher proportion of fluvial sandstones. From the upper two zones of the Lower Williams Fork Formation to the Middle and Upper Williams Fork, a transition from coastal plain to an alluvial plain setting is reflected by a greater proportion of sandstones.

This study combines well-log and 3D seismic data to yield 3D lithology, porosity, permeability, water saturation, bulk volume water, and reservoir pay models to explore the stratigraphic and petrophysical controls on reservoir pay within the Williams Fork Formation in Mamm Creek Field. The data set includes approximately 48 mi^2 (125 km^2) of 3D seismic data in time and depth domains, core porosity and permeability data from the Last Dance 43C-3-792 well, and 234 wells with digital well-logs including gamma ray, neutron porosity, density porosity, and resistivity logs.

Three-dimensional petrophysical property models reveal that Williams Fork Formation sandstones exhibit total and effective porosity ranges of ~5-15% and ~1-8%, respectively, absolute permeability of ~0.7- 10 μD, and bulk volume water of ~0.03-0.06. Core data suggest that matrix permeability is positively correlated with total and effective porosity. Within the study area, 40%

of the Williams Fork Formation is composed of thick, laterally extensive reservoir pay sandstones that on average, reflect total porosity ~9-11%, effective porosity ~3-4%, slightly higher permeability ~7-20 μD, water saturation ~50-85% (avg. ~80%), and bulk volume water ~0.01-0.05 (avg. 0.03). While the range and mean values of petrophysical properties do not vary significantly stratigraphically, lithology, reservoir pay, and pore volume are highly variable stratigraphically. The majority of reservoir pay is confined within the lower two-thirds of the Williams Fork Formation (Lower Williams Fork Formation and Middle Williams Fork). Of the two major reservoir pay contributors, the Lower Williams Fork Formation contains the thickest pay sandstones that range in thickness from ~350-550 ft (106-167 m). 3D reservoir models of lithology, effective porosity, and other petrophysical properties illustrate the stratigraphic and petrophysical controls on high reservoir quality sandstones that form natural gas reservoirs. This work demonstrates that the most prospective reservoir intervals occur within the lower two-thirds of the Williams Fork Formation, with optimal reservoir properties concentrated in thick, laterally extensive sandstone bodies in the central-southeast portion of the study area.

Keywords

Tight-gas reservoirs, reservoir pay sandstones, Williams Fork Formation, Mamm Creek Field, Piceance Basin, 3D modeling, reservoir characterization, petrophysical properties, 3D seismic.

INTRODUCTION

The Upper Cretaceous Williams Fork Formation of the Mesaverde Group within the Piceance Basin of northwestern Colorado is a significant producer of natural gas from low permeability reservoirs (tight-gas sandstones). At Mamm Creek Field (Figure 1), the Williams Fork Formation is informally partitioned into lower, middle, and upper intervals. Responsible for a high percentage of tight-gas production throughout the Piceance Basin, the Lower Williams Fork Formation consists of coastal-plain to shallow-marine deposits including marine sandstones, shales, and coals (Collins, 1976; Hettinger & Kirschbaum, 2002, 2003; Cumella and Ostby, 2003; Cole and Cumella, 2005; Shaak, 2010). The middle and upper Williams Fork Formation is comprised primarily of sandstone and shale dominated alluvial plain deposits (Hettinger and Kirschbaum, 2002, 2003; Foster, 2010). As it is the primary contributor to natural gas production throughout the Piceance Basin, the Williams Fork Formation has been studied previously to address aspects of its stratigraphy, structure, and reservoir properties (e.g., Lorenz and Finley, 1989; Lorenz et al., 1989; Tyler and McMurry, 1995; Hoak and Klawitter, 1997; Kuuskraa et al., 1997a, 1997b; Hettinger and Kirschbaum, 2002, 2003; Patterson et al., 2003; Cole and Cumella, 2003, 2005; Pranter et al., 2007, 2008, 2009; Foster, 2010; Shaak, 2010; Baytok and Pranter, 2013; Keeton et al., 2015).

The Mesaverde Group in the Piceance Basin has been examined in several studies (Tyler and McMurry, 1995; Hettinger and Kirschbaum, 2002, 2003; Patterson et al., 2003; Cole and Cumella, 2003, 2005; Foster, 2010; Shaak, 2010; Keeton et al., 2015) to understand its depositional environment and stratigraphic framework.

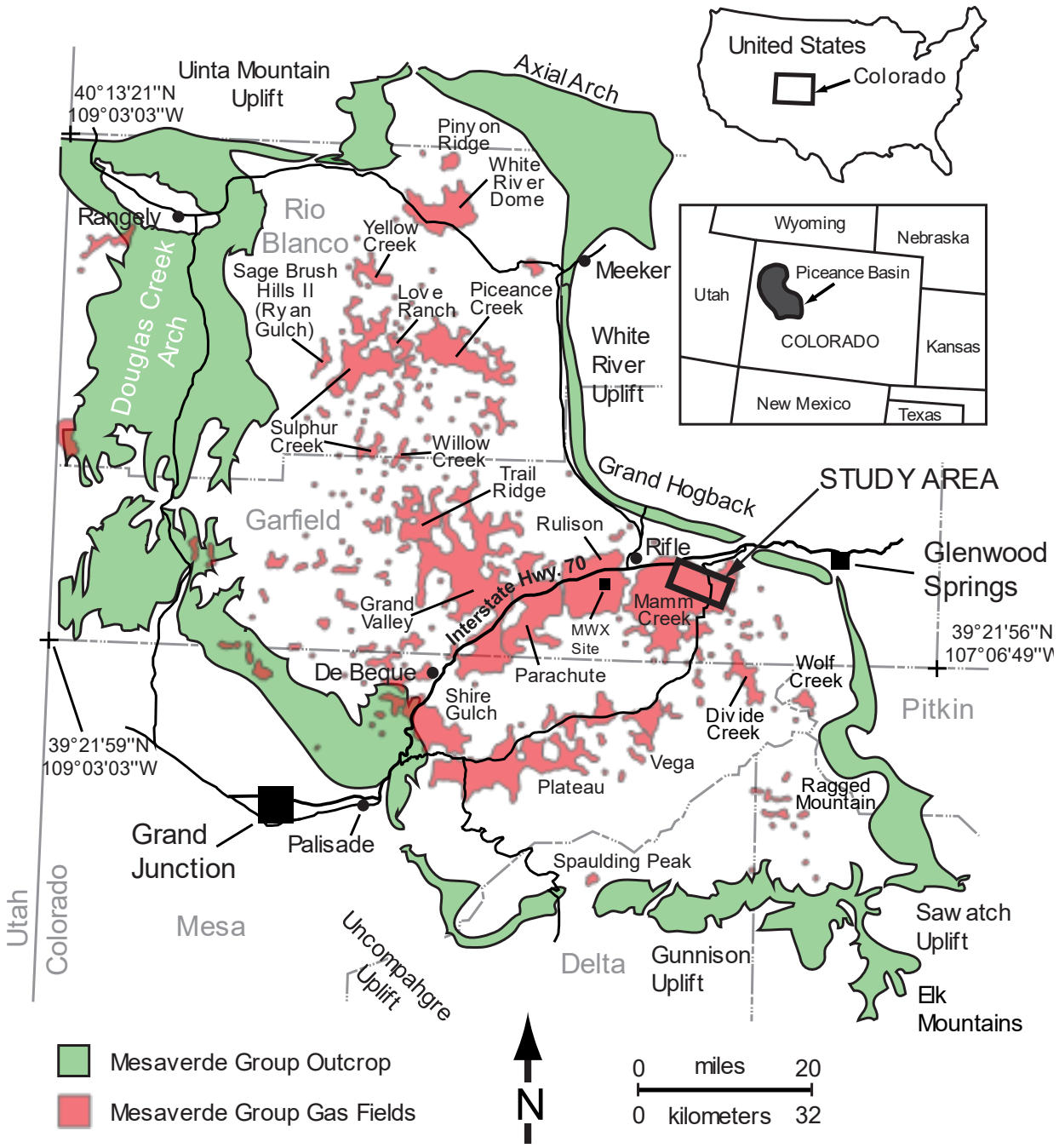

Figure 1: Regional basemap of the Piceance Basin showing exposed Mesaverde Group outcrops along the margins of the basin and major Mesaverde Group gas fields within the basin. The study area is outlined in black. Modified from Hoak and Klawitter (1997), Pranter et al. (2009), and Baytok (2010).

Building on earlier work involving outcrops (Collins, 1976; Hettinger, 1998) and subsurface data (Hettinger, 2000), Hettinger and Kirschbaum (2002, 2003) correlated Upper Cretaceous strata along the southern portion of the Uinta and Piceance basins. As a result of their findings, they divided the Williams Fork Formation into the Bowie Shale Member, Paonia Shale Member, and an "undifferentiated" upper formation primarily consisting of coastal-plain and fluvial deposits (Hettinger and Kirschbaum, 2002, 2003). In this study, units within the Lower Williams Fork Formation extend from the top of the Rollins Sandstone Member of the Iles Formation up to the base of the upper "undifferentiated" Williams Fork Formation, which includes the Paonia and Bowie Shale Members. In 2010, Foster further partitioned the upper “undifferentiated” Williams Fork Formation previously defined by Hettinger and Kirschbaum into the middle Williams Fork 1, middle Williams Fork 2 (Big Kahuna), and upper Williams Fork. While the upper Williams Fork is stratigraphically defined the same, for simplicity, this study combines middle Williams Fork 1 and 2 into a single designation, referred to as the Middle Williams Fork.

Using outcrop observations, core facies analysis, and well-log correlations, Patterson et al. (2003) developed a sequence-stratigraphic framework for the Mesaverde Group and Ohio Creek Conglomerate in the central to northern Piceance Basin. Through their work on the Mesaverde Group and Ohio Creek Conglomerate, they identified seven composite sequences, four of which belong to the Williams Fork Formation. While the lower three sequences associated with the Williams Fork Formation reflect alluvial-plain deposits formed under moderate accommodation, the uppermost sequence represents amalgamated channel-complex deposits from a period of low accommodation (Patterson et al., 2003). Shaak (2010) studied the stratigraphic architecture and sequence-stratigraphy of the coastal-plain to shallow-marine deposits of the Lower Williams Fork Formation. Shaak (2010) identified parasequences that transition landward from wave-dominated

shoreface sandstone deposits into marsh and coal deposits, coastal-plain channel sandstones, and floodplain strata.

To expand upon the stratigraphy and uncover architectural aspects, several studies analyzed sandstone connectivity and structural parameters of sandstone bodies within the Williams Fork Formation. According to Cole and Cumella (2005), it is important to examine heterogeneities in fluvial deposits because they can impede fluid flow (Cole and Cumella, 2005). To enhance subsurface models of gas-producing intervals in the southern Piceance Basin, Cole and Cumella (2005) conducted research on sandstone-body characteristics and connectivity from well-exposed Williams Fork Formation outcrops located in Coal Canyon, Colorado. Observations from these outcrops have facilitated the correlation of stratigraphic architecture and sandstone body connectivity in various fields using core and well-log analysis (e.g., Shaak, 2010), borehole-image logs (e.g., Keeton et al., 2015), and 2D and 3D reservoir modeling (e.g., Pranter et al., 2007, 2008, 2009, 2014; Pranter and Sommer, 2011). Models developed from outcrop data (e.g., Pranter et al., 2008; Pranter and Sommer, 2011) and subsurface data from Rulison Field (e.g., Pranter et al., 2008) and Mamm Creek Field (e.g., Pranter et al., 2014) have examined the sandstone-body architecture and connectivity of the lower, middle, and upper Williams Fork Formation.

To gain further structural insight and expand on reservoir properties of the Williams Fork Formation, multiple studies have investigated fracture systems within the Piceance Basin (Lorenz and Finley, 1989; Lorenz et al., 1989; Hoak and Klawitter, 1997; Kuuskraa et al., 1997a, 1997b; Lorenz, 2003; Baytok and Pranter, 2013). After comparing lower permeability laboratory recordings to field data, Lorenz (2003) attributed the higher field-recorded permeability values to the enhanced conductivity of natural fractures. Using 3D seismic data, borehole-image logs, conventional well logs, and core data, Baytok and Pranter (2013) examined the relationship

between seismic attributes and fracture distribution within the Mesaverde Group at Mamm Creek Field. They employed Ant-track attribute volumes to identify faults and fractures and used interpreted FMI logs to identify fracture orientations and types, generating fracture-intensity logs to correlate fractures with lithology. Their findings indicated a limited correlation between fractures and lithologies within the Williams Fork Formation (Baytok and Pranter, 2013).

Although previous work has addressed aspects of the stratigraphy, structure, and reservoir properties of the Williams Fork Formation, this study expands upon those studies in regard to petrophysical properties and seismic-constrained 3D reservoir modeling. For the Williams Fork Formation in Mamm Creek Field, this study combines well-log data, 3D seismic data, and 3D modeling methods to address the following questions:

- What are the petrophysical characteristics and criteria to define lithology and pay?
- What is the stratigraphic and structural framework?
- How do lithologies, petrophysical properties, and reservoir pay vary spatially?

The study area is at Mamm Creek Field within the southeastern portion of the Piceance Basin in northwest Colorado (Figure 2). The data set (Figure 2) used to address these research questions includes approximately 48 mi^2 (125 km^2) of 3D seismic data in time and depth domains, core porosity and permeability data from the Last Dance 43C-3-792 well, and 234 wells with digital well-logs including gamma ray, neutron porosity, and density porosity. Capturing the interval of interest (Figure 4), each of the 234 wells penetrates through the top of the Williams Fork Formation and into the Rollins Sandstone Member of the underlying Iles Formation. Well data were used to establish proper well-log cut-offs, perform petrophysical calculations, and correlate key formation tops. Various methods were applied to establish a relationship between well and seismic data. Once a relationship was established, seismically

constrained 3D lithology, porosity, permeability, water saturation, bulk volume water, and reservoir pay models were generated to explore the stratigraphic and petrophysical controls on reservoir pay within the Williams Fork Formation in Mamm Creek Field.

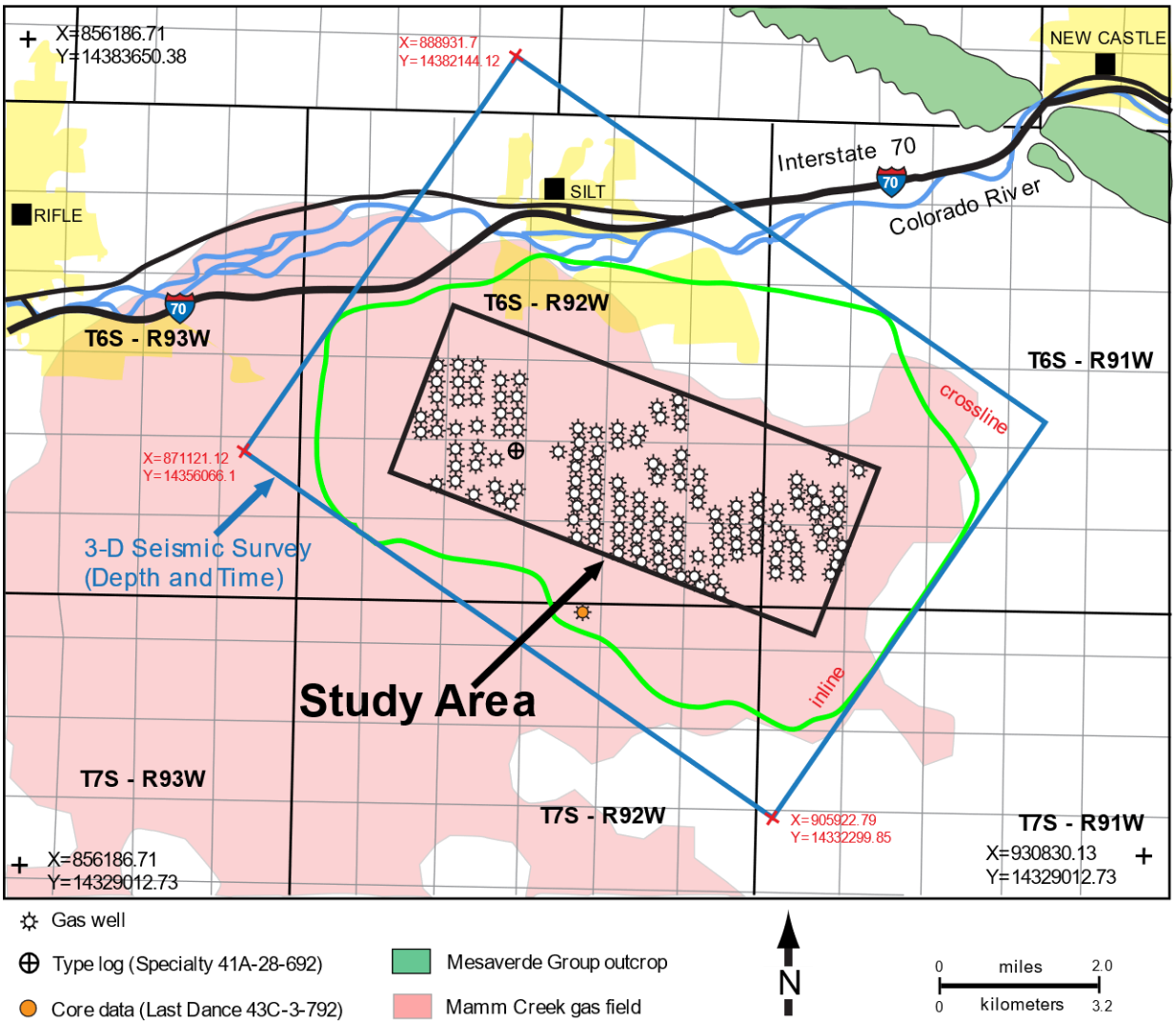

Figure 2: Study area basemap. The green line represents the area in which seismic data is available. The black line outlines the extent of the study area. Core (Appendix K(a)), gas wells, and type log (Figure 4) locations are also shown. Because multiple wells exist at each pad location, the individual gas well symbols represent the location of multiple wells. Modified from Baytok (2010).

GEOLOGIC SETTING

Basin History

The Piceance Basin is an asymmetrical basin trending northwest to southeast in western Colorado (Johnson, 1989; Cole and Cumella, 2003). Covering an area 6000 mi^2 (15539 km^2), the Piceance Basin is bounded by the White River uplift and Elk Mountains to the east, the Uncompahgre Uplift to the southwest, the Gunnison uplift and West Elk Mountains to the southeast, the Uinta Mountains to the northwest, the Axial Basin Anticline to the northeast, and the Douglas Creek arch to the west. The basin features gently dipping flanks, typically between 1 and 20 degrees, with steeper dips that are often sharply upturned or overturned on the eastern flank, particularly at the Grand Hogback (Johnson, 1989; Cole and Cumella, 2003). Comprised of sediments from the Cambrian through Holocene, the thickest section of the Piceance Basin is the Cretaceous-age Mesaverde Group. Across the basin, the Mesaverde Group can range in thickness from less than 1,500 ft (457 m) along the Douglas Creek arch, to over 10,000 ft (3,048 m) in the basin's deepest areas (Johnson and Roberts, 2003).

Structurally, the development of the Piceance Basin can be attributed to two major tectonic events, the Sevier and Laramide orogenies, which included periods of uplift, subsidence, and erosion from the Late Cretaceous to the Paleogene (Johnson, 1989; Hettinger and Kirschbaum, 2002). Four major stages responsible for the development of the Piceance Basin outlined by Johnson (1989) include: 1) the formation of initial depositional patterns due to the Sevier orogeny, 2) the isolation of the Piceance Basin due to Laramide uplift events and establishment of local sediment sources, 3) the production of a regional unconformity as a result of regional uplift associated with the Laramide uplifts and other basin sediments, and 4) the creation of a thermal blanket overlying the Mesaverde Group as a result of the deposition of lower Cenozoic rocks.

Local Stratigraphy

Stratigraphically, the Williams Fork Formation is a member of the Mesaverde Group. Within the Mesaverde Group, lower Cretaceous formations are at the base, followed by the Iles Formation, which is then overlain by the Williams Fork Formation (Cole and Cumella, 2003). Deposited in the Cretaceous Rocky Mountain foreland basin, the Mesaverde Group consists of numerous transgressive and regressive cycles that primarily predate the Laramide orogeny (Johnson, 1989). Within the lower portion of the Mesaverde Group, the Iles Formation contains regressive shoreface sandstones interspersed with transgressive shales. Divided into three members, the Corcoran, Cozzette, and Rollins, the Iles Formation represents inner-shelf, deltaic, shoreface, estuarine, and lower coastal-plain environments (Johnson, 1989; Hettinger and Kirschbaum, 2002, 2003; Cole and Cumella, 2003). Composing the upper two-thirds of the Mesaverde Group, the Williams Fork Formation is defined by the strata from the uppermost Iles Formation, specifically the Rollins Sandstone Member, up to the Cretaceous-Paleocene unconformity denoted by the Ohio Creek Formation (Cole and Cumella, 2003). Figure 3 illustrates the stratigraphic units in the southern basin, highlighting the interval of interest (Figure 3). In greater detail, the modeling interval of interest associated with this study is depicted in Figure 4.

The Williams Fork Formation is informally divided into lower, middle, and upper units. The lower unit is characterized by shallow-marine to coastal-plain deposits, while the middle and upper units consist primarily of alluvial plain deposits (Collins, 1976; Hettinger & Kirschbaum, 2002, 2003; Cole and Cumella, 2005; Shaak, 2010).

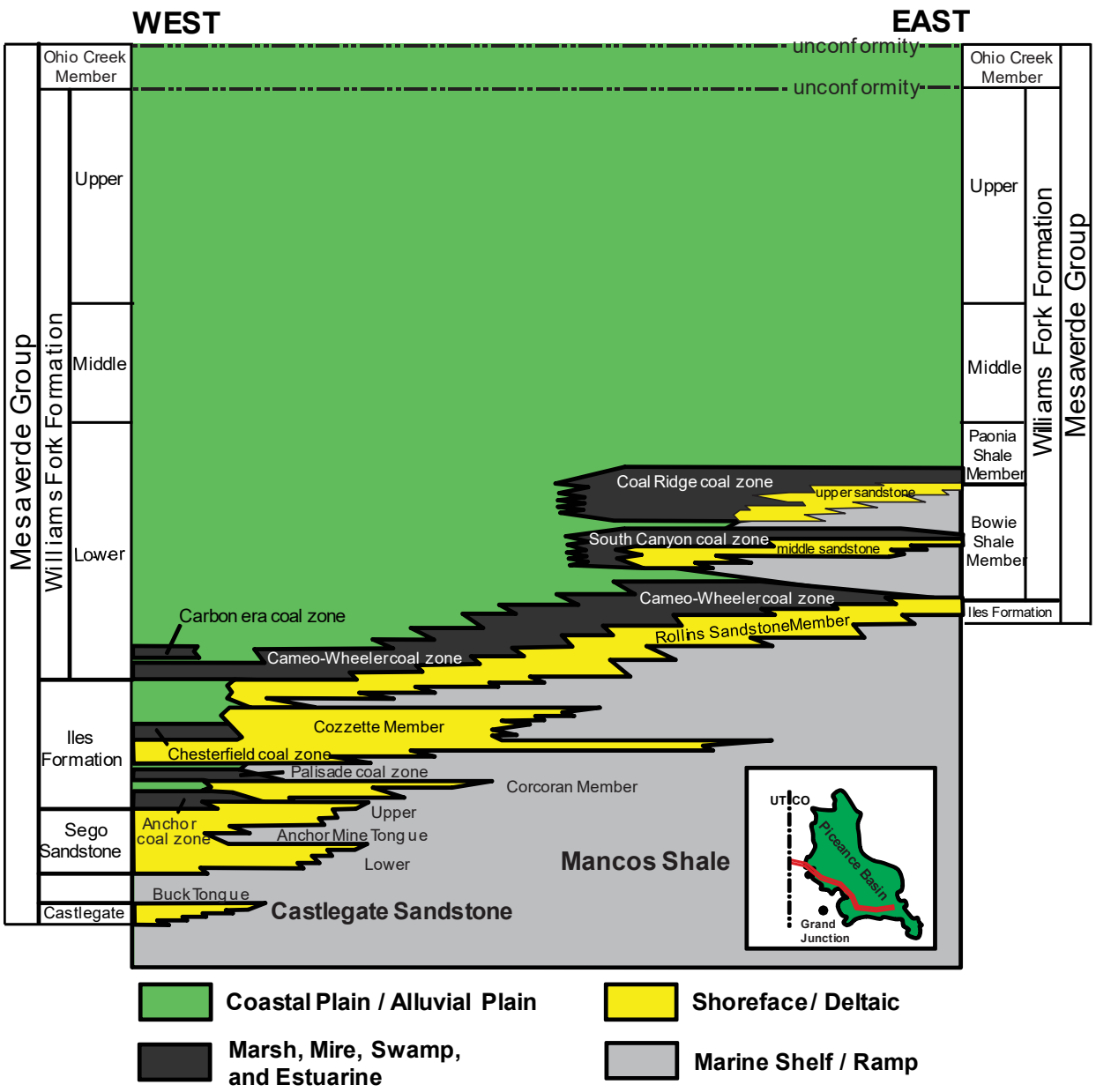

Figure 3: Stratigraphic nomenclature of the Upper Cretaceous strata of the southern Piceance Basin. The Williams Fork Formation is subdivided into lower, middle, and upper intervals in this portion of the basin. Approximate location of transect is shown in map inset. The interval of interest associated with this study runs from the top of the Rollins Sandstone Member (also known as the top of the Iles Formation), to the top of the Upper Williams Fork. Modified from Johnson and May (1980), Johnson and Flores (2003), Hettinger and Kirschbaum (2002, 2003), Patterson et al. (2003), Carroll et al. (2004), Burger (2007), Cole and Pranter (2008), and Baytok (2010).

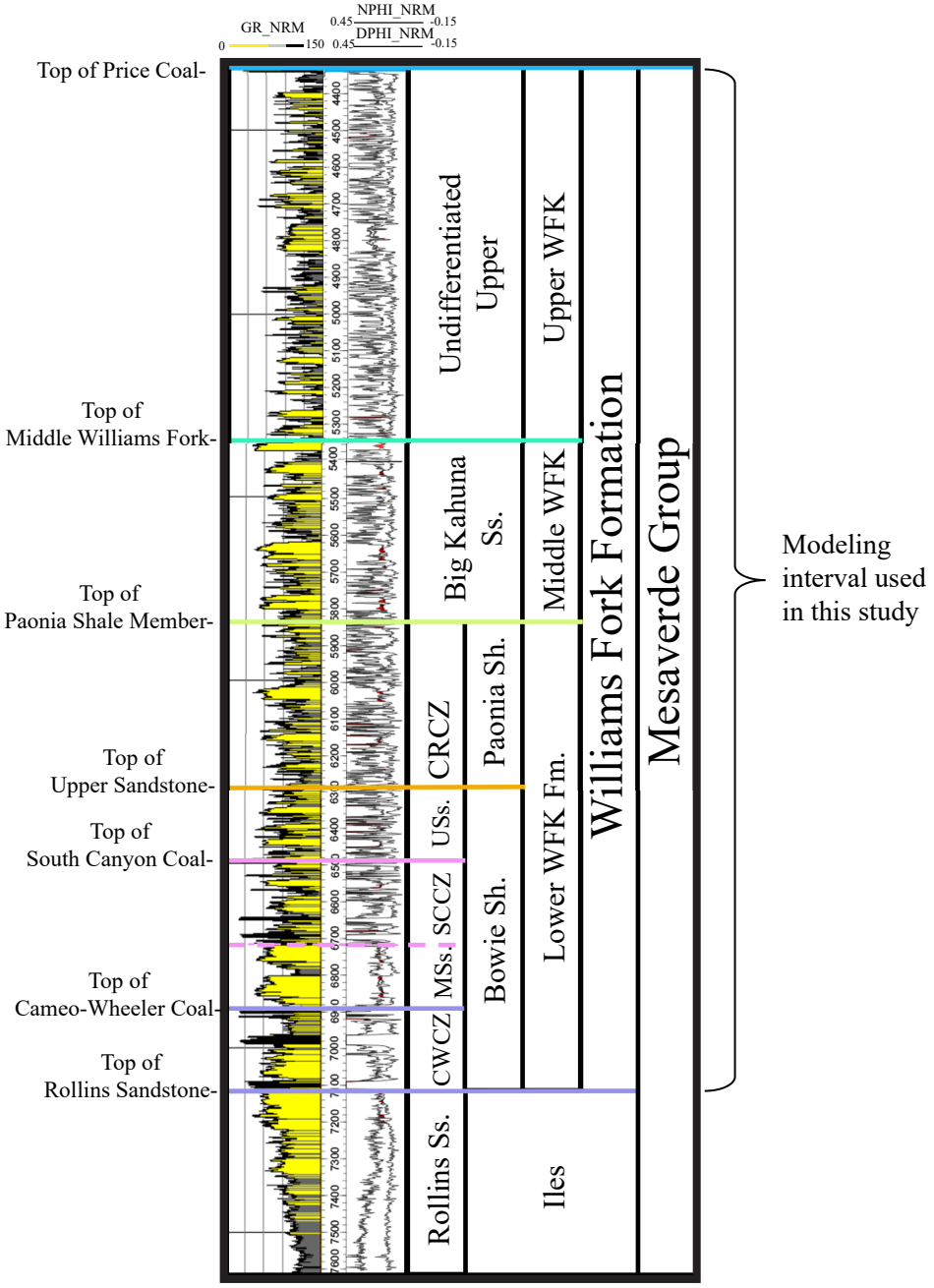

Figure 4: Type log (Specialty 41A-28-692 (see Figure 2 for location)) associated with the modeling interval labeled with abbreviated stratigraphic nomenclature. The modeling interval vertically extends approximately 2,800 ft from the lowermost purple line (top of Rollins Sandstone) to the upper blue line (top of Price Coal). The modeling interval includes: 1) Cameo-Wheeler Coal Zone (CWCZ), 2) Middle Sandstone/ South Canyon Coal Zone (MSs./SCCZ), 3) Upper Sandstone, 4) Paonia Shale, 5) Middle Williams Fork (Middle WFK), and 6) Upper Williams Fork (Upper WFK).

The Lower Williams Fork Formation features several coal zones and marine sandstone units, defined from bottom to top as the Cameo-Wheeler Coal Zone (overlying the Rollins Sandstone Member), the Middle Sandstone unit, the South Canyon Coal Zone, the Upper Sandstone unit, and the Coal Ridge Coal Zone (Lorenz, 1983, 1989; Hettinger & Kirschbaum, 2002, 2003; Shaak, 2010). Although the sandstone and shale dominated alluvial-plain deposits of the middle Williams Fork Formation and upper Williams Fork Formation are not partitioned into other smaller units, they are commonly also defined as the Big Kahuna Sandstone and Undifferentiated Upper, respectively (Hettinger and Kirschbaum, 2002, 2003; Foster, 2010). Although this is the case, within this study they are referred to as the Middle Williams Fork and Upper Williams Fork.

DATA

This study was conducted using data from core, well logs, and high-resolution 3D seismic data (Figure 2). Each facet of data was used in tandem throughout this study to yield seismically constrained 3D models.

Core

Core porosity and permeability data from the Last Dance 43C-3-792 well (Appendix K) was used to conduct a cloud transform method within the 3D modeling process. The Last Dance 43C-3-792 well is located three quarters of a mile south of the study area (Figure 2). The cored interval includes the Ohio Creek, Williams Fork, and Cameo-Wheeler Coal formations and therefore overlies the interval of interest.

Well logs

The 234 wells used throughout this study (Figure 2) each have normalized gamma ray (GR), neutron porosity (NPHI), and density porosity (DPHI) well log curves. Of the 234 wells,

114 also contain resistivity logs (HDRS). In order to conduct the petrophysical analysis and 3D modeling portion of this study, additional well-log curves such as lithology logs, total porosity (ϕ_t), volume of shale (V_{sh}), effective porosity (ϕ_{eff}), water saturation (S_w), and bulk volume water (BVW) were calculated and generated (*see methods section*).

Seismic

The FDmig 3D seismic survey is a post-stack time and depth migrated volume that covers an area of approximately 48 mi^2 (125 km^2) (Figure 2). It consists of 385 inlines and 289 crosslines with traces that have the same coordinate and trace-bin geometry as the original Mamm Creek Survey and a 4 ft sampling rate. The specific corner XY UTM coordinates are as follows:

Origin SW corner (Line 1001, CDP 5001): X=871121.12 Y=14356066.1

NW corner (Line 1001, CDP 5289) X=888931.7 Y=14382144.12

SE corner (Line 1385, CDP 5289) X=905922.79 Y=14332299.85

The FDmig_trimmed_4ft_amplitude_2009_07_17 seismic volume is a depth cube of the average p-wave velocity (vavg) in 32-bit SEGY IBM format referenced to a datum of +7000ft. The upper cube elevation is 3000 ft (914 m) and the base elevation is -2900 ft (883 m).

METHODS

To characterize the spatial distribution of lithologies and petrophysical properties controlling reservoir quality within the Williams Fork Formation at Mamm Creek Field, a comprehensive workflow was employed, integrating well log analysis, core data, and 3D seismic data. Petrophysical properties were first calculated from well logs to establish baseline reservoir characteristics. Key stratigraphic surfaces were then interpreted and mapped using well logs and 3D seismic data to establish a structural framework. Relationships between lithology, porosity,

and seismic attributes were then analyzed to generate lithology thickness probability maps, which helped define the lateral distribution of lithologies between wells. These inputs were subsequently combined to create 3D models depicting lithology distribution, porosity, permeability, water saturation, bulk volume water, and reservoir pay throughout the study area, including an analysis of the impact of faults on the permeability model.

Petrophysical-Property Calculations

Within the 48 mi^2 (125 km^2) 3D seismic survey, a smaller 12 mi^2 (31 km^2) study area boundary was established based on survey quality and adequate well coverage (Figure 2). Wells used in this study were quality controlled and 234 were selected based upon appropriate depth range coverage and the existence of normalized gamma ray, neutron porosity, density porosity, and resistivity curves. Of the 234 wells, 114 contain resistivity logs. Lithology logs were calculated such that sandstone is defined by a gamma ray cut-off of <96 API; shale is defined by a gamma ray cut-off of ≥96API; and coal is defined by a gamma ray cut-off of <96 API and density porosity and neutron porosity cut-offs of >0.25.

Standard techniques and petrophysics-based calculations were applied to digital well-logs associated with this study. As a result, additional logs such as total porosity, volume of shale, effective porosity, water saturation, and bulk volume water were generated.

Total porosity was calculated using the root-mean-square of density porosity and neutron porosity (Asquith and Gibson, 1982):

such that,
$$\phi_t = \frac{\sqrt{\phi_D{}^2 + \phi_N{}^2}}{2}$$

where ϕ_t is total porosity, ϕ_D is density porosity, and ϕ_N is neutron porosity.

Volume of shale (V_{sh}) was calculated from GR logs (Asquith and Gibson, 1982):

such that,
$$V_{sh} = \frac{GR_{log} - GR_{min}}{GR_{max} - GR_{min}}$$

where V_{sh} is shale volume, GR_{log} is log value of GR, GR_{min} is minimum value of GR, and GR_{max} is maximum value of GR. On average, for the Williams Fork Formation, low radioactivity (clean) sandstones represent a GR of 38 API, while radioactive shales represent a GR of 150 API. Therefore, for the purpose of this study, volume of shale was calculated using constant GR_{min} and GR_{max} values set to 38 API and 150 API, respectively.

Total porosity and volume of shale logs were used to calculate effective porosity (Asquith and Gibson, 1982; Stephens et al., 1998):

such that,
$$\phi_{eff} = \phi_t - (V_{sh} * \phi_{sh})$$

where ϕ_{eff} is effective porosity, ϕ_t is total porosity, V_{sh} is volume of shale, and ϕ_{sh} is the average shale porosity. For the Williams Fork Formation, shale possesses an average porosity of 17%. Therefore, effective porosity was calculated using a constant shale porosity (ϕ_{sh}) value of 0.17.

Paired with resistivity logs, effective porosity logs were applied to the empirical Archie equation to calculate water saturation (Archie, 1952):

such that,
$$S_w = \left(\frac{a * R_w}{R_t * {\phi_{eff}}^m}\right)^{\frac{1}{n}}$$

where S_w is water saturation, a is the tortuosity factor, R_w is formation water resistivity, R_t is true formation resistivity, ϕ_{eff} is effective porosity, m is the cementation exponent, and n is the saturation exponent. Because sandstones associated with this study are consolidated, the tortuosity

factor (a) and cementation exponent (m) were set to constant values of $a = 0.81$ and $m = 2$, respectively. The formation water resistivity (R_w) was also set to a constant value of 0.10 ohmm. Resistivity (HDRS) logs were used for true formation resistivity (R_t).

Integrating water saturation with porosity data provides more information about reservoir water content than water saturation alone. To do so, water saturation and effective porosity logs were used to calculate bulk volume water

such that, $$BVW = S_w * \phi_{eff}$$

where BVW is bulk volume water, S_w is water saturation, and ϕ_{eff} is effective porosity. Once BVW was calculated, it was used as criteria to determine pay, such that pay is defined as sandstone that contains a BVW < 0.05.

Stratigraphic Correlation and Mapping

Key stratigraphic surfaces within the Williams Fork Formation were interpreted based on a 48 mi^2 (125 km^2) 3D seismic survey and log data for 234 wells that penetrate the entire Williams Fork Formation within the seismic survey. Of the key stratigraphic surfaces interpreted, the two bounding surfaces of the Williams Fork Formation, top of Rollins Sandstone and top of Price Coal, were correlated first. Resulting structure maps of the top of Rollins Sandstone and top of Price Coal were used to generate a first-pass 3D grid of the Williams Fork Formation within the study area. Covering approximately 12 mi^2 (31 km^2) with aerial cell dimensions of 100 ft x 100 ft (30.5 m x 30.5 m), and proportionally layered cells 2ft (0.6 m) thick, the initial 3D grid was established to 1) provide an initial framework for upscaling lithology logs, 2) enable the analysis of lithologic distribution via the vertical proportion curve of upscaled lithology logs (Figure 5), and 3) determine key stratigraphic boundaries worth interpreting (Figure 5b) and including as stratigraphic framework to capture major depositional events (Figure 5c) within the Williams Fork

Formation. At Mamm Creek Field, the Williams Fork Formation is informally partitioned into lower, middle, and upper intervals. However, when analyzing the vertical proportion curve associated with the upscaled lithology logs, six main depositional events were visible (Figure 5). Therefore, for this study, the Williams Fork Formation is subdivided into six zones. From base to top, these zones include the Lower Williams Fork Formation including 1) Cameo-Wheeler Coal Zone, 2) Middle Sandstone/South Canyon Coal Zone, 3) Upper Sandstone, and 4) Paonia Shale Member, and the 5) Middle Williams Fork, and 6) Upper Williams Fork (Figure 5d). The seven key stratigraphic surfaces that were mapped to define the six zones include from base to top, 1) top of Rollins Sandstone, 2) top of Cameo-Wheeler Coal, 3) top of South Canyon Coal, 4) top of Upper Sandstone, 5) top of Paonia Shale, 6) top of the Middle Williams Fork, and 7) top of Price Coal (Figures 6 and 7). Consistent with interpretations conducted by Baytok (2010), the seven formation tops were correlated, quality checked, and further refined in all 234 wells. In agreement with seismic horizon interpretations from Baytok (2010), within the seismic depth volume, horizon interpretations of the top of Rollins Sandstone, top of Cameo-Wheeler Coal, top of Paonia Shale, and top of Price Coal were each mapped and quality checked. The remaining associated key horizons such as the top of South Canyon Coal, top of Upper Sandstone, and top of Middle Williams Fork were manually interpreted in the seismic volume using 1) seeded 2D/ 3D auto-tracking, 2) guided auto-tracking, and 3) manual interpretation tools. After interpreting horizons every five lines, an additional 3D auto-tracking feature was applied to interpolate between manual picks. Using resulting horizon interpretations and associated formation top correlations as inputs, seismically constrained structure-contour maps were then generated for all seven key stratigraphic surfaces (Figure 8a).

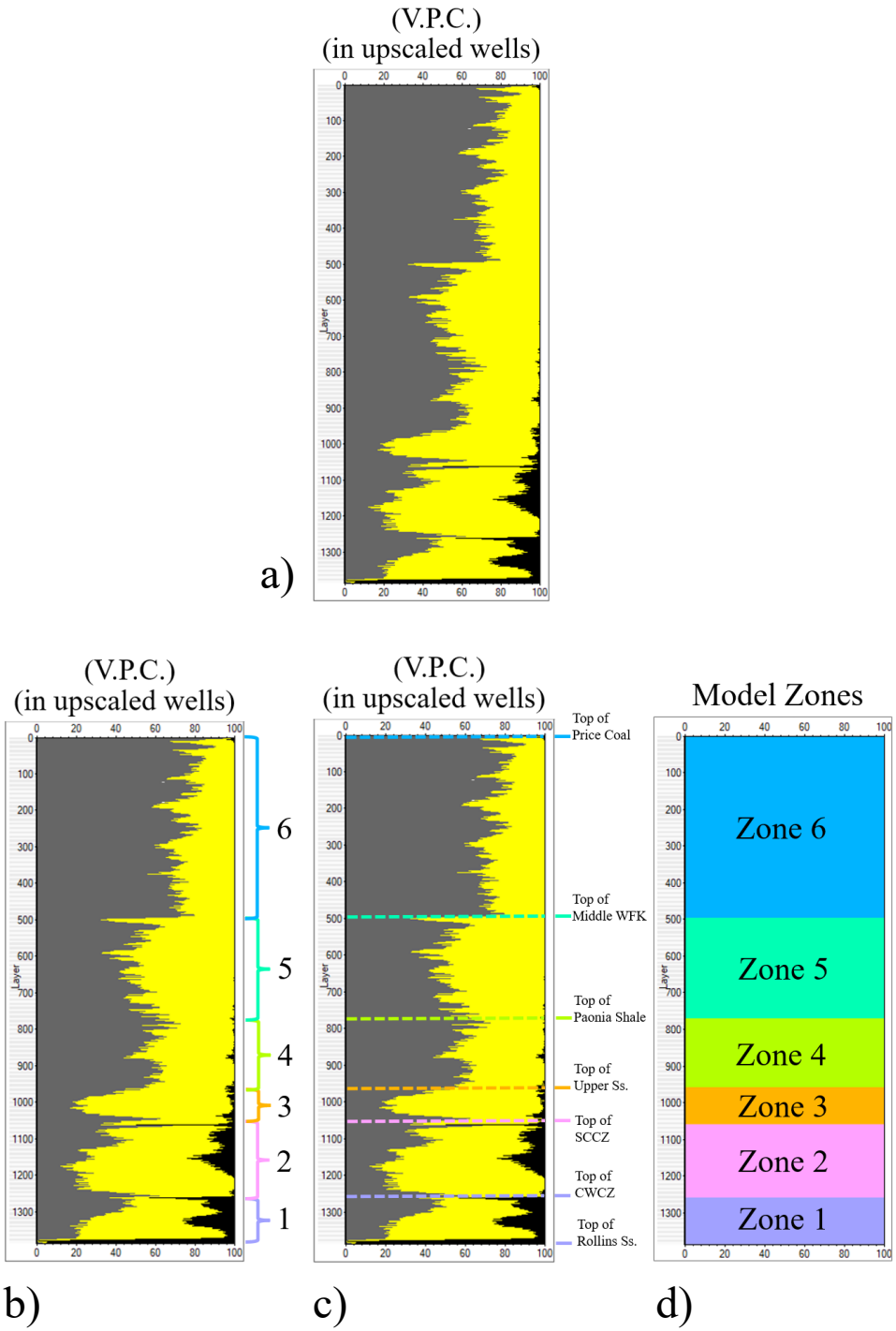

Figure 5: **a)** Vertical proportion curve associated with the initial grid and upscaled lithology logs. Lithologies are depicted such that shale is gray, sandstone is yellow, and coal is black. **b)** The six main depositional events visible within the vertical proportion curve are denoted via brackets, and **c)** the associated formation tops that were picked as a result are denoted by dashed lines. **d)** For visual comparison, the resulting zones used in the final 3D grid associated with the study are partitioned via color.

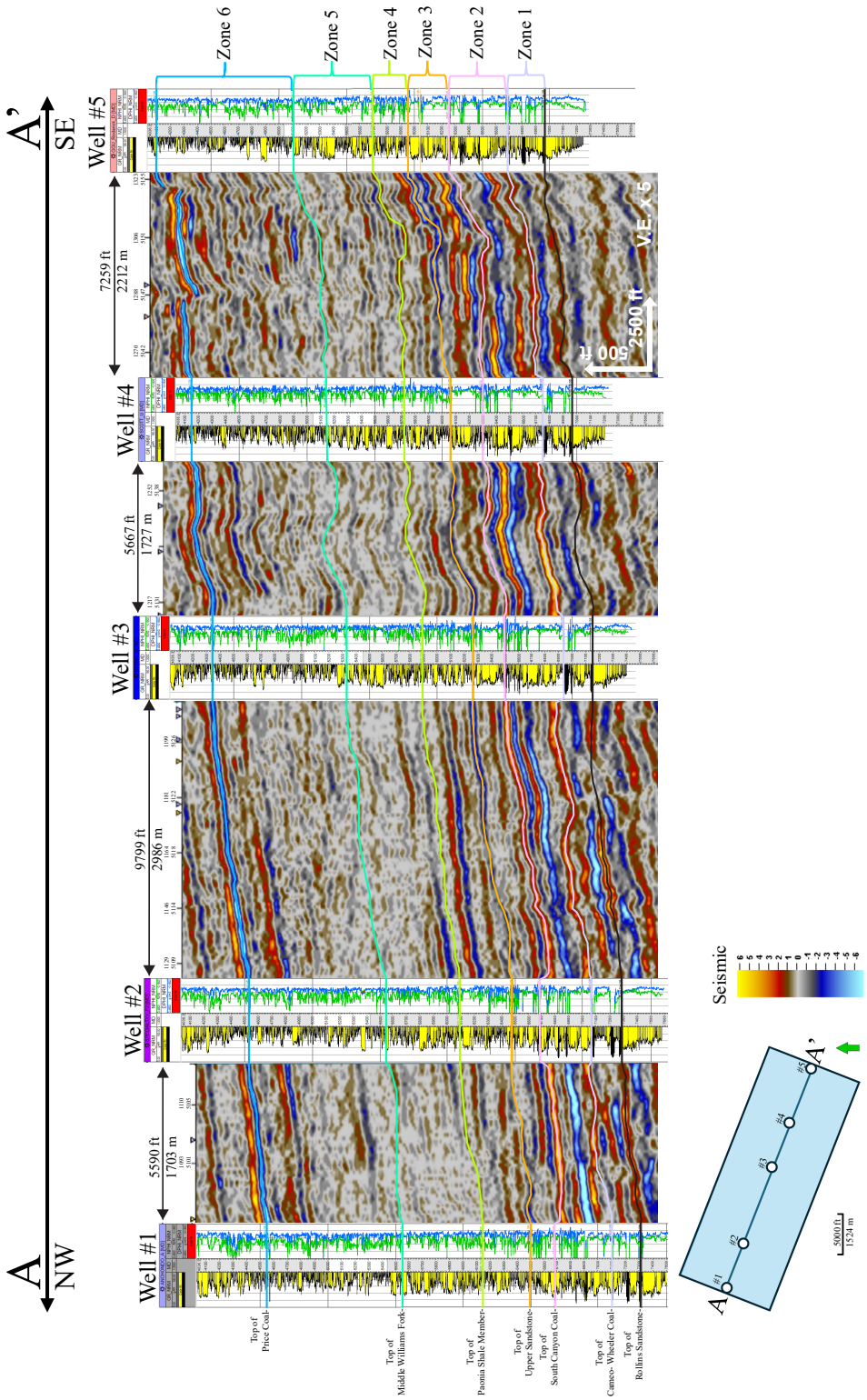

Figure 6: NW-SE structural cross section along A-A' (approximate location of cross section also displayed in Figure 8b) depicting the conformance between well-top and seismic-horizon interpretations for the seven formation tops used as stratigraphic framework to define six zones.

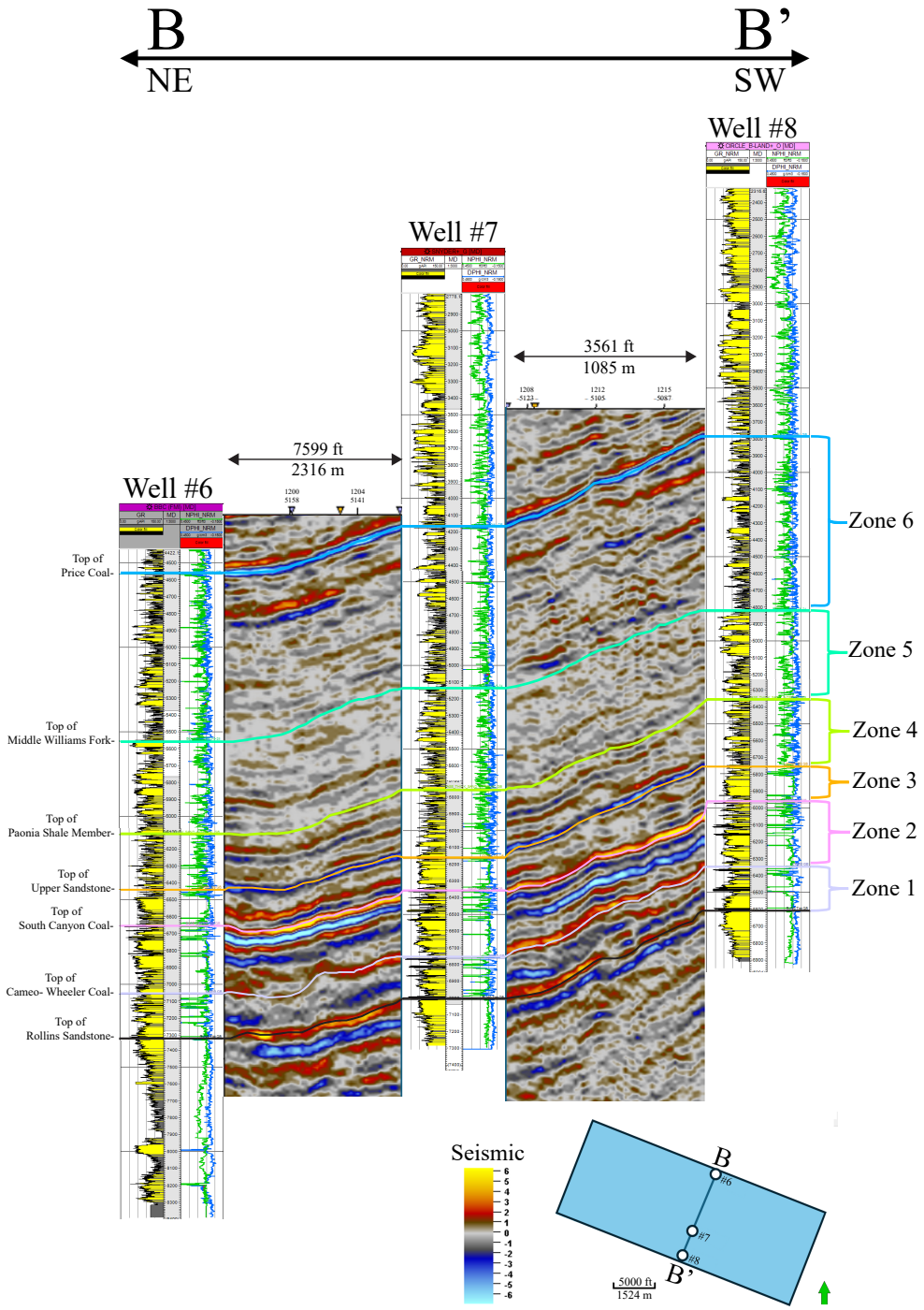

Figure 7: NE-SW structural cross section along B-B' depicting the conformance between well-top and seismic-horizon interpretations for the seven formation tops used as stratigraphic framework to define six zones.

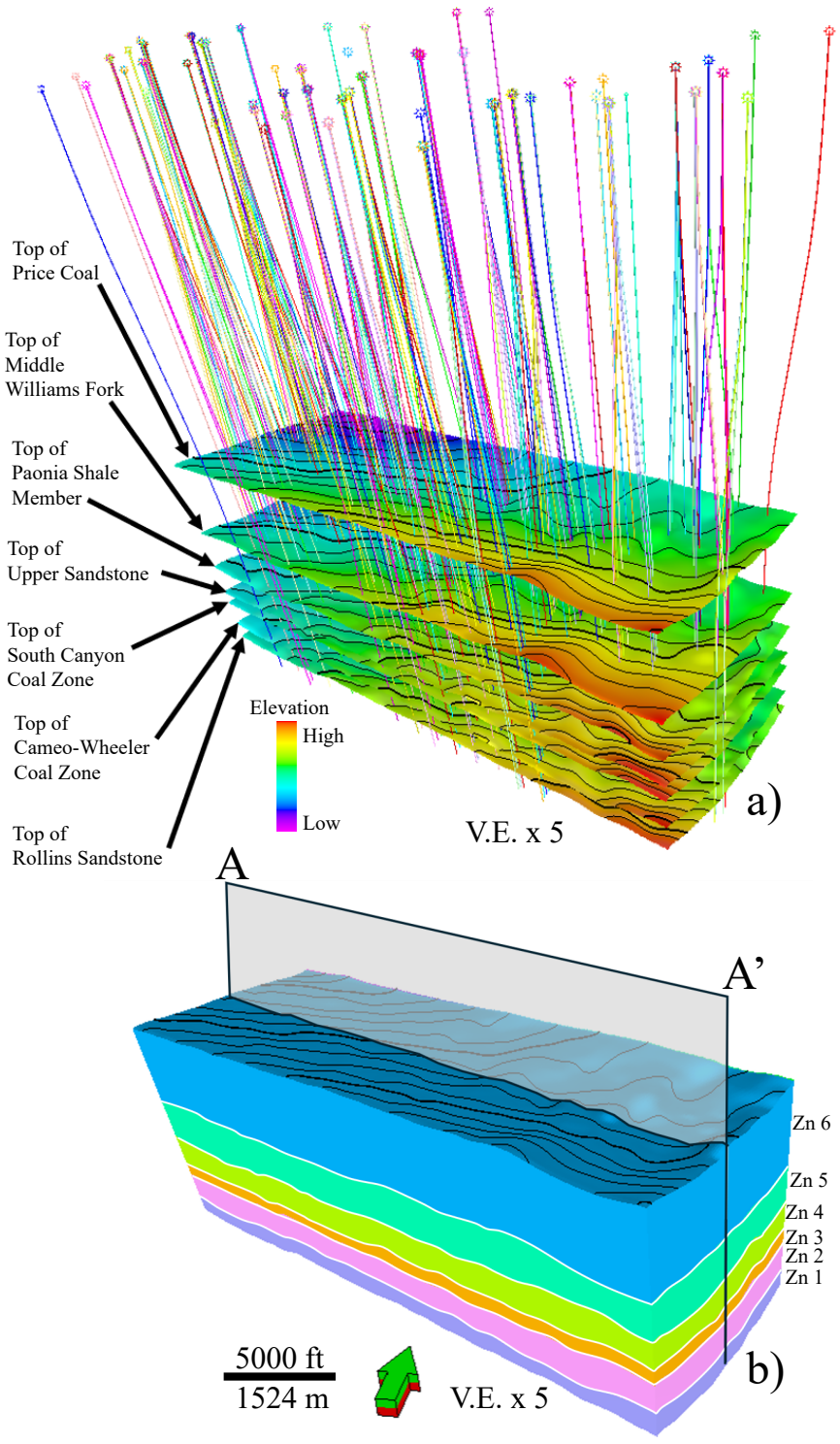

Figure 8: a) Structure contour maps of the 7 main formation tops associated with this study. Well density coverage of the 234 well penetrations are depicted. **b)** Displayed are the 6 zones associated with the modeling interval of this study. The transparent plane denotes the location of cross-section A-A' that will be referenced throughout this study.

Seismically Constrained Lithology Thickness Probability Map Generation

To constrain the lateral lithology distribution during the 3D modeling process, I explored the relationship between lithology, porosity, and sweetness. For a more thorough explanation describing how these three variables were selected and how cross plots were used to reveal the relationship, see Appendices B and C. In general, a positive relationship exists between lithology and total porosity such that sandstone has the lowest total porosity values, shale has middle-range porosity values, and coal has the highest porosity values. Though sweetness helped further define this relationship, there was considerable overlap between each lithology, especially between sandstone and shale. To address the lithological overlap, polygons were drawn dynamically on the at-well-location cross plot to better refine and distinguish each lithology. Once these polygons were defined, they were applied to a cross plot between a 3D model of total porosity (Appendix F) and the 3D sweetness attribute volume (Appendix D). By applying the lithology polygons to the 3D model cross plot, each voxel within the sweetness volume was assigned to a specific lithology based on the polygon and associated sweetness and porosity values it fell within. Once applied, sandstone and coal thickness maps were generated per zone (*see* Appendix H *for a more thorough explanation for the negation of shale*). This general relationship and resulting thickness maps were utilized as lithology thickness probability maps to constrain the lateral distribution of lithologies between wells when constructing the 3D lithology model (Appendix G).

3D Geological Modeling

To assess how lithology, porosity, permeability, water saturation, and bulk volume water influence reservoir pay and its spatial variability, 3D lithology and petrophysical property models were generated for the Williams Fork Formation. Utilizing structure-contour maps derived from seismic horizons and well tops (Figure 8a), a 3D reservoir model grid was developed to represent

the structural and stratigraphic framework of the Williams Fork Formation. The 7 structure-contour maps used to construct the model grid defined 6 model zones (1-6) (Figure 8b). The grid dimensions were established based on well spacing, preservation of the vertical resolution with respect to the stratigraphic variability of lithology, and a computationally adequate number of cells. This grid covers approximately 12 mi^2 (31 km^2) with aerial cell dimensions of 100 ft x 100 ft (30.5 m x 30.5 m) and a cell layer thickness of about 2 ft (0.6 m). It consists of 115 x 297 x 1386 cells in the I, J, and K directions, totaling 47,338,830 cells arranged with a proportional layering scheme (Figure 9). The number of layers per zone (Figure 9) was calculated by dividing the average thickness of each zone by the vertical cell height.

Once generated, lithology logs were then upscaled to the 3D model grid. A comparison of the original and upscaled logs was conducted using frequency histograms and cross sections to validate the accuracy of the upscaling. Frequency histograms were used to validate rock-type proportions, while cross sections were used to validate rock-type presence. This validation process was repeated until each cell within the resulting upscaled logs represented the most abundant rock type (lithology).

The 3D lithology model was generated using sequential indicator simulation (SIS), constrained by the following: (1) the 3D model grid (stratigraphic framework), (2) 234 upscaled lithology logs, (3) vertical lithology proportion curves, (4) horizontal and vertical variogram parameters (Appendix J(b)) for each lithology per zone, and (5) thickness probability maps for sandstone and coal per zone. Variogram ranges were established to capture the variability of log properties with respect to distance and direction. Shale was set as the background lithology during the modeling process.

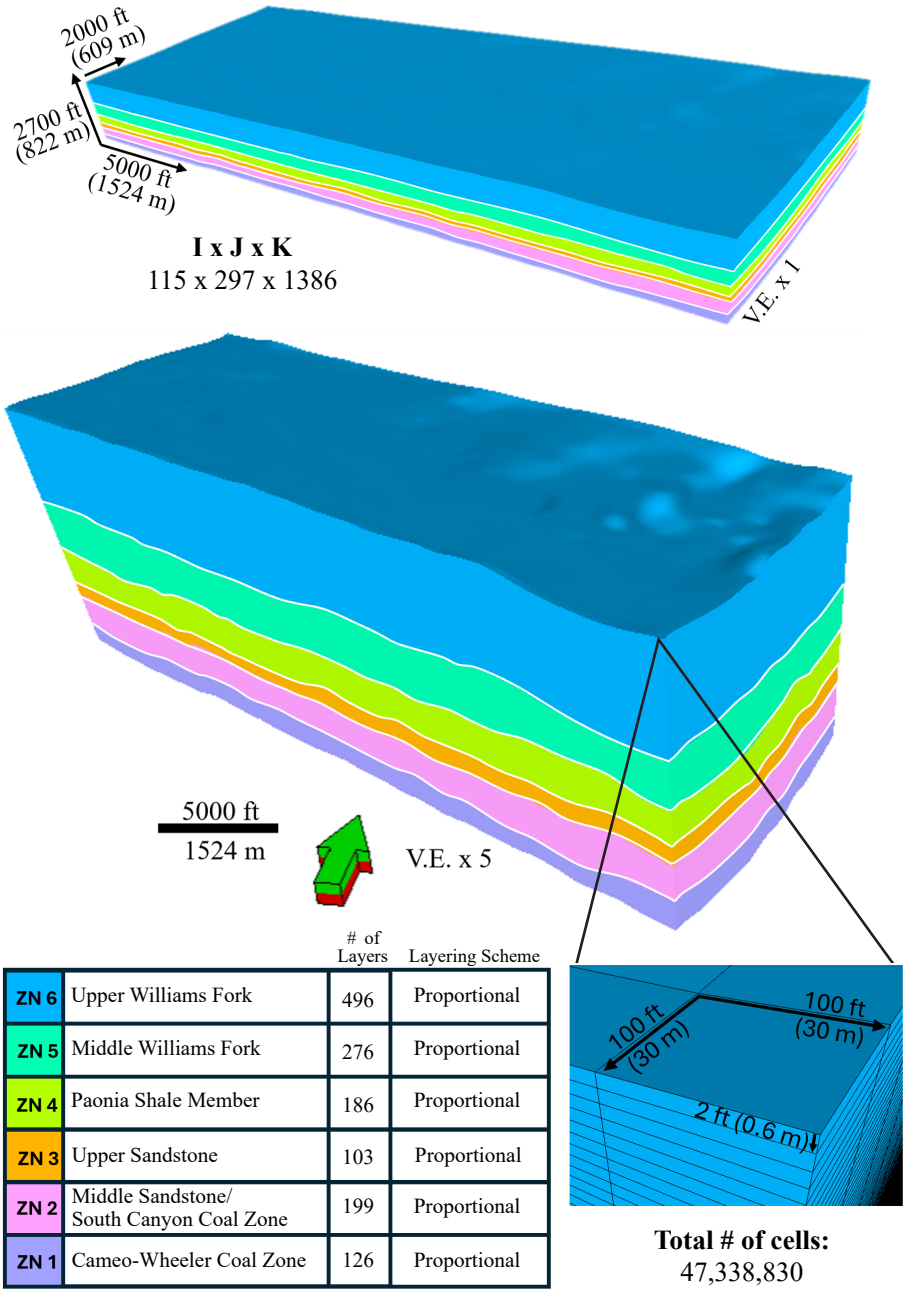

		# of Layers	Layering Scheme
ZN 6	Upper Williams Fork	496	Proportional
ZN 5	Middle Williams Fork	276	Proportional
ZN 4	Paonia Shale Member	186	Proportional
ZN 3	Upper Sandstone	103	Proportional
ZN 2	Middle Sandstone/ South Canyon Coal Zone	199	Proportional
ZN 1	Cameo-Wheeler Coal Zone	126	Proportional

Figure 9: Depiction of the 3D grid generated and used throughout this study. The uppermost image displays the 3D grid dimensions at a vertical exaggeration of 1 while the image beneath depicts the same 3D grid at a vertical exaggeration of 5 to accentuate the stratigraphic framework. This grid covers approximately 12 mi² (31 km²) with aerial cell dimensions of 100 ft x 100 ft (30.5 m x 30.5 m) and a cell layer thickness of about 2 ft (0.6 m). It consists of 115 x 297 x 1386 cells in the I, J, and K directions, totaling 47,338,830 cells arranged with a proportional layering scheme. The number of layers per zone was calculated by dividing the average thickness of each zone by the vertical cell height.

Because the seismically derived thickness probability maps were used as constraints to guide the lateral lithology distribution, the variogram range parameters associated with the major and minor horizontal directions for each lithology per zone were set to 3000 ft (914.4 m). Vertical variogram ranges applied to each lithology were set based on the log data and, depending on lithology and zone; generally, between 24-36 ft (7-10 m). After running several iterations and applying stochastic adjustments where needed, the accuracy of the resulting 3D lithology model was qualitatively evaluated by comparing the vertical proportion curve of the upscaled wells at well location vs. the vertical proportion curve of the lithology model. A visual summary of the workflow used to generate the seismically constrained 3D lithology model is displayed in Figure 10.

To analyze the spatial distribution of porosity throughout the Williams Fork Formation, 3D models of total porosity (ϕ_t) and effective porosity (ϕ_{eff}) were created. Shale and coal lithologies were assigned a constant value of 0 (as they are not considered pay). The 3D total porosity model was generated using sequential-Gaussian simulation (SGS), constrained by the following: (1) the 3D lithology model, (2) upscaled ϕ_t logs biased to the lithology logs using an arithmetic mean, (3) porosity histograms for sandstone per zone, and (4) horizontal and vertical variogram parameters (Appendix J(c)) for sandstone per zone. The 3D effective porosity model was generated using sequential-Gaussian simulation (SGS) as well, constrained to: (1) the 3D lithology model, (2) upscaled ϕ_{eff} logs biased to the lithology logs using an arithmetic mean, (3) porosity histograms for sandstone per zone, and (4) horizontal and vertical variogram parameters (Appendix J(d)) for sandstone per zone.

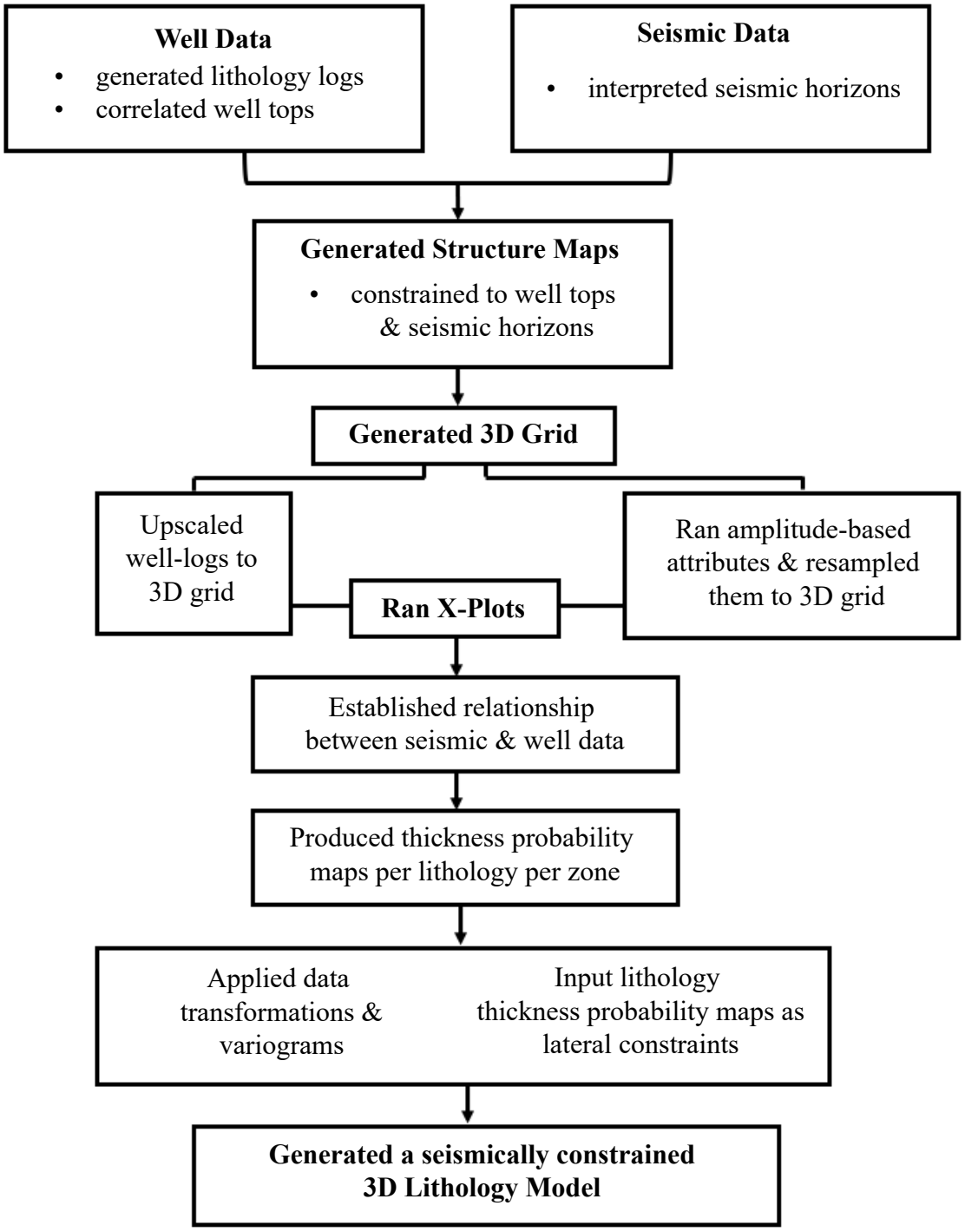

Figure 10: Depiction of the workflow used in this study to generate a seismically constrained 3D lithology model.

Normal score transforms were applied to the total porosity and effective porosity models. For both 3D porosity models, the major and minor horizontal variogram parameters were set to 2000 ft (609 m), while the vertical variogram parameters were set to approximately 30 ft (9 m).

To assess the relationship between porosity and absolute permeability within the tight-gas sandstones of the Williams Fork Formation and the spatial variability of absolute permeability, a 3D permeability model was established. Before producing a 3D permeability model, core permeability and porosity data associated with the Last-Dance 43C-3-792 well were cross-plotted. The cross-plot correlation was then applied to all wells as a cloud transform with twenty equally spaced bins (Appendix K(b)). Using sequential-Gaussian simulation (SGS), a 3D permeability model was generated by applying a bivariate distribution method to the secondary property, (the upscaled 3D effective porosity model), guided by the core porosity vs core permeability cloud transform. Shale and coal were assigned a constant value of 0 for permeability. Permeability variogram parameters (Appendix J(e)) applied to the sandstones were set to match those used in the total and effective porosity models. The permeability distribution of sandstone was set to a minimum of 0 and maximum of 2.25 based on the minimum and maximum of the cloud transform cross-plot data.

Because sandstones within the Williams Fork Formation are tight-gas reservoirs, faults and fractures are important as they can affect permeability along and within proximity to the faults. While faults can sometimes act as a barrier to flow, the faults identified by Baytok (2010) were analyzed and incorporated into the permeability model as conduits. This approach was used herein to qualitatively assess the potential positive impact of faults on permeability within the study area (in the absence of production data). To incorporate the faults, I began by applying a discrete method within geometric modeling to generate a “distance from fault” 3D volume (Figure 11b),

constrained to the analyzed faults and 3D model grid. To create a model representing the highest values along the faults that decrease to zero with distance, I calculated an inverse of the 3D "distance from fault" model (Figure 11c). Qualitatively, the resulting "inverse distance from fault" 3D model was then analyzed numerically and partitioned into different regions based on proximity to faulting. Numerically, these regions were used to create a separate permeability multiplier model (Figure 11d), assigning values as follows: areas along the faults (≥ 1) were assigned a multiplier of 5, areas near the faults (1-0.2) a multiplier of 2, and areas beyond the faults (≤ 0.2) a multiplier of 1. Once the permeability multiplier model was generated, it was multiplied by the existing permeability model to yield a fault-enhanced 3D permeability model (Figure 11f). These methods were applied to produce 1) a fault-enhanced 3D permeability model representing a select group of quality-checked faults (Appendix L(a)) previously interpreted by Baytok (2010), and 2) a fault-enhanced 3D permeability model that incorporates all faults (Appendix L(b)) interpreted by Baytok (2010).

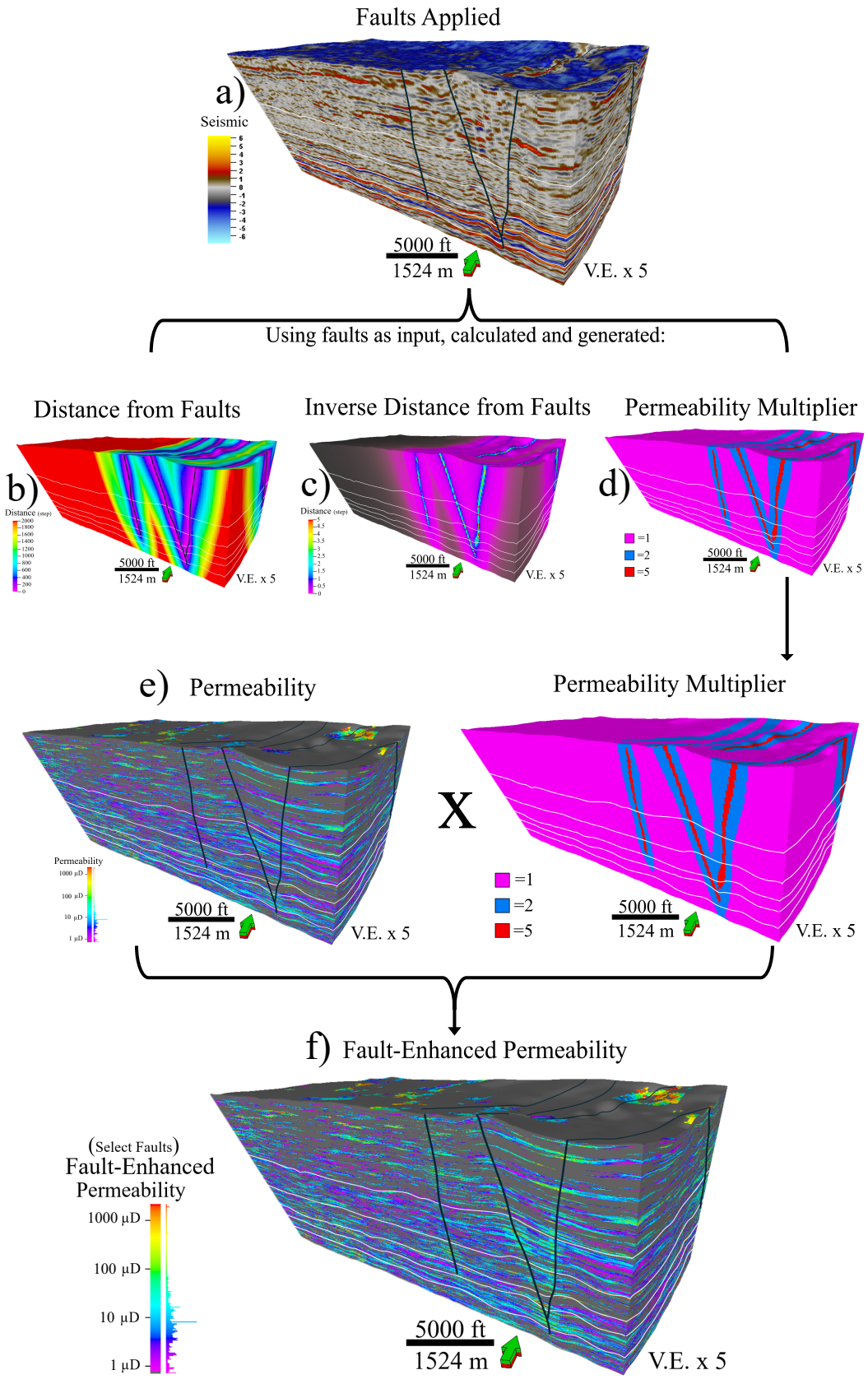
Faults Applied
a)
Seismic
5000 ft
1524 m
V.E. x 5
Using faults as input, calculated and generated:
Distance from Faults
b)
Distance (step)
5000 ft
1524 m
V.E. x 5
Inverse Distance from Faults
c)
Distance (step)
5000 ft
1524 m
V.E. x 5
Permeability Multiplier
d)
=1
=2
=5
5000 ft
1524 m
V.E. x 5
e) Permeability
Permeability
1000 µD
100 µD
10 µD
1 µD
5000 ft
1524 m
V.E. x 5
x
=1
=2
=5
Permeability Multiplier
5000 ft
1524 m
V.E. x 5
f) Fault-Enhanced Permeability
(Select Faults)
Fault-Enhanced
Permeability
1000 µD
100 µD
10 µD
1 µD
5000 ft
1524 m
V.E. x 5

Figure 11: Visual depiction of the workflow used to generate 3D fault-enhanced permeability models. The select group of faults (interpreted by Baytok (2010) and quality checked) represented in **a)** were used as inputs to calculate and generate **b)** a 3D "distance from faults" model. To create a model representing the highest values along the faults that decrease to zero with distance, calculations were applied to generate **c)** an "inverse distance from faults" 3D model (an inverse of the 3D "distance from fault" model). Qualitatively, the resulting "inverse distance from fault" 3D model was then analyzed numerically and partitioned into different regions based on proximity to faulting. Numerically, these regions were used to create a separate **d)** "permeability multiplier" model, assigning values as follows: areas along the faults (≥ 1) were assigned a multiplier of 5, areas near the faults (1-0.2) a multiplier of 2, and areas beyond the faults (≤ 0.2) a multiplier of 1. Once the permeability multiplier model was generated, it was multiplied by the existing **e)** permeability model to yield a **f)** fault-enhanced 3D permeability model. This process was applied a second time (using all faults interpreted by Baytok (2010) (Appendix L(b))) to generate a separate fault-enhanced permeability model that incorporates all faults (Appendix N(c)).

Expanding upon the S_w logs calculated using the basic Archie equation, a 3D water saturation (S_w) model was developed to assess the spatial distribution of water saturation. Shale and coal were assigned a constant S_w value of 1. The 3D S_w model was generated using sequential-Gaussian simulation (SGS), constrained to: (1) the 3D lithology model, (2) upscaled S_w logs biased to the lithology logs using an arithmetic mean, (3) S_w histograms for sandstone per zone, and (4) horizontal and vertical variogram parameters (Appendix J(f)) for sandstone per zone. In addition to the application of a normal score transform, the major and minor horizontal variogram parameters were set to 2000 ft (609 m), while the vertical variogram parameters were set around 30ft (9 m).

To evaluate the spatial distribution of bulk volume water (BVW) for future analysis of pay, a 3D BVW model was created. Utilizing the 3D models already produced, a property calculator was used to multiply the 3D S_w model by the 3D ϕ_{eff} model. The resulting 3D BVW model was then analyzed to assess a cut off for pay. A discrete model of pay was then generated such that pay represents sandstones that have a BVW < 0.05. A visual summary of the workflows used to generate all petrophysical models mentioned is displayed in Figure 12.

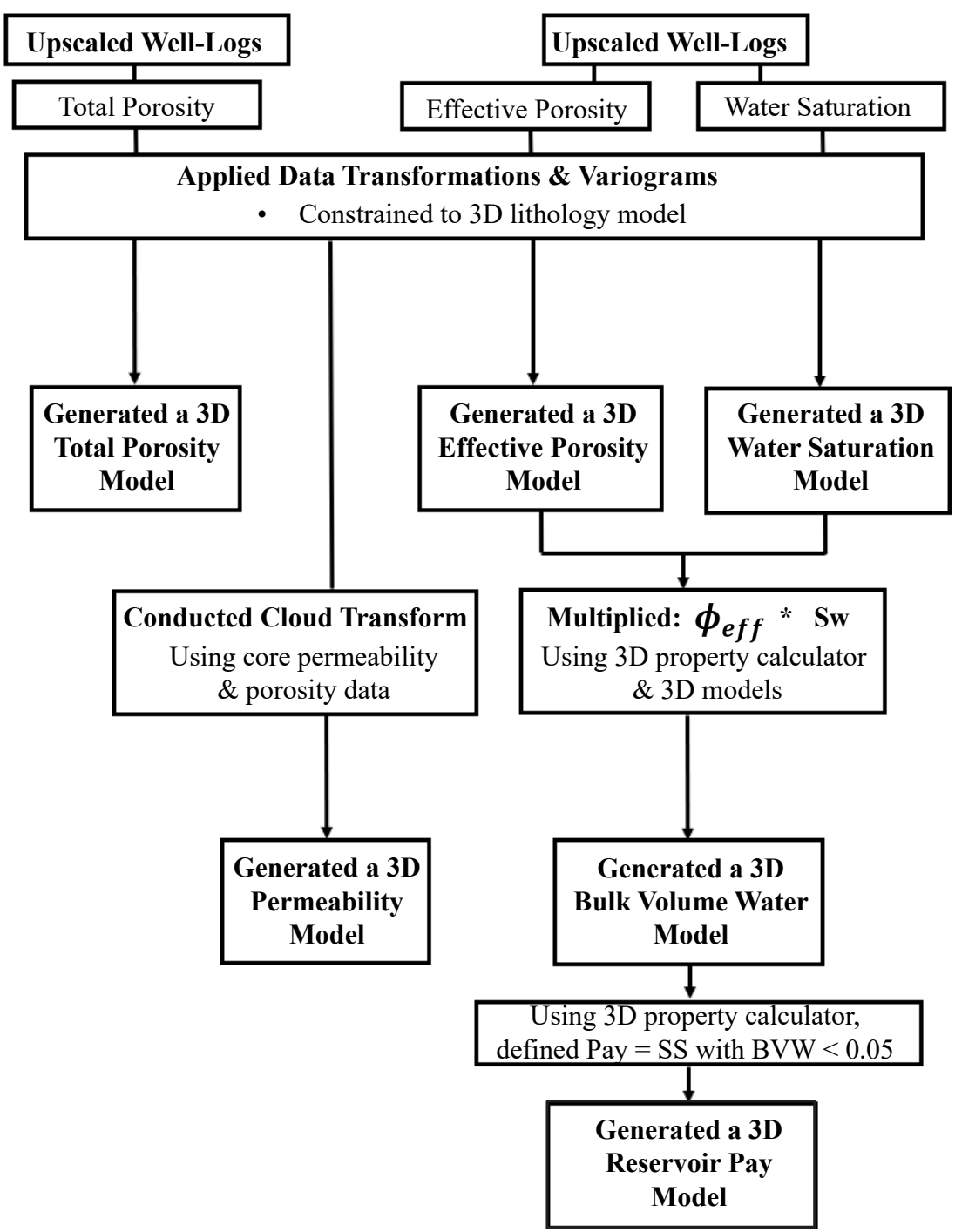

Figure 12: A generalized summary of the various workflows used throughout this study to generate 3D total porosity, effective porosity, permeability, water saturation, bulk volume water, and reservoir pay models.

RESULTS

Lithologies and Petrophysical Properties

Based on work involving core descriptions by Shaak (2010), core to log correlations by Foster (2010), and lithology log cut-offs defined by Hewlett (2010) and Baytok (2010), three lithologies were defined within the Williams Fork Formation including: 1) sandstone, 2) shale, and 3) coal, and were used in this study. Lithology logs calculated within this study define: 1) sandstone by a gamma ray cut-off of <96 API, 2) shale by a gamma ray cut-off of ≥96API, and 3) coal by a gamma ray cut-off of <96 API and density porosity and neutron porosity cut-offs of >0.25. While the cleanest sandstones exemplify approximate gamma ray, NPHI, and DPHI values of 38 API, 11%, and 17% respectively, the majority reflect a GR of 60-70 API, and depending on presence of gas-effect, a NPHI of 6.5-11% and a DPHI of 7-15%.

The Williams Fork Formation sandstone, shale, and coal lithologies have somewhat unique well-log responses (Figure 13). Williams Fork Formation sandstones typically exhibit: 1) moderate resistivity readings of 40-50 ohmm, 2) a volume of shale (Vsh) of 17-20%, 3) effective porosity of 1-8%, 4) water saturation range in value of 50-90% (avg. ~87%), and 5) BVW ranging from 0.03-0.06. While shales exhibit significantly higher NPHI values in comparison to DPHI values (shale effect), they also typically represent: 1) resistivity readings of 25-50 ohmm, 2) a higher Vsh of 60-80%, 3) effective porosity of 0.2-3%, 4) water saturation of 60-100%, and 5) BVW values of 0.4-0.6. Similar to the high NPHI and DPHI readings they exhibit, Williams Fork Formation coals also have very high resistivity and effective porosity values followed by extremely low readings of Vsh, water saturation, and BVW.

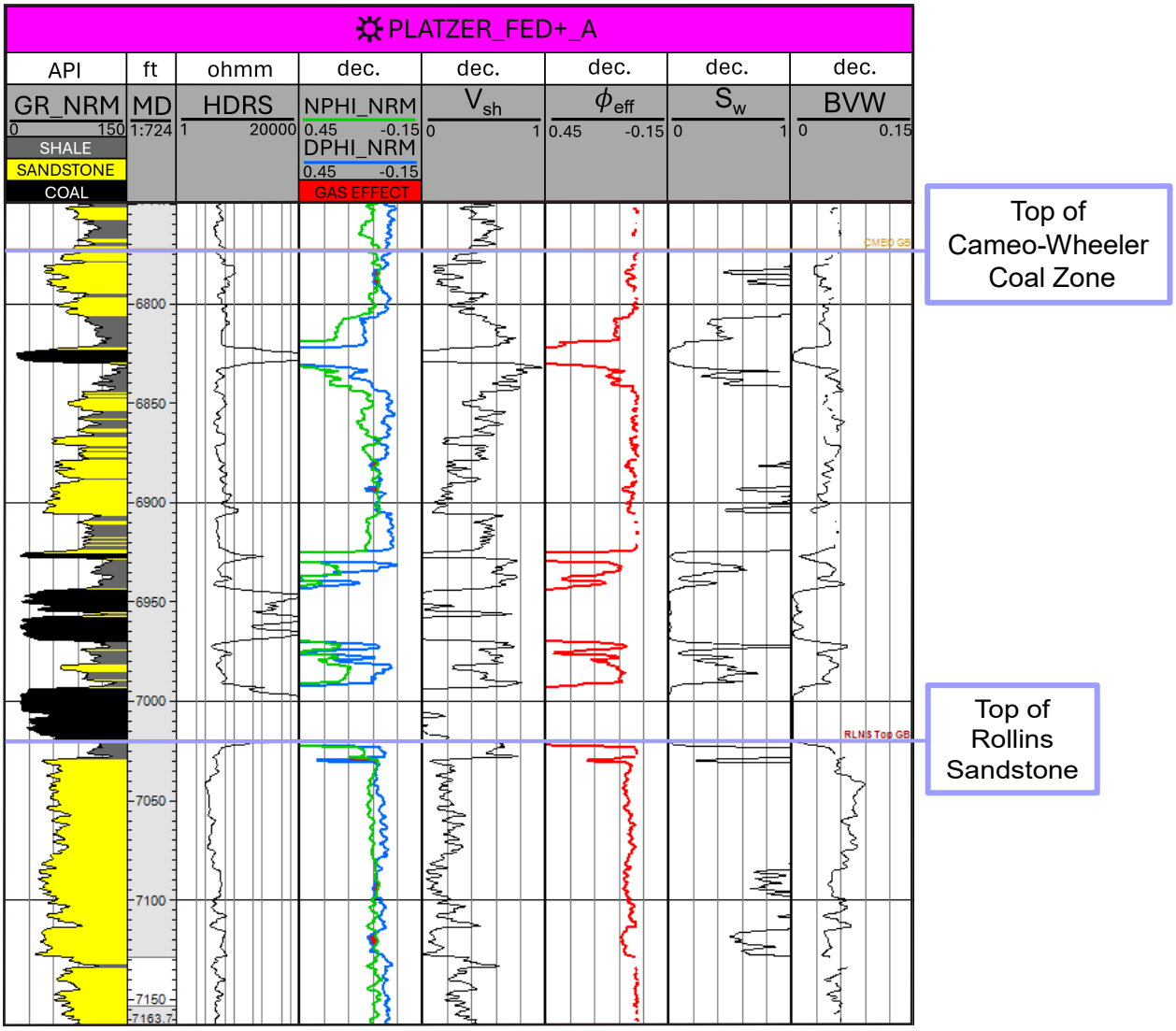

Figure 13: Typical log and petrophysical responses present in Williams Fork Formation sandstone, shale, and coal within the study area. Williams Fork Formation sandstones typically exhibit: 1) GR 60-70 API, 2) gas-effect depicted by NPHI/DPHI crossover, 3) moderate resistivity readings of 40-50 ohmm, 4) a volume of shale (Vsh) of 17-20%, 5) effective porosity of 1-8%, 6) water saturation range in value of 50-90% averaging ~87%, and 7) BVW ranging from 0.03-0.06. Williams Fork Formation shales exhibit: 1) significantly higher NPHI values in comparison to DPHI values (shale effect), 2) resistivity readings of 25-50 ohmm, 3) a higher Vsh of 60-80%, 4) effective porosity of 0.2-3%, 5) water saturation of 60-100%, and 6) BVW values of 0.4-0.6. Williams Fork Formation coals exhibit: 1) high NPHI and DPHI readings, 2) very high effective porosity and resistivity readings, and 3) extremely low readings of Vsh, water saturation, and BVW.

Stratigraphic Framework

Within the study area, the Williams Fork Formation ranges in thickness from approximately 2670-2880 ft (813-877 m), with an average thickness of 2780 ft (847 m). Dipping to the northwest, the Williams Fork Formation is thinner in the northwest and thickens towards the southeast (Figure 14).

The Williams Fork Formation is divided into six laterally continuous zones. Stratigraphically, from base to top these zones include the Lower Williams Fork Formation including 1) Cameo-Wheeler Coal Zone, 2) Middle Sandstone/South Canyon Coal Zone, 3) Upper Sandstone, and 4) Paonia Shale Member, and the 5) Middle Williams Fork, and 6) Upper Williams Fork. Structurally, all six zones exhibit a consistent northwest dip, gradually transitioning from the deepest northwest corner of the study area to the shallowest southeast corner (Figure 14).

As a unit, the Lower Williams Fork Formation (zone 1-4) is the thickest portion of the Williams Fork Formation with a thickness range of 1130-1380 ft (344-420 m), and an average thickness of 1230 ft (374 m) (Figure 15c). Thin to the west, the thickest part of the Lower Williams Fork Formation resides in the southeastern portion of the study area (Figure 15c). The Middle Williams Fork (zone 5), thinnest in comparison to the Upper Williams Fork and Lower Williams Fork Formation, has a thickness range of 370-680 ft (112-207 m), averaging approximately 553 ft (168 m) thick (Figure 15b). Apart from a few thicker areas in the center and to the east and west of the study area, the Middle Williams Fork generally maintains uniform thickness (Figure 15b). The Upper Williams Fork (zone 6) is slightly thinner than the Lower Williams Fork Formation, exhibiting an approximate thickness range of 880-1090 ft (268-332 m), and average thickness of 990 ft (301 m) (Figure 15a).

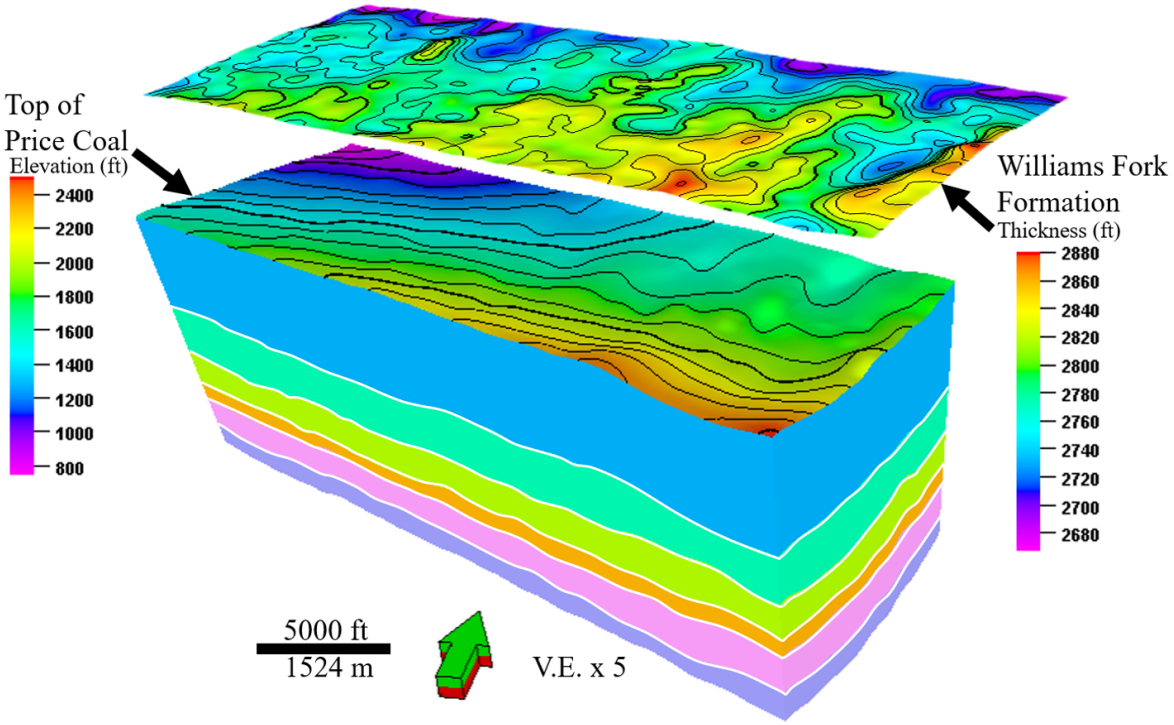

Figure 14: Draped by the structure contour map associated with the top of the Price Coal, the 3D grid of the Williams Fork Formation displays a northwest dipping trend within the study area. All 6 zones within the model follow this structural northwest-dipping trend. Positively correlated to the structure map displayed, a thickness map of the Williams Fork Formation reveals that the formation is thinner to the northwest and thickens towards the southeast. The Williams Fork Formation ranges in thickness from approximately 2670-2880 ft (813-877 m), with an average thickness of 2780 ft (847 m).

Upper Williams Fork Structure vs. Thickness

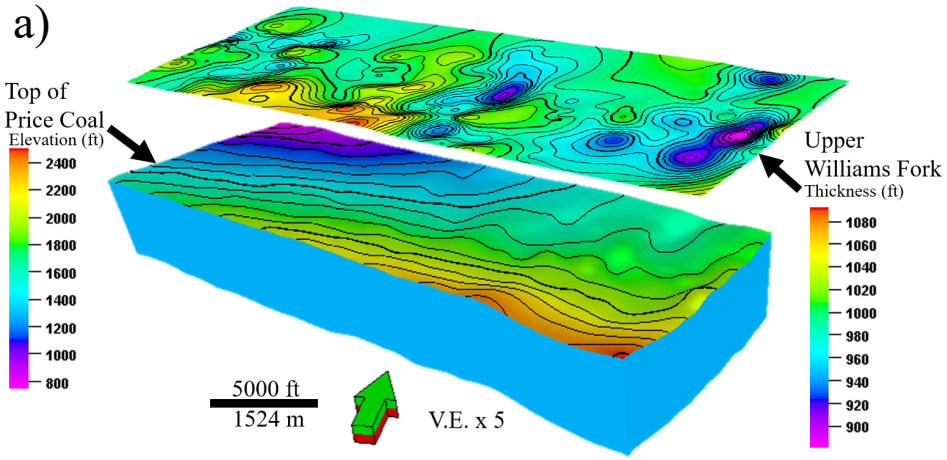

Middle Williams Fork Structure vs. Thickness

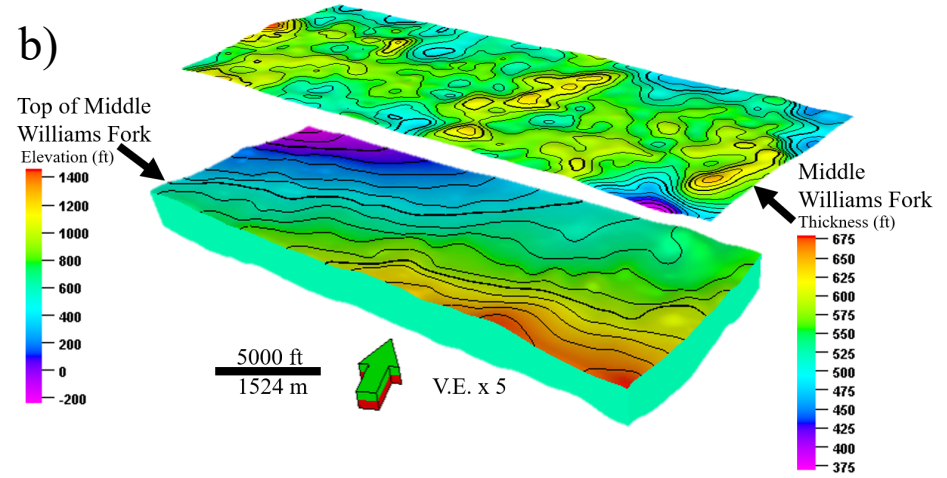

Lower Williams Fork Formation Structure vs. Thickness

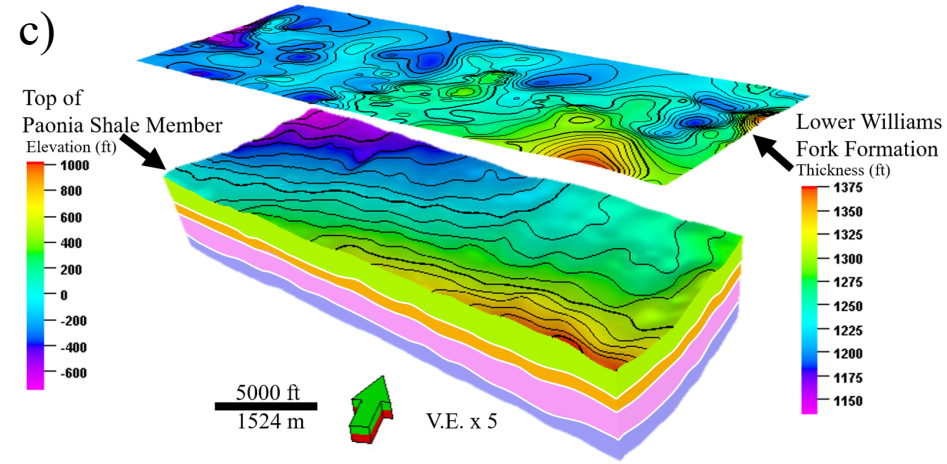

Figure 15: a) Upper Williams Fork (Zone 6) structure vs. thickness. Draped by the Upper Williams Fork top structure-contour map, the Upper Williams Fork displays a northwest dipping trend and has a range in thickness of ~880-1090 ft (268-332 m), averaging 990 ft (301 m). Thinner areas present to the north and east, thicker towards the central southwest. **b)** Middle Williams Fork (Zone 5) structure vs. thickness. Draped by the Middle Williams Fork top structure-contour map, the Middle Williams Fork displays a northwest dipping trend and has a thickness range of 370-680 ft (112-207 m), averaging ~553 ft (168 m) thick. Apart from a few thicker areas in the center and to the east and west of the study area, the Middle Williams Fork generally maintains uniform thickness. **c)** Lower Williams Fork Formation (zone 1-4) structure vs. thickness. Draped by the Paonia Shale Member top structure-contour map, the Lower Williams Fork Formation has a thickness range of 1130-1380 ft (344-420 m), an average thickness of 1230 ft (374 m), and is thin to the west, and thickest in the southeastern portion of the study area.

Generally, the Upper Williams Fork is thin to the north, with some thinner areas to the east, and it thickens toward the central southwest (Figure 15a).

Although the Lower Williams Fork Formation is thickest as a unit in comparison to the Middle Williams Fork and Upper Williams Fork, the individual zones within it are much thinner. The lowest zone of the Lower Williams Fork Formation, the Cameo-Wheeler Coal Zone (zone 1), has a thickness range of 190-340 ft (57-103 m), and an average thickness of 250 ft (76 m) (Figure 16p). Thinnest in centralized regions within the study area, the Cameo-Wheeler Coal Zone thickens radially to the northwest and southeast (Figure 16p). The thickest portion of the Lower Williams Fork Formation, the Middle Sandstone/South Canyon Coal Zone (zone 2), ranges in thickness from 330-490 ft (100-149 m), averaging an approximate thickness of 400 ft (121 m) (Figure 16m). The Middle Sandstone/South Canyon Coal Zone thickens from the west to east, exhibiting thickest deposits in the southeast (Figure 16m). The thinnest portion of the Lower Williams Fork Formation, the Upper Sandstone (zone 3), exhibits a thickness range of 140-240 ft (42-73 m), and an average thickness of 207 ft (63 m) (Figure 16j). Thin to the southwest, the Upper Sandstone thickens radially to the northeast and southeast (Figure 16j). Slightly thinner than zone 2, the Paonia Shale Member (zone 4) has a thickness range of 280-470 ft (m) and average thickness of 370 ft, ranking it as the second thickest zone within the Lower Williams Fork Formation (Figure 16g). Thin to the northeast, the Paonia Shale Member gradually thickens to the southwest and southeast (Figure 16g).

Upper Williams Fork Thickness vs. Sandstone Thickness

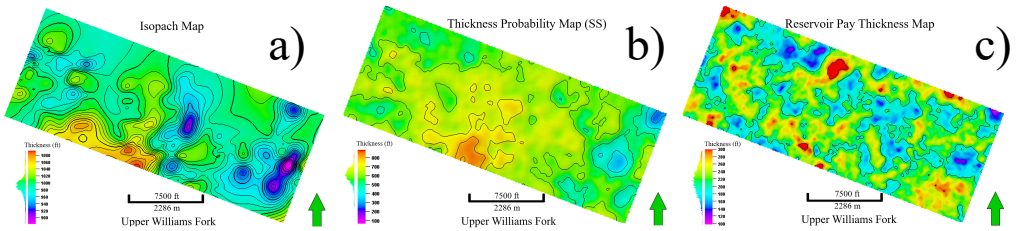

Middle Williams Fork Thickness vs. Sandstone Thickness

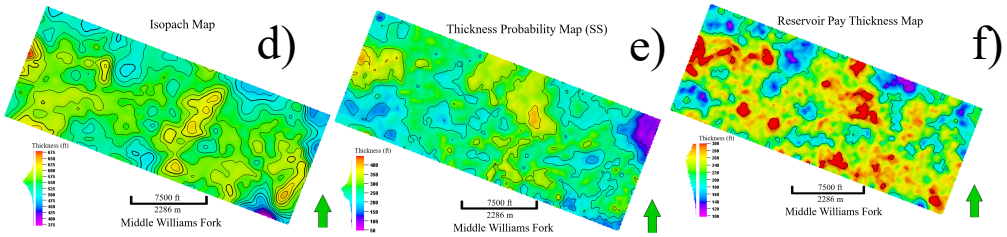

Lower Williams Fork Formation Thickness vs. Sandstone Thickness

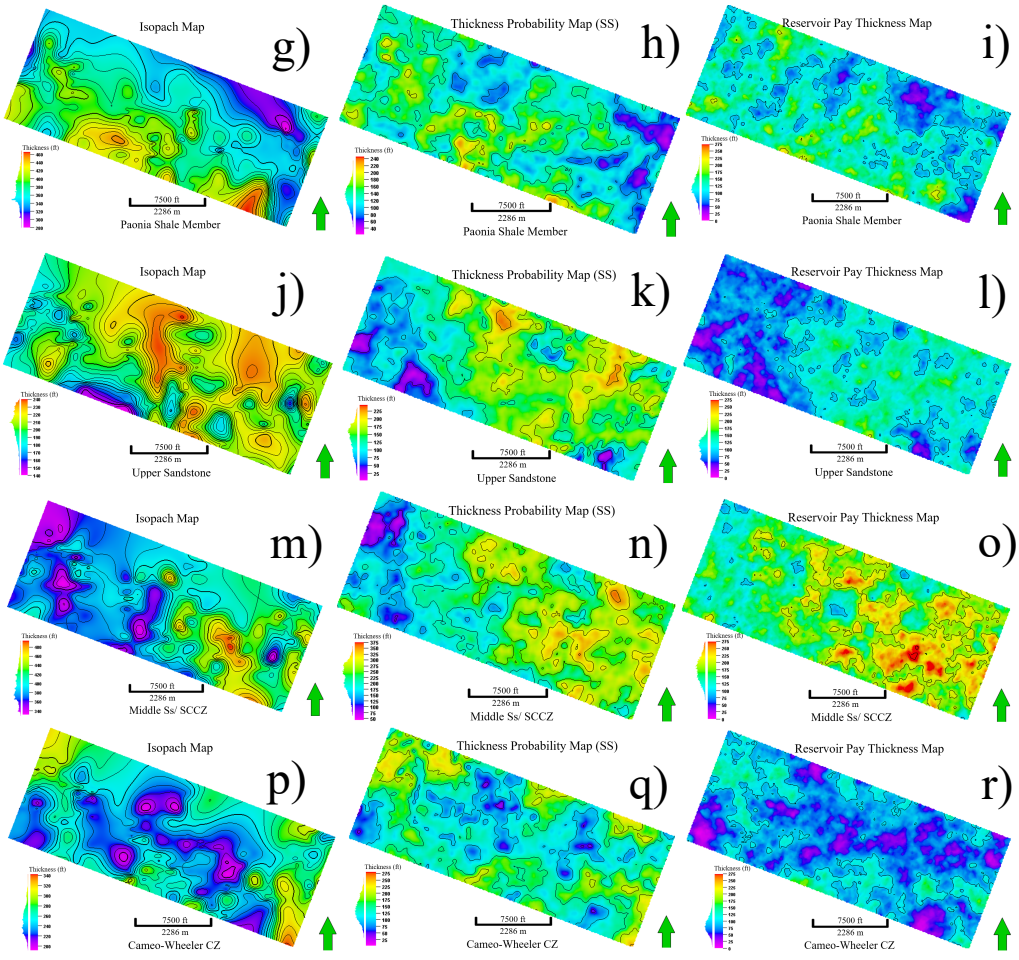

Figure 16: Formation thickness vs sandstone thickness vs pay thickness comparisons within each zone of the Williams Fork Formation. The left column **(a, d, g, j, m,** and **p)** depicts formation thickness maps associated with each of the 6 zones within the Williams Fork Formation. The middle column **(b, e, h, k, n,** and **q)** depicts the probability sandstone thickness maps (*see methods section*) used to constrain the lateral distribution of sandstone per zone in the 3D lithology model. The column on the right, **(c, f, i, l, o,** and **r)**, depicts the reservoir pay thickness within each zone. Within all 6 zones of the Williams Fork Formation, there is a positive correlation between the thickest regions of each zone and the thickest sandstone and reservoir pay deposits.

Lithology Thickness Probability Maps/ Lateral Lithology Distribution

The trends identified within the seismically constrained lithology thickness probability maps ((Figure 16b, e, h, k, n, and q) and (Figure 17)), used as lateral constraints during the 3D lithology modeling process, provide additional insights into the lithologic distribution of each zone. Although the Williams Fork Formation was modeled to include three lithologies, shale was set as the background lithology (*see methods section*) and is not discussed. In addition, while thickness probability maps were used to laterally constrain sandstone and coal, because they were only applied to coal in zones 1 and 2 where its presence was most prevalent (*see* (Appendix C) *for further explanation*), the lateral distribution of coal in zones 3-6 is not discussed.

Within the Cameo-Wheeler Coal Zone (zone 1), the thickness probability maps of sandstone (Figure 17c) and coal (Figure 17d) coincide such that high sandstone presence to the northwest, southeast, and central edges of the study area corresponds with low coal presence. Conversely, areas to the southwest, northeast, and central interior are predominantly coal rich (Figure 17d). Within the Middle Sandstone/South Canyon Coal Zone (zone 2), the lateral distribution of sandstones and coals displayed by the lithology thickness probability maps showcase similar conformance. Areas of higher coal presence (Figure 17b) in the northwest and southwest correspond to lower sandstone presence (Figure 17a), while higher sandstone presence in the east is associated with lower coal presence. The lithology thickness probability map associated with the Upper Sandstone (zone 3), depicts a higher sandstone presence throughout the central and eastern portion of the study area (Figure 16k). Within the Paonia Shale Member (zone 4), sandstone is most predominant to the northwest, and centrally along a southwest/ northeast trend (Figure 16h).

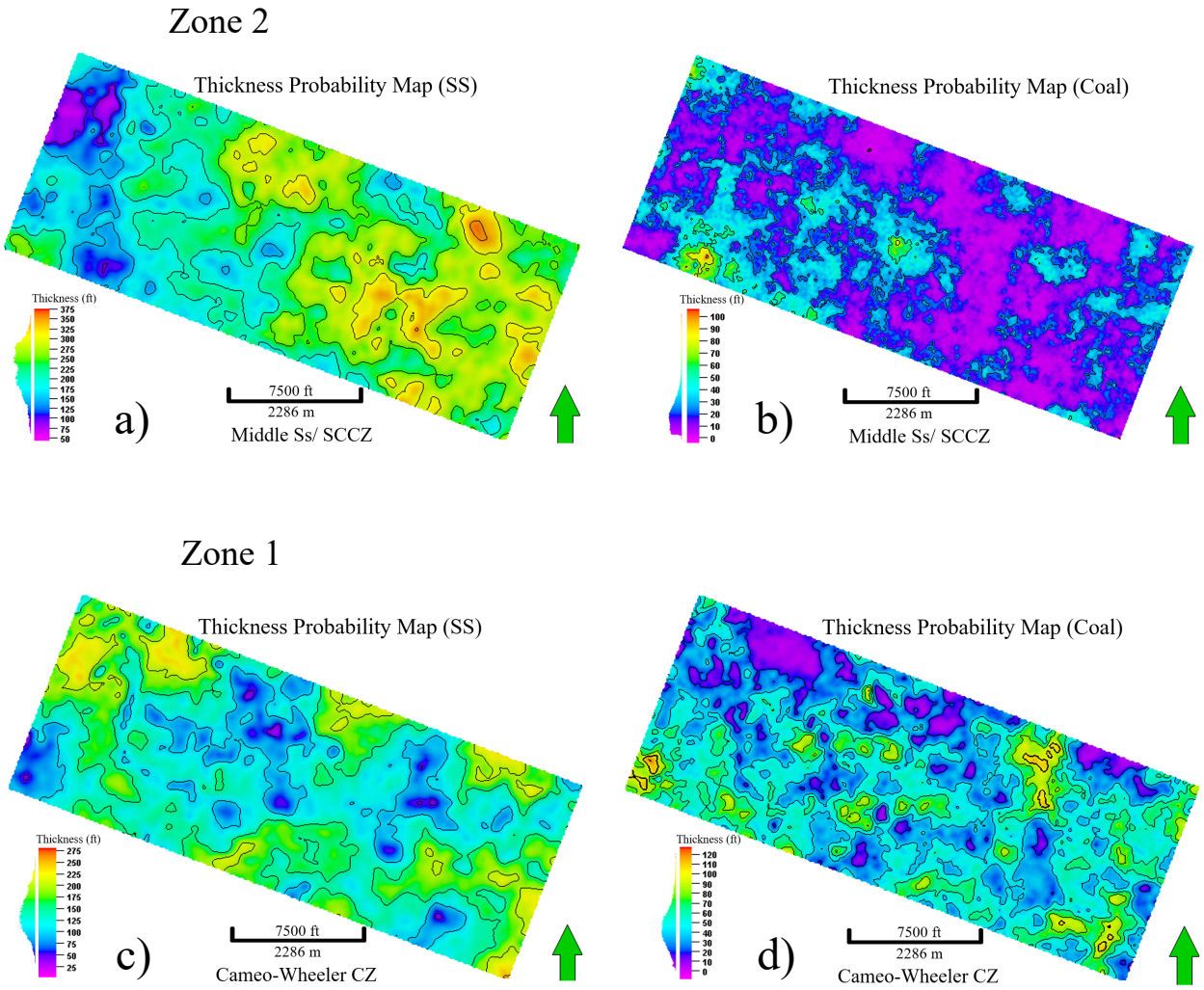

Figure 17: Visual comparison of the sandstone and coal thickness probability maps associated with zone 1 and zone 2. Within the Cameo-Wheeler Coal Zone (zone 1), the thickness probability maps of **c)** sandstone and **d)** coal coincide such that high sandstone presence to the northwest, southeast, and central edges of the study area corresponds with low coal presence. Conversely, areas to the southwest, northeast, and central interior are predominantly coal rich **(d)**. Within the Middle Sandstone/South Canyon Coal Zone (zone 2), the lateral distribution of sandstones and coals displayed by the lithology thickness probability maps showcase similar conformance. Areas of higher **b)** coal presence in the northwest and southwest correspond to lower **a)** sandstone presence, while higher sandstone presence in the east is associated with lower coal presence.

Although sandstone is present throughout most of the Middle Williams Fork (zone 5), the associated thickness probability map depicts higher sandstone thickness in the northwest, central-northeast, and eastern portions of the study area (Figure 16e). Prevalent throughout the majority of the Upper Williams Fork (zone 6), sandstone thickness is greatest within the central-interior and central-southern areas of the study area (Figure 16b).

3D Lithology Model

When comparing the lithologic vertical proportion curve of the upscaled wells (54% shale, 43% sandstone, 3% coal) to that of the resulting 3D lithology model (54% shale, 42% sandstone, 4% coal) (Figure 18a), the model honors the stratigraphic trends in lithology (Figure 18b).

The two lowermost zones of the Lower Williams Fork Formation, the Cameo-Wheeler Coal Zone (zone 1) and the Middle Sandstone/South Canyon Coal Zone (zone 2), contain laterally extensive coal deposits interbedded with sandstone and shale. Together, these two coal-dominated zones are composed of 31% shale, 54% sandstone, and 15% coal (Figure 19e). In comparison to the lithologic composition of the Middle Sandstone/South Canyon Coal Zone (31% shale, 61% sandstone, 8% coal), the Cameo-Wheeler Coal Zone contains higher coal presence as it is 30% shale, 50% sandstone, and 20% coal.

In comparison to the lower two coal-dominated zones, the two uppermost zones of the Lower Williams Fork Formation, Upper Sandstone (zone 3) and Paonia Shale Member (zone 4), reflect a decrease in coal and sandstone content, and an increase in shale. As a unit, zones 3 and 4 are composed of 50% shale, 47% sandstone, and 3% coal (Figure 19d).

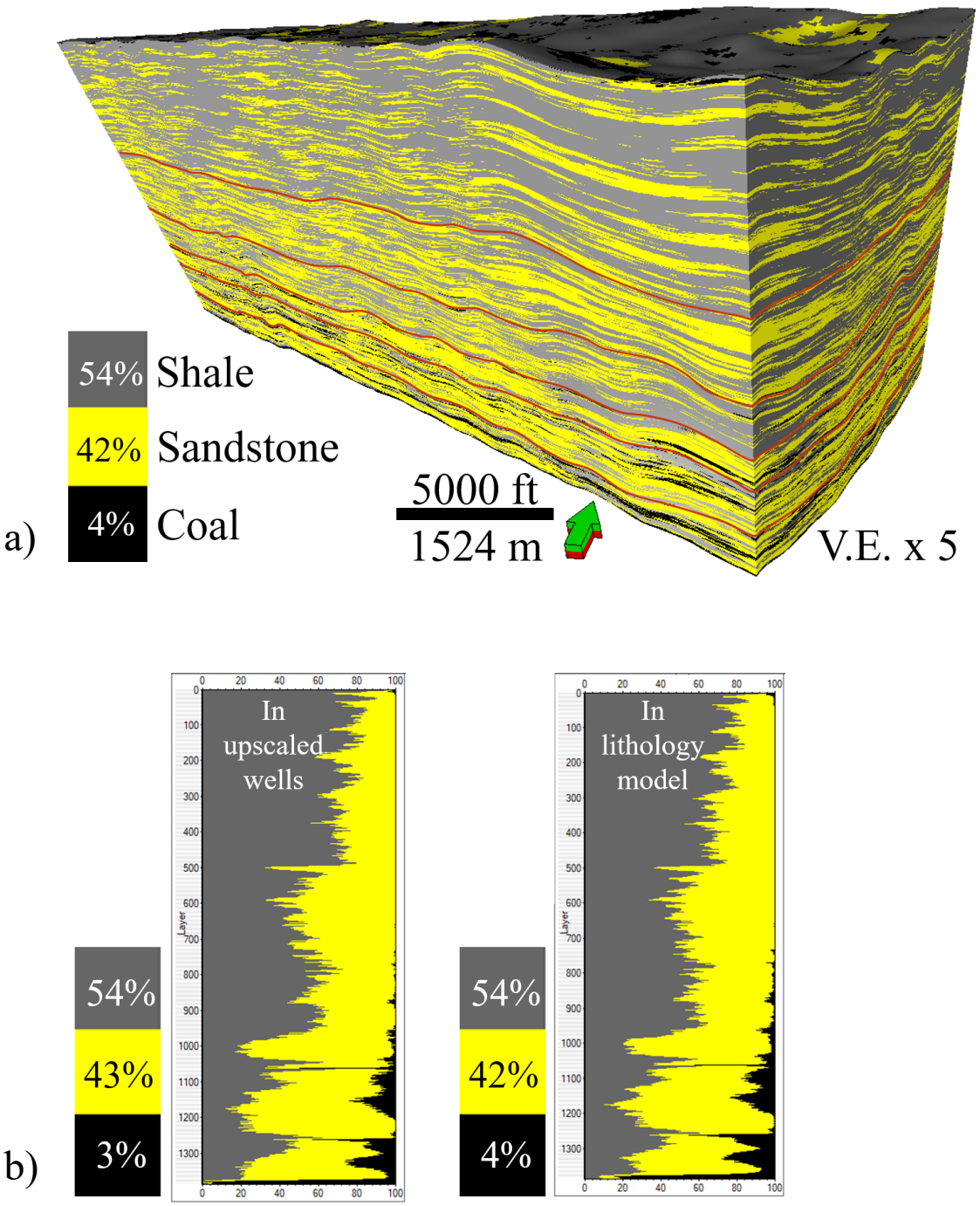

Figure 18: a) Seismically constrained 3D lithology model of the Williams Fork Formation. Within the study area, the Williams Fork Formation is composed of ~54% shale, 42% sandstone, and 4% coal. Brown lines denote the 6 different zones within the entire formation. **b)** Comparison of the upscaled wells' vertical proportion curve and lithology model's vertical proportion curve displays how the model honors the stratigraphic trends in lithology.

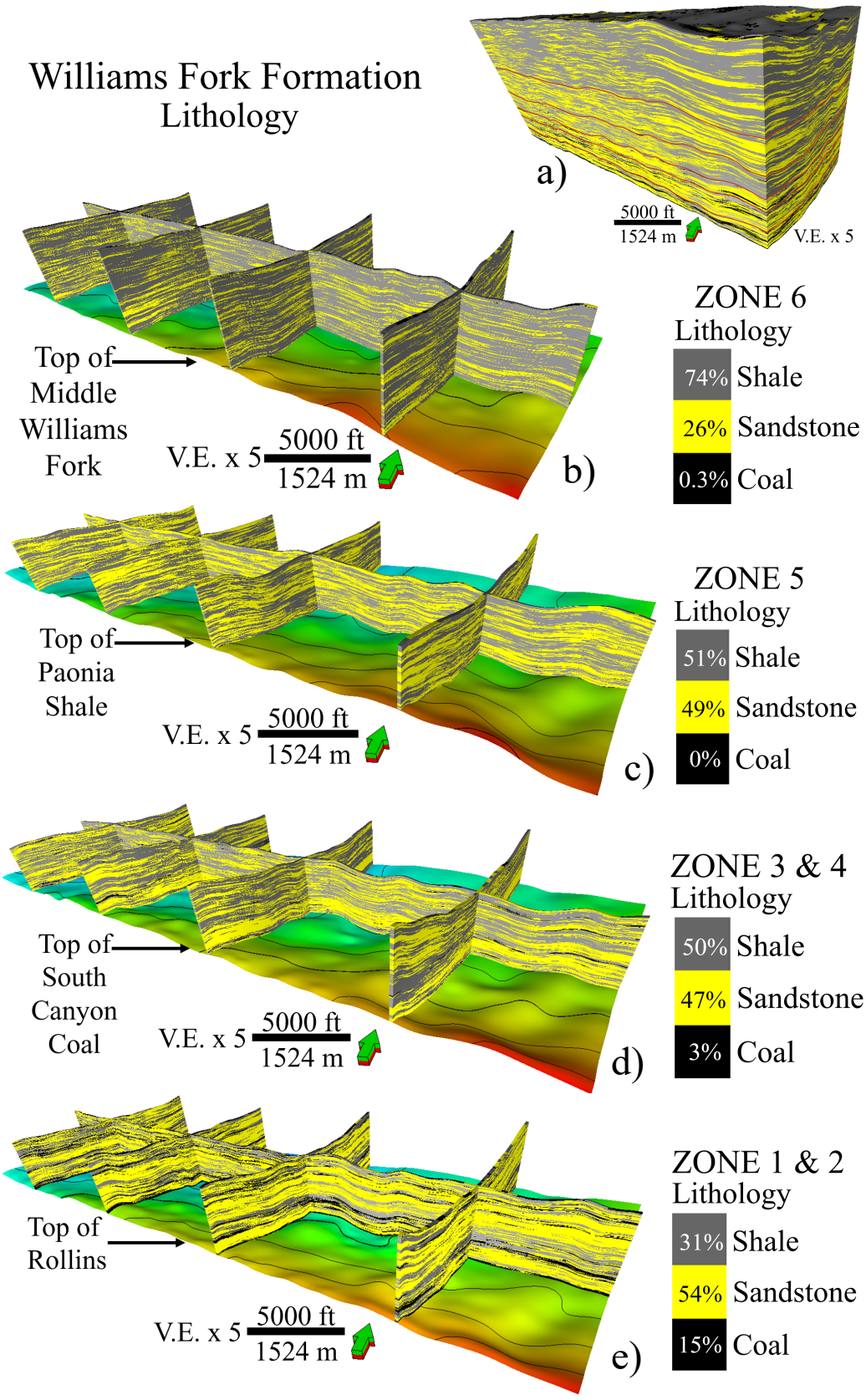
Williams Fork Formation
Lithology
a)
5000 ft
1524 m
V.E. x 5
Top of
Middle
Williams
Fork
V.E. x 5
5000 ft
1524 m
b)
ZONE 6
Lithology
74% Shale
26% Sandstone
0.3% Coal
Top of
Paonia
Shale
V.E. x 5
5000 ft
1524 m
c)
ZONE 5
Lithology
51% Shale
49% Sandstone
0% Coal
Top of
South
Canyon
Coal
V.E. x 5
5000 ft
1524 m
d)
ZONE 3 & 4
Lithology
50% Shale
47% Sandstone
3% Coal
Top of
Rollins
V.E. x 5
5000 ft
1524 m
e)
ZONE 1 & 2
Lithology
31% Shale
54% Sandstone
15% Coal

Figure 19: Model and fence diagram depictions of Williams Fork Formation lithology within the study area. **a)** 3D lithology model of the Williams Fork Formation. **b)** The Upper Williams Fork (zone 6) is composed of ~74% shale, ~26% sandstone, and ~0.3% coal, representative of an alluvial plane depositional environment. **c)** The Middle Williams Fork (zone 5) is composed of 51% shale, 49% sandstone, and 0% coal, representative of a depositional transition from coastal to alluvial plain. **d)** Grouped together based on depositional environment, the upper 2 zones of the Lower Williams Fork Formation (zones 3&4), are composed of 50% shale, 47% sandstone, and 3% coal, representing a depositional transition from swamp to coastal plain. **e)** Grouped together based on representing swamp depositional environments, the lower 2 zones of the Lower Williams Fork Formation are composed of 31% shale, 54% sandstone, and 15% coal.

Of the two zones, the Upper Sandstone has higher coal and sandstone content (35% shale, 63% sandstone, 2% coal), whereas the Paonia Shale Member contains higher shale content (59% shale, 40.5% sandstone, and 0.5% coal.

The Middle Williams Fork (zone 5) contains laterally extensive sandstones interbedded with shale. In comparison to the upper two zones of the Lower Williams Fork Formation (zones 3 and 4) (50% shale, 47% sandstone, 3% coal), the Middle Williams Fork reflects a slight increase in shale (51%) and sandstone (49%) content, and a complete deficit in coal (0%) (Figure 19c).

Denoted by its high shale content, the Upper Williams Fork (zone 6) contains interbedded sandstone and shale and has a negligible coal presence at the top associated with the Price Coal formation. In comparison with the Middle Williams Fork (51% shale, 49% sandstone, 0% coal), the Upper Williams Fork reflects a significant increase in shale (73.75%), a substantial decrease in sandstone (26%), and a slight increase in coal (0.25%) (Figure 19b).

Spatial Distribution of Reservoir Properties and Reservoir Pay Sandstone

To analyze the spatial distribution of reservoir properties within the Williams Fork Formation sandstones at Mamm Creek Field, 3D models of total porosity (Figure 20), effective porosity (Figure 21), permeability (Figure 22), water saturation (Figure 23), bulk volume water (Figure 24), and reservoir pay (Figure 25) were generated.

Williams Fork Formation sandstone total porosity, effective porosity, and permeability range from 5-15%, 1-8%, and 0.7-10 µD, respectively (Figure 20, 21, and 22).

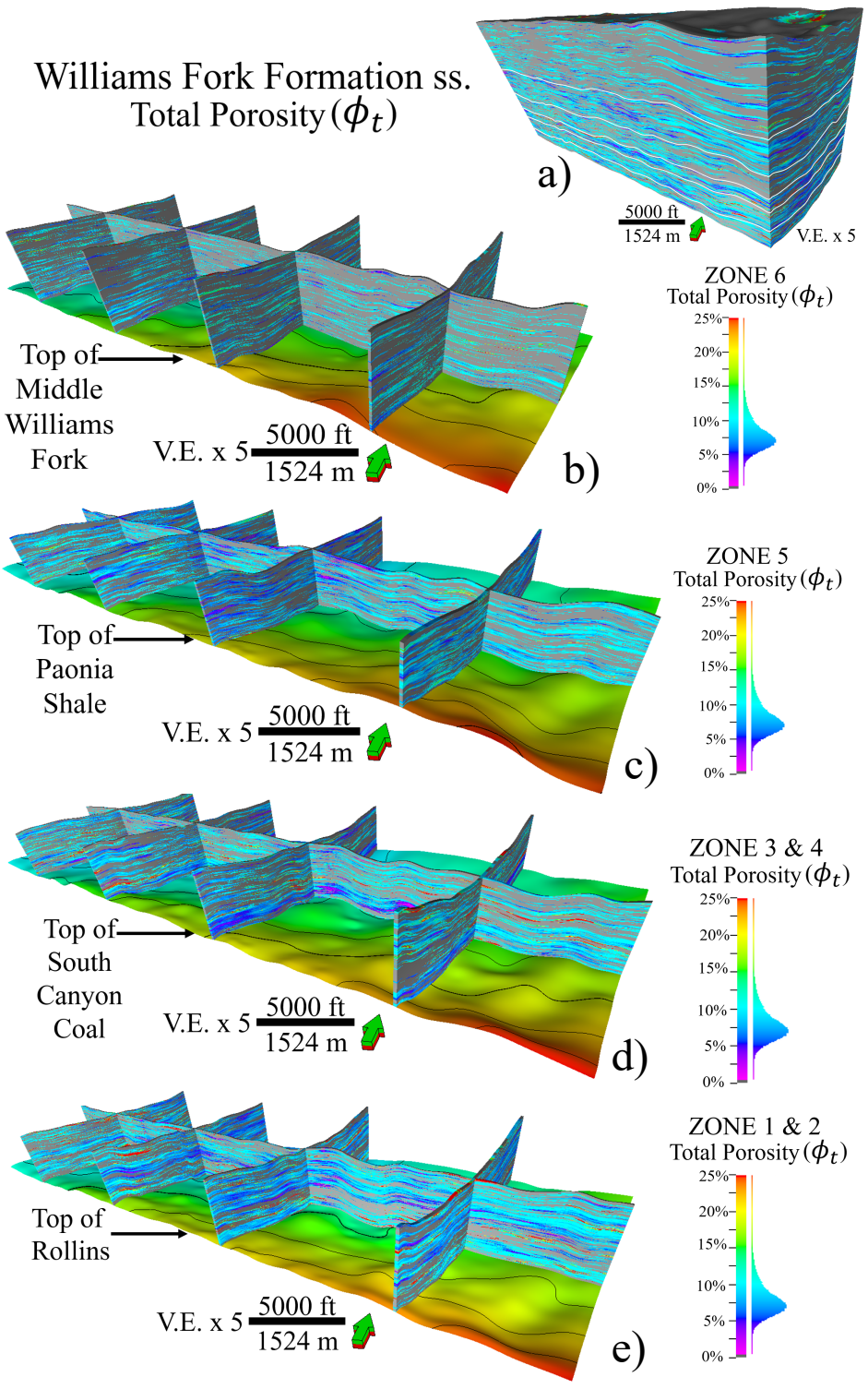

Figure 20: Model and fence diagram depictions of total porosity within Williams Fork Formation sandstone within the study area. **a)** 3D total porosity model of the Williams Fork Formation. **b-e)** on average, total porosity consistently reflects a range in value of 5-15% regardless of zone/ stratigraphy.

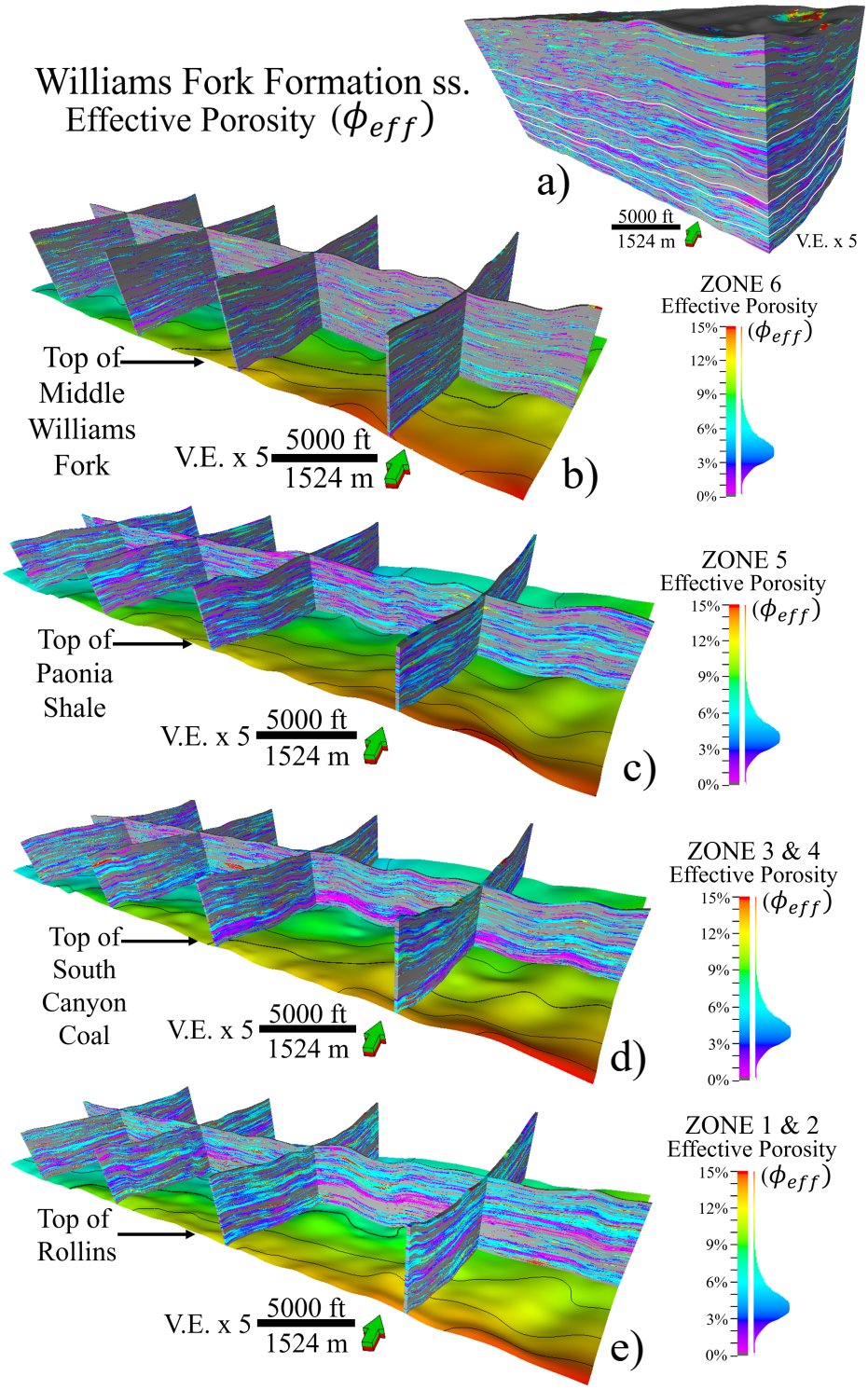

Figure 21: Model and fence diagram depictions of effective porosity within Williams Fork Formation sandstone within the study area. **a)** 3D effective porosity model of the Williams Fork Formation. **b-e)** on average, effective porosity consistently reflects a range in value of 1-8% regardless of zone/ stratigraphy.

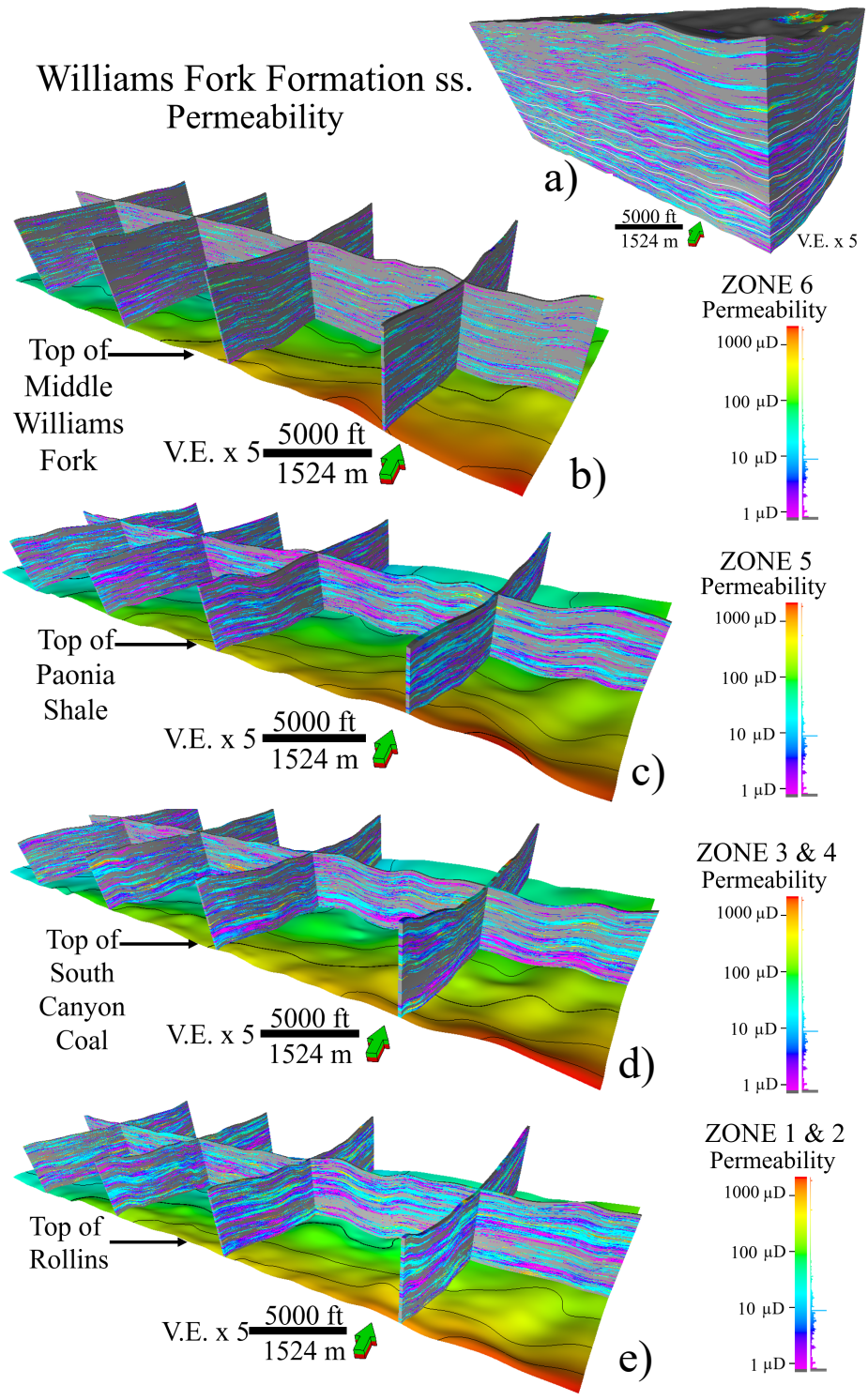

Figure 22: Model and fence diagram depictions of permeability within Williams Fork Formation sandstone within the study area. **a)** 3D permeability model of the Williams Fork Formation. **b-e)** on average, permeability consistently reflects a range in value of 0.7-10 µD regardless of zone/ stratigraphy.

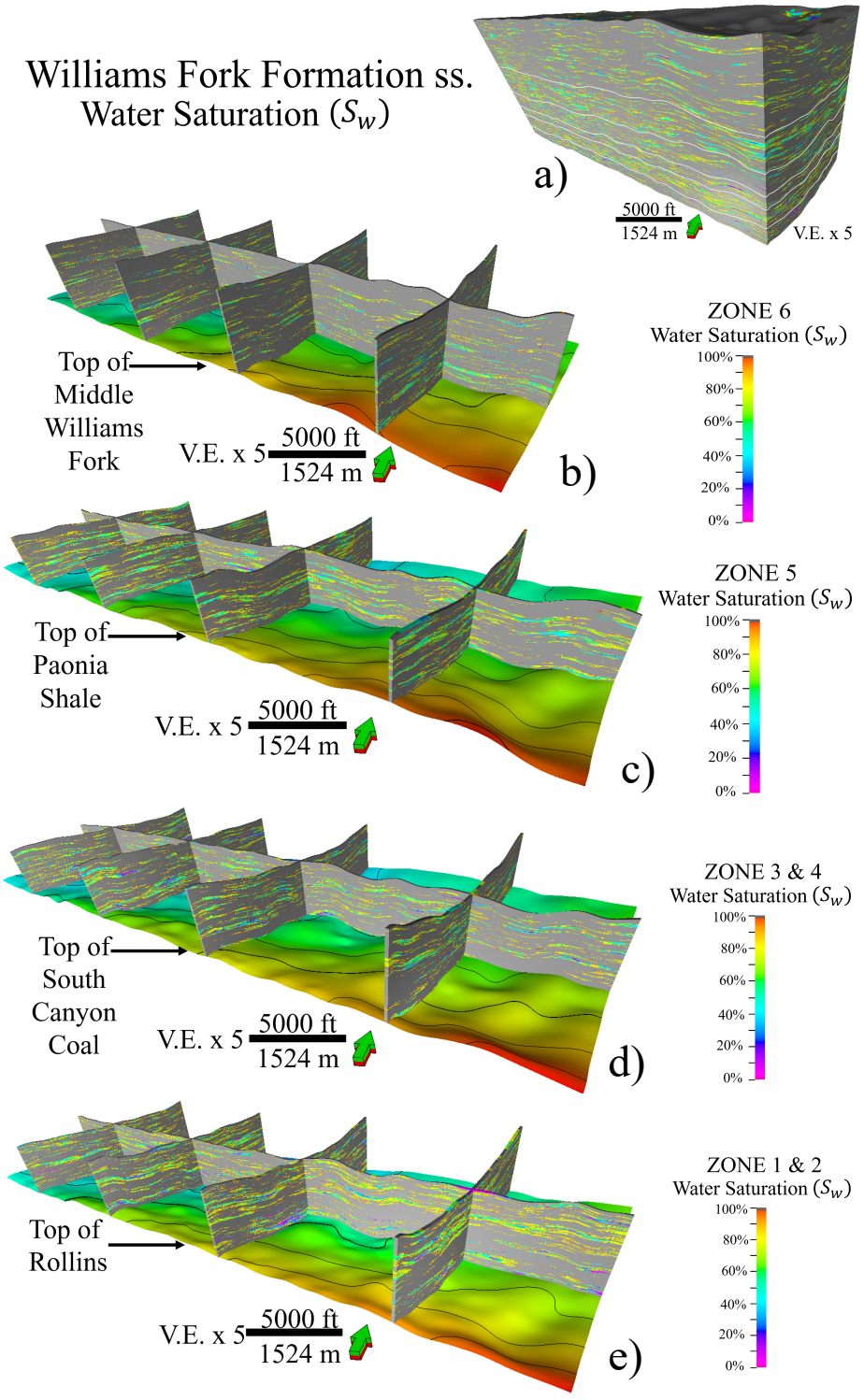

Figure 23: Model and fence diagram depictions of water saturation within Williams Fork Formation sandstone within the study area. **a)** 3D water saturation model of the Williams Fork Formation. **b-e)** water saturation consistently reflects a range in value of ~50-90%, and on average ~87% regardless of zone/ stratigraphy.

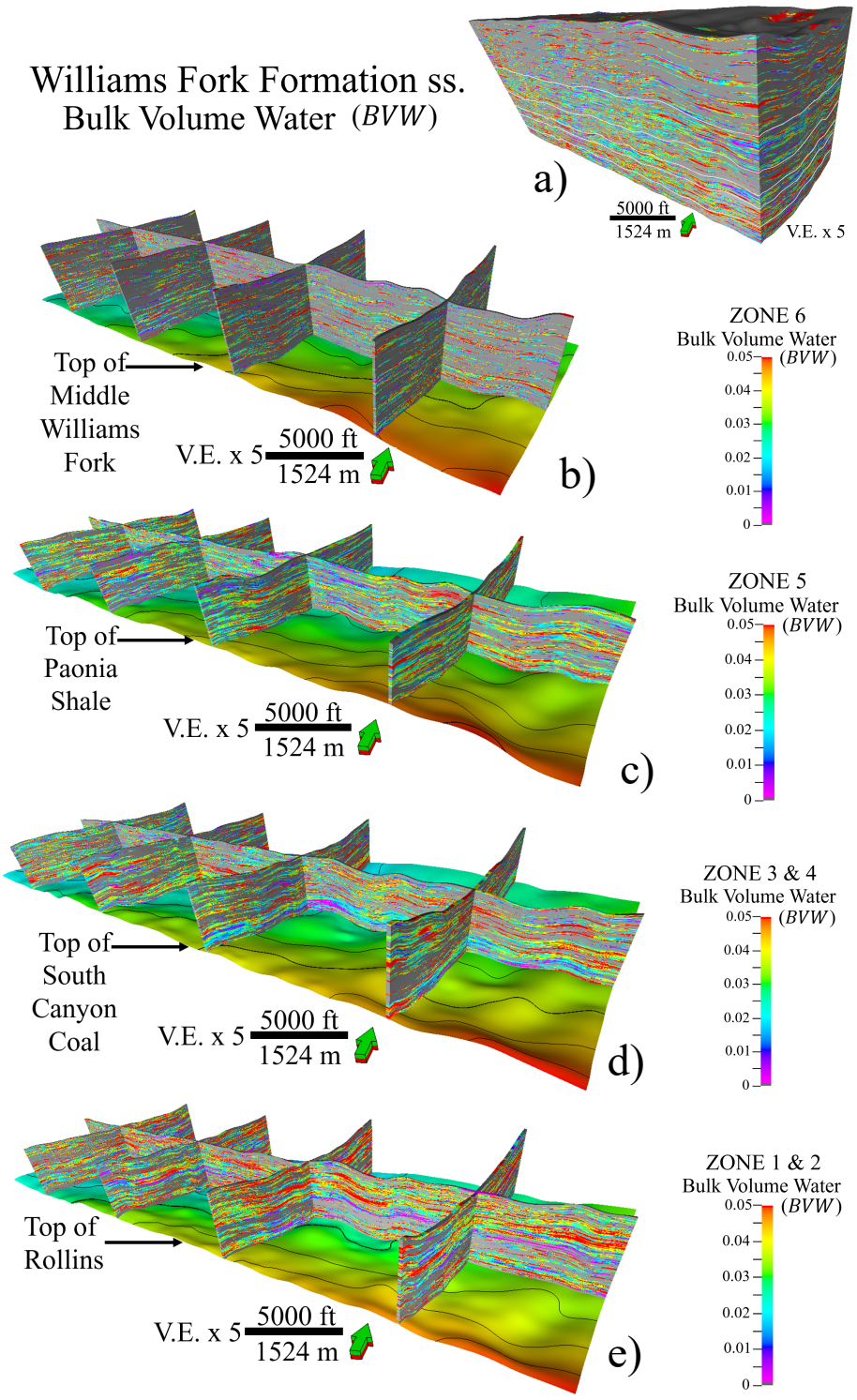

Figure 24: Model and fence diagram depictions of bulk volume water within Williams Fork Formation sandstone within the study area. **a)** 3D bulk volume water model of the Williams Fork Formation. **b-e)** on average, bulk volume water consistently reflects a range in value of 0.03-0.06 regardless of zone/ stratigraphy.

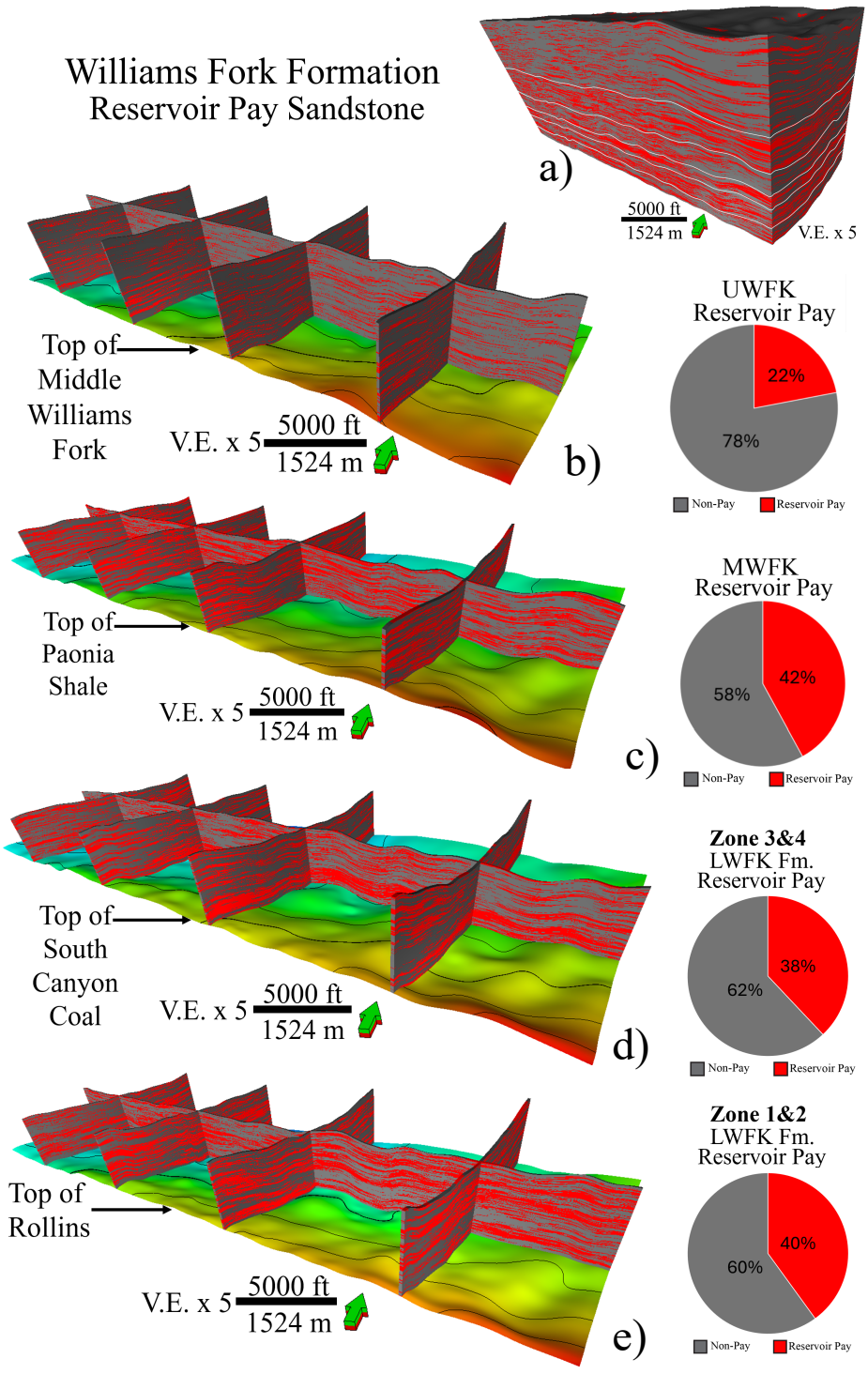

Figure 25: Model and fence diagram depictions of reservoir pay sandstone within the Williams Fork Formation within the study area. **a)** 3D reservoir pay sandstone model of the Williams Fork Formation. **b-e)** Depicted in the pie charts and fence diagrams, the Lower Williams Fork Formation (zones 1-4) and Middle Williams Fork (zone 5) are composed of a higher percentage of reservoir pay sandstone than the Upper Williams Fork (zone 6).

Although the general ranges associated with these petrophysical properties do not vary stratigraphically, the average values of each do vary slightly depending on zone. On average, sandstones within the Cameo-Wheeler Coal Zone (zone 1), for example, not only contain the highest total porosity (12%), effective porosity (6%), and permeability values (6 µD) within the Lower Williams Fork Formation, but also throughout the entire Williams Fork Formation. Within the remaining three zones (zones 2-4) of the Lower Williams Fork Formation, the average total porosity (10%), effective porosity (5%), and permeability (6 µD) values exhibited within sandstones are generally higher in comparison to that of the Middle Williams Fork (9% total porosity, 4% effective porosity, 7 µD permeability), and Upper Williams Fork (10% total porosity, 4% effective porosity, 7 µD permeability). Although stratigraphic variability of water saturation (50-90%, averaging ~87%) (Figure 23) and bulk volume water (0.03-0.06) (Figure 24) is minimal between zones, average values contained by sandstones do vary slightly between zones. The lower two zones of the Lower Williams Fork Formation, the Cameo-Wheeler Coal Zone (zone 1) and Middle Sandstone/South Canyon Coal Zone (zone 2), contain sandstones with approximate S_w values of 87%, while sandstones in the upper two zones, Upper Sandstone (zone 3) and Paonia Shale Member (zone 4), contain S_w values of 88% and 86%, respectively. Not much water saturation fluctuation takes place between sandstones in the Lower Williams Fork Formation and the Middle Williams Fork (86% S_w), however, an increase in water saturation does take place transitioning from the Middle Williams Fork to the Upper Williams Fork (89% S_w). Related to bulk volume water, on average, sandstones in the Lower Williams Fork Formation vary from 0.04-0.05 BVW, while sandstones in the Middle Williams Fork and Upper Williams Fork represent BVW values of 0.03-0.04. Faults factored into the enhanced permeability model that structurally cut through zones 2-6 are regionally fixated in the eastern portion of the study area. Throughout

the fault-enhanced permeability model, permeability values along the faults saw an increase in value, in some cases to ~550 µD (Figure 31). In summary, on average, Williams Fork Formation sandstones within the study area 1) contain total porosity, effective porosity, permeability, water saturation, and bulk volume water values of 10%, 6%, 7 µD, 87%, and 0.04 , respectively, and 2) comprise petrophysical properties that do not vary much stratigraphically, yet still reflect trends that suggest a slight elevation in reservoir quality within the lower two-thirds of the Williams Fork Formation, in comparison to the Upper Williams Fork.

Within the study area, 40% of the Williams Fork Formation is composed of reservoir pay sandstone (Figure 26). While the thickest reservoir pay is in the central southeastern portion of the study area, throughout the Williams Fork Formation, reservoir pay sandstones vary in thickness from ~700-1100 ft (213-335 m), averaging around 1000 ft (304 m) (Figure 26). Contributing the thickest reservoir pay deposits (~350-550 ft) (106-167 m) of the Williams Fork Formation, the Lower Williams Fork Formation (zones 1-4) is composed of 38% reservoir pay, while 42% of the Middle Williams fork (zone 5) and 22% of the Upper Williams Fork (zone 6) is composed of evenly dispersed reservoir pay sandstone deposits ~(300-400 ft) (91-121 m) thick (Figure 27). Within the Lower Williams Fork Formation (zones 1-4), 33% of zone 1, 44% of zone 2, 49% of zone 3, and 32% of zone 4 is composed reservoir pay sandstones (Figure 28). After criteria were applied to sandstones to define reservoir pay within the study area (*see methods*), the petrophysical properties associated with reservoir pay were analyzed.

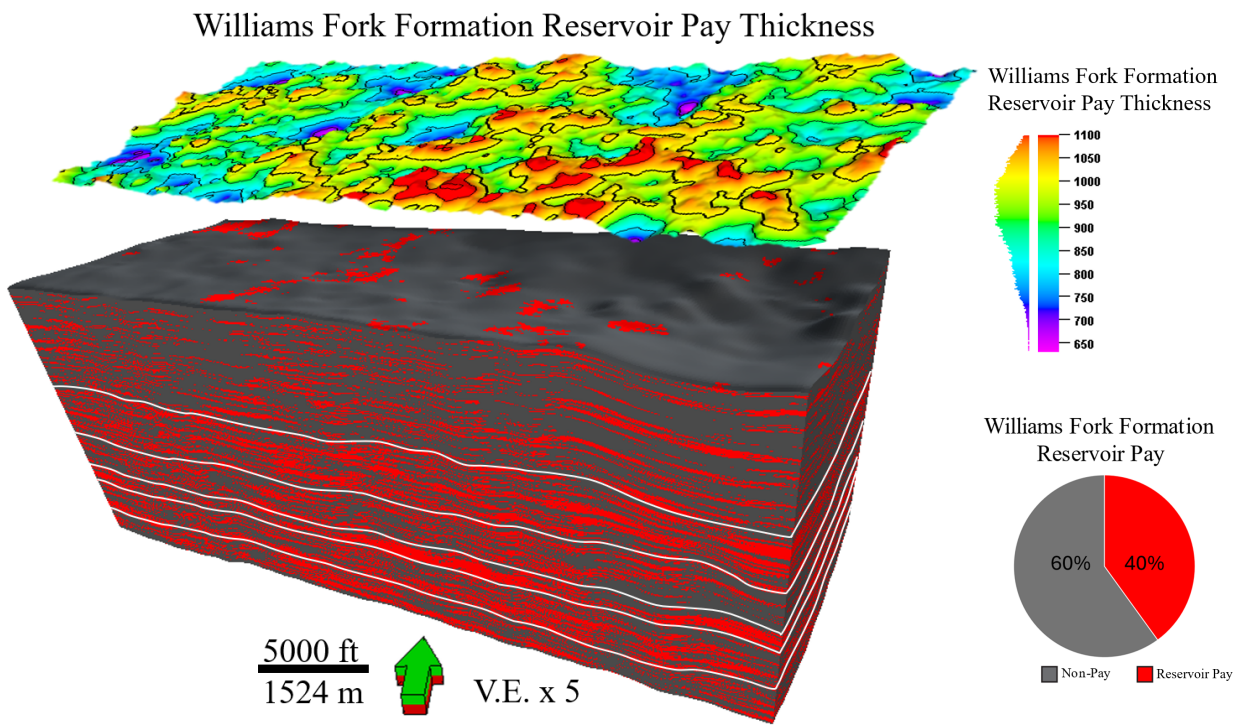

Figure 26: 3D reservoir pay sandstone model of the Williams Fork Formation. On average, 40 % of the entire Williams Fork Formation within the study area is composed of reservoir pay sandstone, while the thickest reservoir pay deposits are located to the central southeast of the study area. Throughout the Williams Fork Formation, reservoir pay sandstone deposits vary in thickness from ~700-1100 ft (213-335 m), averaging around 1000 ft (304 m).

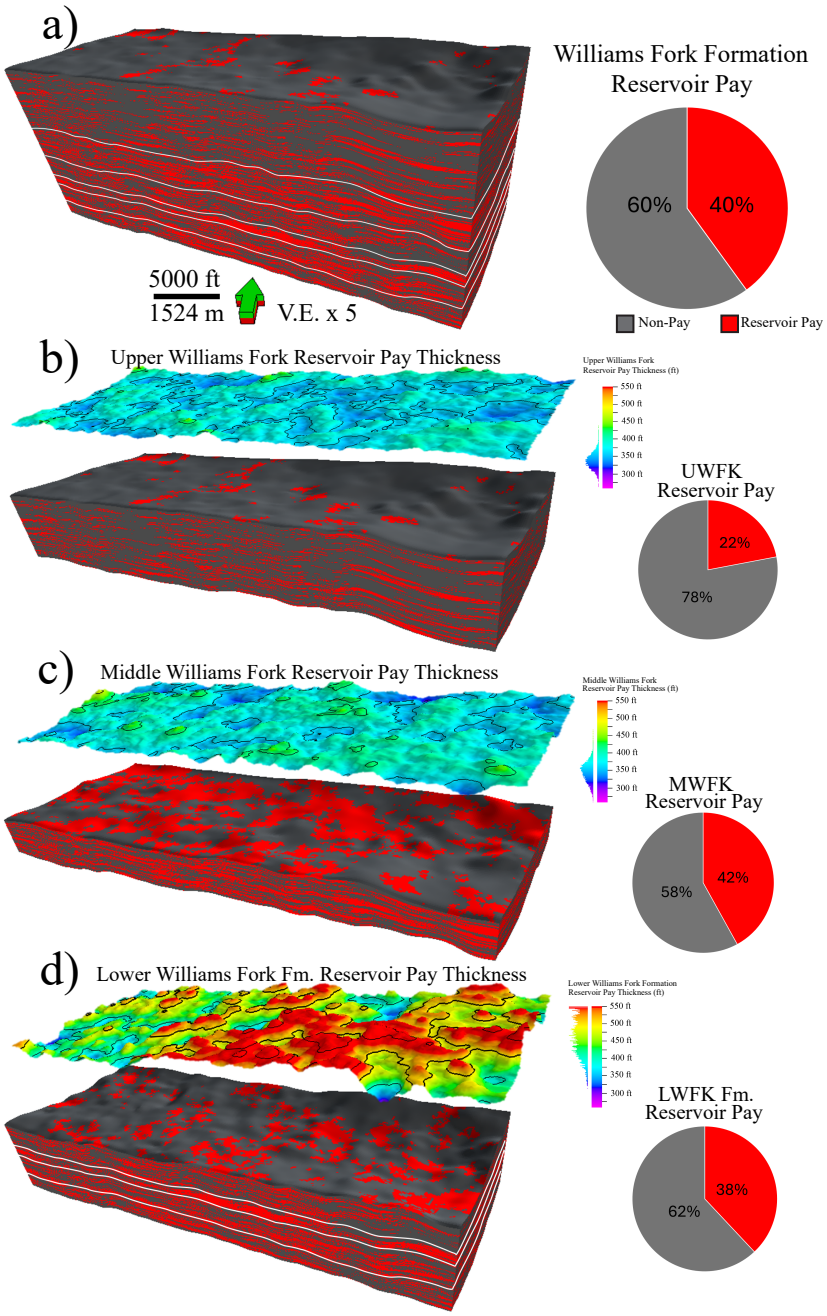

Figure 27: Model zones and associated reservoir pay thickness maps depicting the distribution of reservoir pay sandstone within the Williams Fork Formation within the study area. **a)** 3D reservoir pay sandstone of the Williams Fork Formation. On average, 40 % of the entire Williams Fork Formation within the study area is composed of reservoir pay sandstone. **b)** The Upper Williams Fork (zone 6) is composed of 22% reservoir pay deposits, evenly dispersed, that range in thickness from ~ (300-375 ft) (91-114 m). **c)** The Middle Williams Fork (zone 5) is composed of 42% reservoir pay deposits, evenly dispersed, that range in thickness from ~ (300-400 ft) (91-121 m). **d)** The Lower Williams Fork Formation (zones 1-4) is composed of 38% reservoir pay deposits, focused in the central-southeast, that range in thickness from ~ (350-550 ft) (106-167 m).

Lower Williams Fork Formation Reservoir Pay

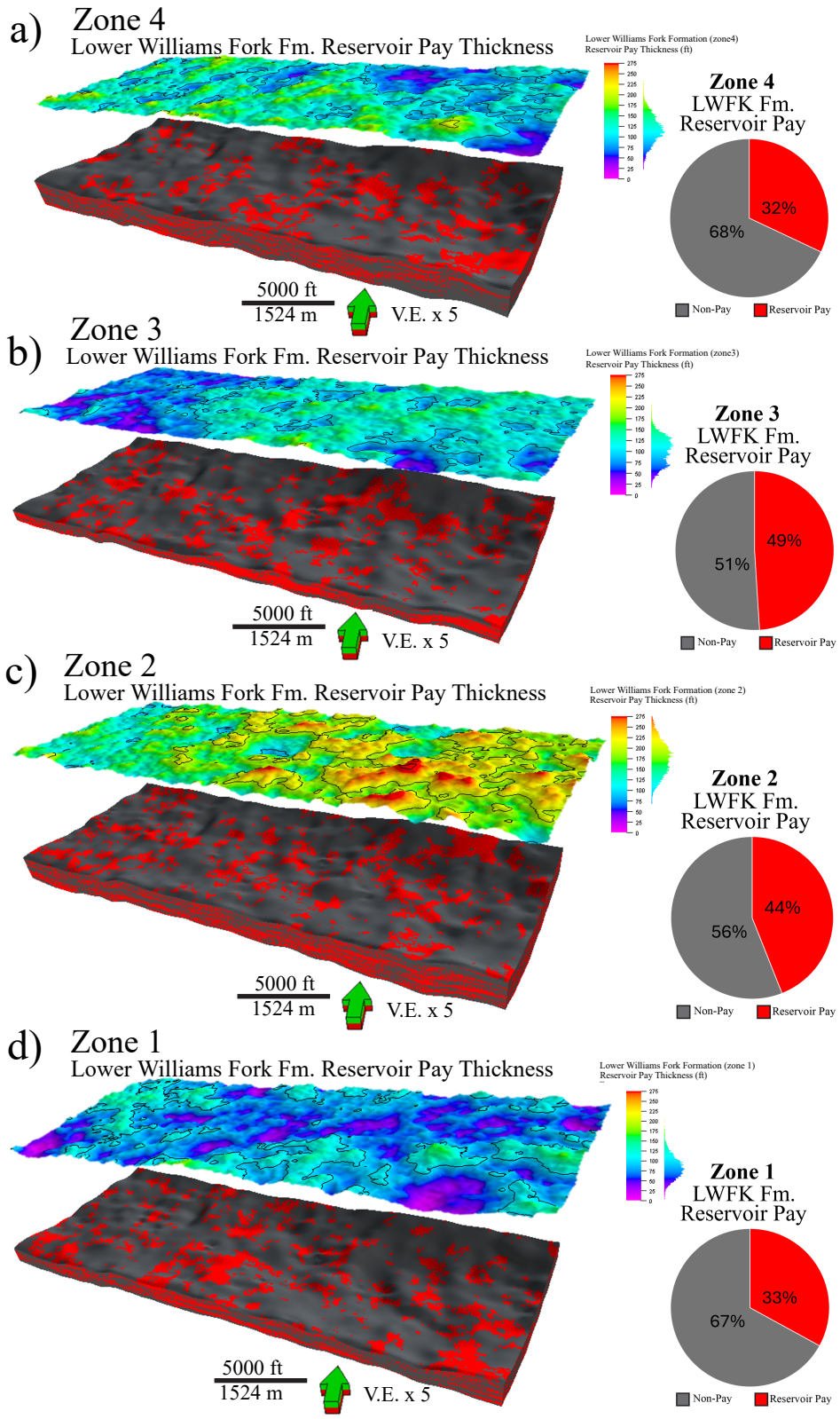

Figure 28: Model zones and associated reservoir pay thickness maps depicting the distribution of reservoir pay sandstone within the Lower Williams Fork Formation within the study area. **a)** The Paonia Shale Member (zone 4) is composed of 32% reservoir pay sandstone, thickening from the northeast to the south and southwest, that range in thickness from ~ (20-240 ft) (6-73 m), averaging 120 ft (36 m) thick. **b)** The Upper Sandstone (zone 3) is composed of 49% reservoir pay sandstone, focused in the central-southeast, that range in thickness from ~ (10-210 ft) (3-64 m), averaging 100 ft (30 m) thick. **c)** The Middle Sandstone/ South Canyon Coal Zone (zone 2) is composed of 44% reservoir pay sandstone, focused in the central-southeast, that range in thickness from ~ (60-330 ft) (18-100 m), averaging 180 ft (54 m) thick. **d)** The Cameo-Wheeler Coal Zone (zone 1) is composed of 33% reservoir pay sandstone, thickening radially to the northwest and southeast from the thinner centralized region of the study area, that range in thickness from ~ (2-225 ft) (0.5-68 m), averaging 80 ft (24 m) thick.

Although at a broad scale the same range in values of total porosity (5-15%), effective porosity (1-8%), and permeability (0.7-10 µD) previously defined for sandstone still apply for reservoir pay, on average, the majority of reservoir pay sandstone within the study area represents total porosity, effective porosity, and permeability values of ~9-11%, ~3-4%, and ~7-20 µD, respectively. In alignment with previous trends, general ranges associated with these petrophysical properties do not vary stratigraphically, however, the average values of each do vary slightly depending on zone. Consistent with previously mentioned trends, just slightly less in value, on average, reservoir pay sandstones within the Cameo-Wheeler Coal Zone (zone 1) exhibit the highest total porosity (11%), effective porosity (4%), and permeability values (20 µD) within the Lower Williams Fork Formation, but also throughout the entire Williams Fork Formation. Within the remaining three zones (zones 2-4) of the Lower Williams Fork Formation, the average total porosity (9-10%), effective porosity (3-4%), and permeability values (10 µD) exhibited within reservoir pay sandstones are roughly the same or higher in comparison to that of the Middle Williams Fork (9% total porosity, 3% effective porosity, 7 µD permeability), and Upper Williams Fork (10% total porosity, 3% effective porosity, 7 µD permeability). Similarly, trends exhibited within sandstones regarding water saturation also applied to reservoir pay sandstones at a reduced value such that the bottom two zones of the Lower Williams Fork Formation, the Cameo-Wheeler Coal Zone (zone 1) and Middle Sandstone/South Canyon Coal Zone (zone 2), contain reservoir pay sandstones with approximate S_w values of 85%, while reservoir pay sandstones in the upper two zones, Upper Sandstone (zone 3) and Paonia Shale Member (zone 4) contain S_w values of 87% and 83%, respectively. Not much water saturation fluctuation takes place between reservoir pay sandstones in the Lower Williams Fork Formation and the Middle Williams Fork (84% S_w), however, an increase in water saturation does take place transitioning from the Middle Williams Fork to the

Upper Williams Fork (87% S_w). Related to bulk volume water, reservoir pay sandstones contain a range in BVW of (0.01-0.05) but most average ~0.03 BVW throughout all six zones of the Williams Fork Formation at Mamm Creek Field. Permeability values associated with reservoir pay as a result of the fault-enhanced permeability model reflected similar trends as previously stated, equating to an increase in permeability along the faults, in some cases to ~550 μD (Figure 31b). In summary, most Williams Fork Formation reservoir pay sandstones within the study area 1) contain total porosity, effective porosity, permeability, water saturation, and bulk volume water values of approximately 9%, 3%, 10 μD, 85%, and 0.03 respectively, and 2) comprise petrophysical properties that do not vary much stratigraphically, yet still reflect trends that suggest a slight elevation in reservoir quality within the lower two-thirds of the Williams Fork Formation, in comparison to the Upper Williams Fork.

DISCUSSION

Lithologies and Petrophysical Properties

When analyzed together, log properties and petrophysical characteristics offer valuable insights and potential reservoir implications associated with each lithology. Resistivity, for example, can give insights into porosity and fluid content of a rock, while total and effective porosity can help delineate the amount of storage space a rock has, and how interconnected the pores are. When paired with water saturation and bulk volume water, one can further explore reservoir quality by delineating how much of the open pore space is consumed by water, and how much storage space is left for storing potential hydrocarbons. Essential to the assessment of tight-gas reservoirs such as the Williams Fork Formation sandstone, permeability then helps us assess fluid flow capability within a rock, and therefore determine reservoir production potential.

Williams Fork Formation Sandstones:

While the cleanest sandstones represent a gamma ray of 38 API, paired average readings of 60 API and 20% shale (V_{sh}) suggest a moderate level of shale content within sandstones throughout the study area. Since higher shale content (denoted by higher API and V_{sh} % values) can affect the overall porosity and restrict fluid flow, reservoir quality of tight-gas sandstones throughout the Williams Fork Formation can be impacted regarding gas storage and flow as a result of higher shale content. Commonly used to indicate the presence of gas, the NPHI and DPHI crossover (gas-effect) frequently associated with most sandstones throughout the study area helps assess gas saturation and evaluate the potential productivity of the reservoir. Although it's a critical indicator between gas and water bearing zones, if the crossover is not significant, the presence of gas-effect in sandstones may also just indicate non-producible gas vapor. Since higher resistivity often suggests lower salinity fluid content (less water saturation), the moderate sandstone resistivity range of 40-50 ohmm indicates that they could potentially hold hydrocarbon. Porosity values in unconventional reservoirs typically range from 2-10% (Satter and Iqbal, 2016). Since the tight-gas sandstones of the Williams Fork Formation are unconventional reservoirs, their average effective porosity of 6% is conducive for hydrocarbon storage. Although the average water saturation in Williams Fork Formation sandstones is relatively high (S_w =87%), when multiplied by the low effective porosity values, the resulting bulk volume water BVW of ~0.04 further suggests favorable conditions for hydrocarbon presence. On average, most tight sandstone within the study area contains permeability values of 7 µD. Although reservoir pay sandstone within the study area exhibits a higher average permeability of 10 µD, hydraulic fracture stimulation is still necessary to enhance permeability enough for production. In addition to higher permeability values, the reservoir quality of Williams Fork Formation reservoir pay sandstone is also reflected

by its lower water saturation ~ (80%), and bulk volume water ~ (0.03) values (presents more favorable conditions for hydrocarbon presence). To further analyze the relationship between sandstone and reservoir pay sandstone within the Williams Fork Formation (within the study area), the vertical proportion curves of lithology (from the 3D lithology model) and reservoir pay (from the 3D reservoir pay model) were visually compared (Figure 29). The close alignment between sandstone (in the 3D lithology model's vertical proportion curve) and reservoir pay sandstone (in the 3D reservoir pay model's vertical proportion curve) demonstrates that most of the Williams Fork Formation sandstone in the study area consists of reservoir pay (Figure 29).

Williams Fork Formation Shales:

Reflected by their lower resistivity, and higher water saturation and bulk volume water values, shales within the Williams Fork formation at Mamm Creek are likely water saturated. Shales often retain water due to capillary forces, which can occupy the pore spaces. This high water saturation reduces the volume of pore space available for hydrocarbons, contributing to its lower effective porosity of ~0.2-3%.

Williams Fork Formation Coals:

Due to their high carbon content, low water saturation, complex pore structure, and organic material composition, Williams Fork Formation coals exhibit extremely high resistivity and effective porosity readings, and low readings of bulk volume water. Although they have high hydrocarbon content, the producibility of coal depends on its permeability and presence of fractures. The costs associated with coal extraction can be significant, particularly in regions with challenging geology such as the Piceance Basin and therefore usually makes production unprofitable.

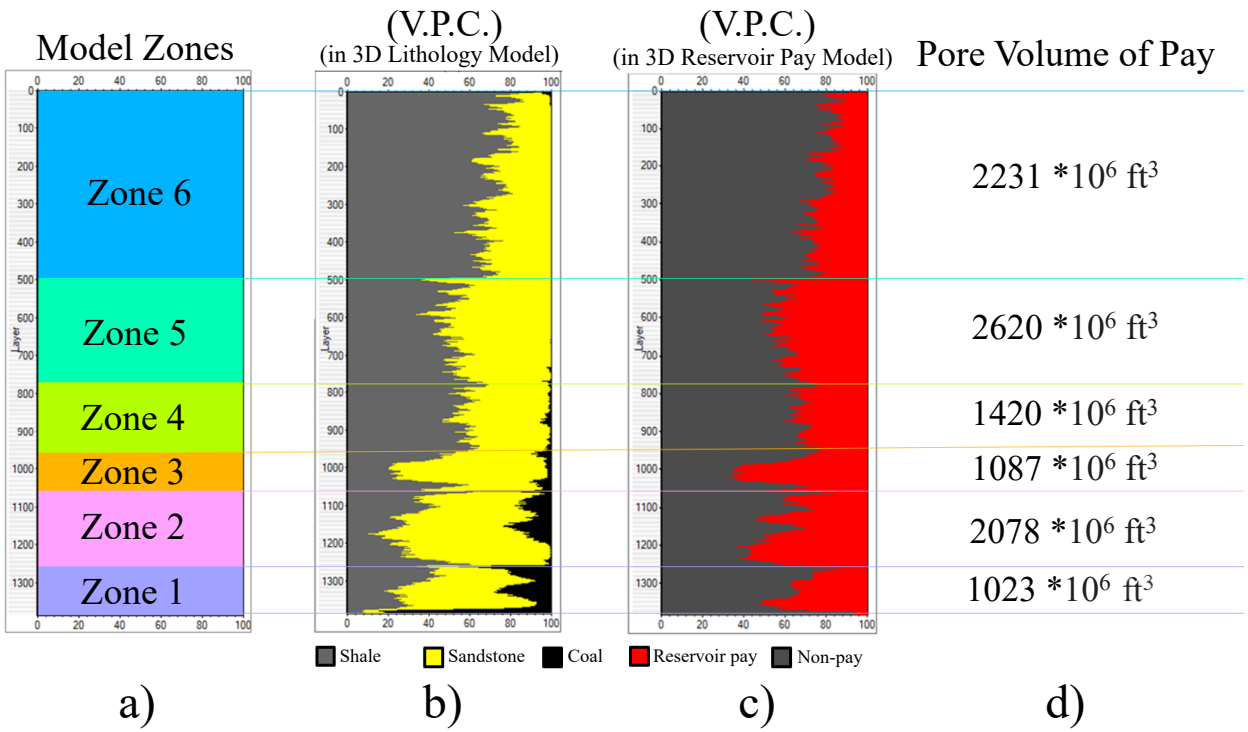

Figure 29: Per **a)** each zone within the stratigraphic modeling interval, a visual comparison between the **b)** vertical proportion curve of lithology (within the 3D lithology model), **c)** vertical proportion curve of reservoir pay sandstone (within the 3D reservoir pay model), and **d)** pore volume of pay depicts several stratigraphic trends. The strong conformance between sandstone (yellow) within the **b)** 3D lithology model's vertical proportion curve and reservoir pay sandstone (red) within the **c)** 3D reservoir pay model's vertical proportion curve demonstrates that most of the Williams Fork Formation sandstone in the study area consists of reservoir pay. In addition, throughout the modeling interval, the variation in magnitude of those trends varies stratigraphically such that the majority of reservoir pay sandstone exists in the lower three zones of the Lower Williams Fork Formation, followed by the Middle Williams Fork, while the Upper Williams Fork is the lowest pay contributor. The **d)** pore volume of pay also displays a higher cumulative pore volume contribution from the Lower Williams Fork Formation and Middle Williams Fork compared to the Upper Williams Fork.

Depositional Environment Implications

Based upon lithology (Figure 19), zones within the Williams Fork Formation are representative of three main depositional environments. Dominated by laterally extensive coals, the two lowermost zones of the Lower Williams Fork Formation (zones 1 and 2) are representative of a swamp environment of deposition (Figure 19e) (Hettinger and Kirschbaum, 2002, 2003; Shaak, 2010). Moving stratigraphically upward, the upper two zones of the Lower Williams Fork Formation (zones 3 and 4) represent a depositional transition from swamp to coastal plain as represented by fewer coal deposits and a higher proportion of fluvial sandstones (Figure 19d) (Hettinger and Kirschbaum, 2002, 2003; Shaak, 2010). From the upper two zones of the Lower Williams Fork Formation (zones 3-4) to Middle Williams Fork (zone 5), a transition from coastal plain to alluvial plain settings is reflected by a greater proportion of sandstones as compared to the Lower Williams Fork Formation with more laterally extensive coals (Figure 19c) (Hettinger and Kirschbaum, 2002, 2003; Patterson et al., 2003; Foster, 2010). Transitioning from the Middle to Upper Williams Fork (zone 6), the shale percentage increases relative to sandstone, yet still representing an alluvial plain setting (Figure 19b) (Hettinger and Kirschbaum, 2002, 2003; Patterson et al., 2003; Foster, 2010).

Spatial Distribution of Reservoir Properties and Reservoir Pay Sandstone

Although the range and mean values of petrophysical properties do not vary significantly stratigraphically, they do relate to each other in various ways. Depicted in (Figure 30), the 3D permeability model derived from core data suggests matrix permeability is positively correlated with total and effective porosity. In addition to these relationships, zones 1-5 contain a higher concentration of reservoir pay sandstone (and associated petrophysical properties within them) in comparison to the Upper Williams Fork (Figure 30). Depicting this trend further, the magnitude

of lithology and reservoir pay sandstone varies stratigraphically such that 1) the majority of reservoir pay sandstone exists in the lower three zones of the Lower Williams Fork Formation, 2) the Middle Williams Fork contains the second highest concentration of reservoir pay sandstone, and 3) the Upper Williams Fork is the lowest pay contributor (Figure 29). The pore volume of pay also displays a higher cumulative pore volume contribution from the Lower Williams Fork Formation and Middle Williams Fork in comparison to the Upper Williams Fork (Figure 29). Further analysis comparing formation thickness, sandstone thickness, and pay thickness within each zone of the Williams Fork Formation revealed a positive correlation between the thickest regions of each zone and the thickest sandstone and reservoir pay deposits (Figure 16). This suggests that reservoir pay in the Williams Fork is primarily composed of thick, laterally extensive sandstones. Further, while the majority of reservoir pay is confined within the lower two-thirds of the Williams Fork Formation (Lower Williams Fork Formation and Middle Williams Fork), the Lower Williams Fork Formation (zones 1-4) contains the thickest reservoir pay deposits, focused in the central-southeast portion of the study area, that range in thickness from ~350-550 ft (106-167 m) (Figure 27d). A visual representation of the stratigraphic variability of Williams Fork Formation reservoir pay sandstone within the study area is depicted in Figure 29c.

Fault-Enhanced Permeability

Faults interpreted by (Baytok, 2010) were applied to the 3D permeability model as conduits to flow. This approach aimed to assess the potential positive impact of faults on permeability within the study area (in the absence of production data). Increasing permeability along faults, in some cases as high as ~550 µD, faults within the study area positively correlate with areas of highest reservoir quality (Figure 31b).

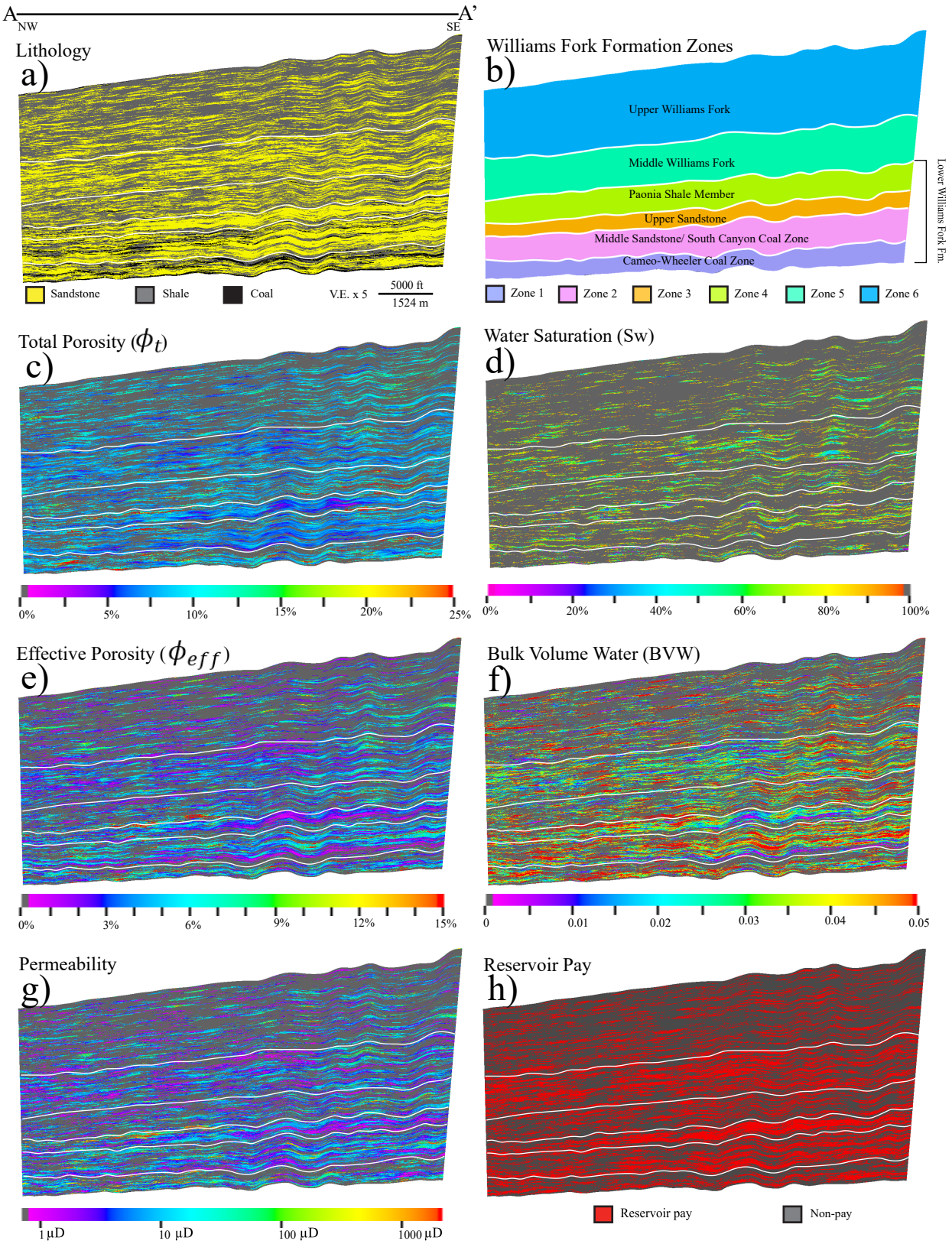
A
NW
A'
SE
Lithology
a)
Sandstone
Shale
Coal
V.E. x 5
5000 ft
1524 m
Williams Fork Formation Zones
b)
Upper Williams Fork
Middle Williams Fork
Paonia Shale Member
Upper Sandstone
Middle Sandstone/ South Canyon Coal Zone
Cameo-Wheeler Coal Zone
Lower Williams Fork Fm.
Zone 1
Zone 2
Zone 3
Zone 4
Zone 5
Zone 6
Total Porosity (ϕ_t)
c)
0%
5%
10%
15%
20%
25%
Water Saturation (Sw)
d)
0%
20%
40%
60%
80%
100%
Effective Porosity (ϕ_{eff})
e)
0%
3%
6%
9%
12%
15%
Bulk Volume Water (BVW)
f)
0
0.01
0.02
0.03
0.04
0.05
Permeability
g)
1 µD
10 µD
100 µD
1000 µD
Reservoir Pay
h)
Reservoir pay
Non-pay

Figure 30: Cross-sectional slices along A-A' (approximate location of cross section displayed in (Figure 8b)) depicting 3D **a)** lithology, **b)** zones within the model grid, **c)** total porosity, **d)** water saturation, **e)** effective porosity, **f)** bulk volume water, **g)** permeability, and **h)** reservoir pay modeling results for comparison purposes. The 3D permeability model derived from core data suggests matrix permeability is positively correlated with total and effective porosity. Although the range and mean values of petrophysical properties do not vary significantly stratigraphically, the magnitude of lithology, reservoir pay, and associated petrophysical properties are highly variable stratigraphically.

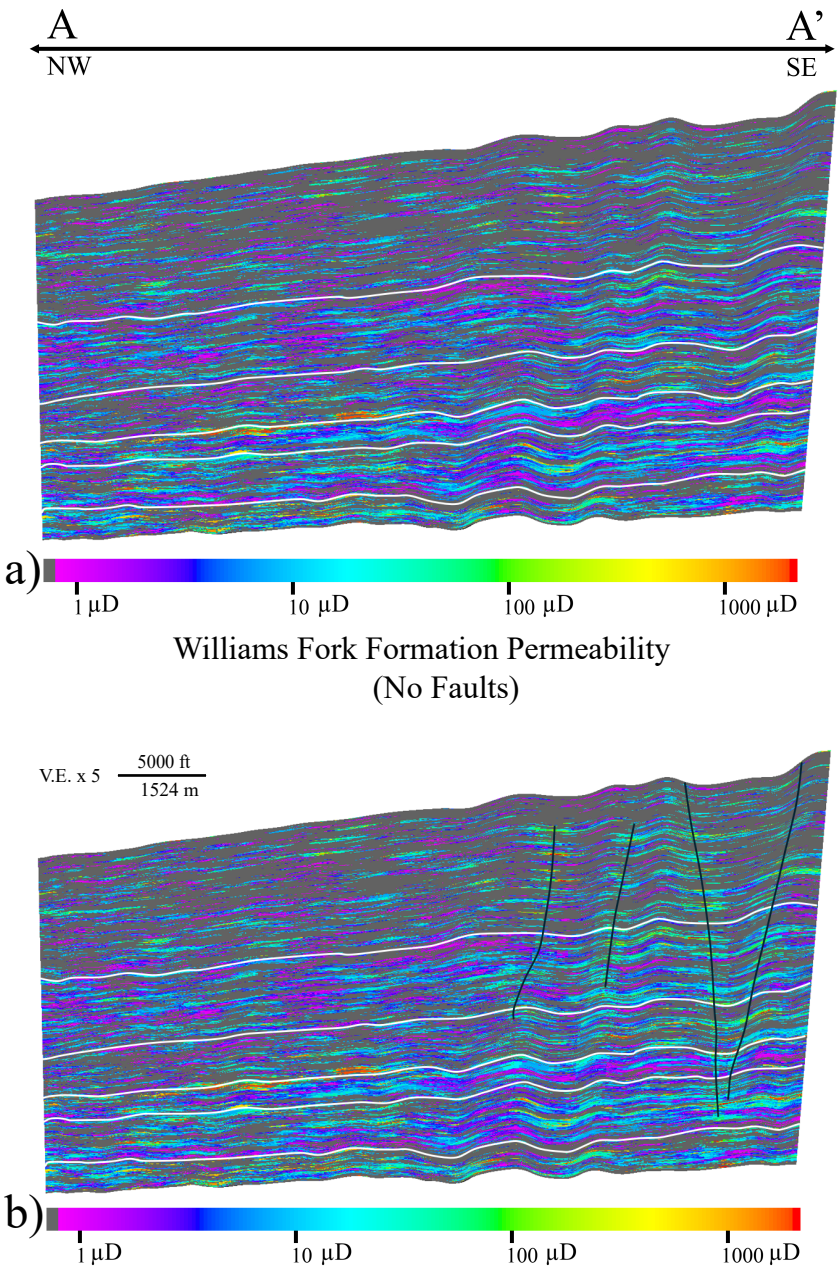

Figure 31: A comparison of the **a)** original Williams Fork Formation 3D permeability model (no faults incorporated) and **b)** fault-enhanced 3D permeability model (incorporating a select group of quality-checked faults interpreted by Baytok (2010)) in cross-sectional view along A-A'. (See Figure 8b for approximate location of A-A'). Increasing permeability along faults, in some cases as high as ~550 µD, faults within the study area positively correlate with areas of highest reservoir quality. See Appendix M for an additional comparison between the original Williams Fork Formation 3D permeability model and fault-enhanced 3D permeability model (incorporating all faults interpreted by Baytok (2010)).

Additionally, the two main grabens included in the permeability model cut through the same southeastern region of the study area that contains the thickest reservoir pay deposits which may explain why reservoir pay (and therefore reservoir quality) within that region is favorable. Although one might expect fracture intensity or fracture density to be higher near the faults (as demonstrated throughout this fault-enhanced permeability modeling process), from a practical standpoint since these are tight-gas sandstones, hydraulic fracture stimulation is still necessary to sufficiently enhance permeability enough to produce the pay zones.

Limitations

One of the main goals of this study was to yield a seismically constrained 3D lithology model (and therefore all associated 3D petrophysical models biased to it as well). To accomplish this, a lithological relationship needed to be established between the well logs and seismic. Although a relationship between wells (total porosity logs) and seismic (3D sweetness attribute volume) was established, it was not much of a linear relationship, but instead rather flat (meaning there were multiple sweetness values for the same porosity because of overlap). To address the lithological overlap, polygons were drawn dynamically on at-well-location cross plots to better refine and distinguish each lithology. The intended goal of the polygons was to take the relationship between well-log-based porosity (total porosity logs), well-log-based lithology (lithology logs), and sweetness (extracted at the well locations), and assign/ propagate it to the rest of the 3D sweetness attribute volume. However, when trying to assign the relationship to the 3D sweetness attribute volume, it was only propagating at each well location. To address this, the at-well-location relationship polygons were applied to a cross plot between a 3D model of total porosity (not biased to lithology) (Appendix F) and the 3D sweetness attribute volume (Appendix D). An additional way seismic was incorporated into the modeling process involves faults

interpreted previously by Baytok, 2010. Throughout their work, Baytok (2010) employed Ant-track attribute volumes to identify faults and fractures and used interpreted FMI logs to identify fracture orientations and types, generating fracture-intensity logs to correlate fractures with lithology. Although Ant-tracking fault interpretation is an accelerated fault extraction technique that can help reduce bias when picking faults, newer fault interpretation workflows including 1) machine learning, 2) deep learning convolutional neural networks (CNNs), and 3) nearest neighbor learning and principal component analysis, could be beneficial to apply to faults within this study. Additionally, since this study was conducted in the absence of production data, the faults that were incorporated into the fault-enhanced permeability models were applied as conduits to flow. Although this approach was used to qualitatively assess the potential positive impact of faults on permeability within the study area, production data would help improve the accuracy of the fault-enhanced permeability models. Furthermore, because the faults were incorporated in the absence of production data, values associated with the permeability multiplier model were set to values of 1, 2, and 5 based on visual analysis of the "inverse-fault-distance" model, however, production data would also aid in the selection of these values.

CONCLUSION

In conclusion, the Upper Cretaceous Williams Fork Formation of the Mesaverde Group within the Piceance Basin at Mamm Creek Field consists of 6 zones that are composed of tight-gas sandstone, shale, and coal deposits. From base to top, these zones include the Lower Williams Fork Formation including 1) Cameo-Wheeler Coal Zone, 2) Middle Sandstone/South Canyon Coal Zone, 3) Upper Sandstone, and 4) Paonia Shale Member, and the 5) Middle Williams Fork, and 6) Upper Williams Fork. Of the sandstone present, reservoir pay sandstone composes 40% of the Williams Fork Formation within the study area. Although at a broad scale the same range in values

of total porosity (5-15%), effective porosity (1-8%), and permeability (0.7-10 µD) previously defined for sandstone still apply for reservoir pay, on average, the majority of reservoir pay sandstone within the study area represents total porosity, effective porosity, and permeability values of ~9-11%, ~3-4%, and ~7-20 µD, respectively. Related to water saturation and bulk volume water, most reservoir pay sandstones within the study area also reflect ~50-85% (avg. ~80% Sw), and ~0.01-0.05 (avg. ~0.03). In alignment with previous trends, general ranges associated with these petrophysical properties do not vary stratigraphically. Although the range and mean values of petrophysical properties do not vary significantly stratigraphically, lithology, reservoir pay, and pore volume are highly variable stratigraphically. The two lowermost zones of the Lower Williams Fork Formation (zones 1-2) are dominated by coal zones that are laterally extensive. Moving stratigraphically upward into the upper two zones of the Lower Williams Fork Formation (zones 3-4), a depositional transition from swamp to coastal plain deposits takes place as represented by fewer coal deposits and a higher proportion of fluvial sandstones. From the upper two zones of the Lower Williams Fork Formation (zones 3-4) to Middle Williams Fork (zone 5), a transition from coastal plain to alluvial plain settings is reflected by a greater proportion of sandstones as compared to the Lower Williams Fork Formation with more laterally extensive coals. The majority of reservoir pay is confined within the lower two-thirds of the Williams Fork Formation (Lower Williams Fork Formation and Middle Williams Fork). Of the two major reservoir pay contributors, the Lower Williams Fork Formation (zones 1-4) contains the thickest reservoir pay deposits, focused in the central-southeast portion of the study area, that range in thickness from ~350-550 ft (106-167 m). Transitioning from the Middle to Upper Williams Fork (zone 6), the shale percentage increases relative to sandstone while still representing an alluvial plain setting. Core data suggest that matrix permeability is positively correlated with total and

effective porosity. 3D reservoir models of lithology, effective porosity, and other petrophysical properties illustrate the stratigraphic and petrophysical controls on high reservoir quality sandstones that form natural gas reservoirs. This detailed characterization of reservoir distribution and quality provides a practical framework for field development optimization and a predictive understanding of stratigraphic and petrophysical controls on reservoir quality in tight-gas sandstone systems. These insights can guide well placement, completion design, and exploration strategies in similar tight-gas reservoirs throughout the region.

REFERENCES

Archie, G. E., 1952, Classification of carbonate reservoir rocks and petrophysical considerations: AAPG Bulletin, vol. 36, no. 2, p. 218–298.

Asquith, G. B., & Gibson, C. R., 1982, Basic well log analysis for geologists: American Association of Petroleum Geologists, vol. 3.

Baytok, S., 2010, Seismic investigation and attribute analysis of faults and fractures within a tight-gas sandstone reservoir: Williams Fork Formation, Mamm Creek Field, Piceance Basin, Colorado: MS thesis, University of Colorado, Boulder, CO. 243 p.

Baytok, S., and M. J. Pranter, 2013, Fault and fracture distribution within a tight-gas sandstone reservoir: Mesaverde Group, Mamm Creek Field, Piceance Basin, Colorado, U.S.A., Petroleum Geoscience, vol. 19, p. 203-222.

Blakey, R. C., 2010, Paleogeographic and Paleotectonic Maps-Use, Construction, Interpretation, and Example, RMAG Short Course CD, January 28, 2010.

Burger, B., 2007, A new Late Paleocene Vertebrate Fauna from the Ohio Creek Formation of Western Colorado: Mountain Geologist, vol. 44.

Carroll, C. J., E. Robeck, G. Hunt, and W. Koontz, 2004, Structural implications of underground coal mining in the Mesaverde Group in the Somerset coal field, Delta and Gunnison counties, Colorado; field trips in the southern Rocky Mountains, USA. GSA Field Guide, 5, p. 41-58.

Cole, R.D., and S.P. Cumella, 2003, Stratigraphic architecture and reservoir characteristics of the Mesaverde Group, southern Piceance Basin, Colorado, in K. M. Peterson, T. M. Olson, and D. S. Anderson eds., Piceance Basin 2003 guidebook: RMAG, p. 385-442.

Cole, R.D., and S.P. Cumella, 2005, Sand-body architecture in the lower Williams Fork Formation (Upper Cretaceous), Coal Canyon, Colorado, with comparison to the Piceance Basin subsurface; Cretaceous sand body geometries in the Piceance Basin area of northwest Colorado: The Mountain Geologist, v. 42, p. 85-107.

Cole, R. D., and M. J. Pranter, 2008, Stratigraphic variability of sandstone-body dimensions in the Williams Fork Formation: outcrop data from the southwest Piceance Basin, Colorado, AAPG Rocky Mountain Section Convention, Denver, Colorado, 15 p.

Collins, B. A., 1976, Coal deposits of the Carbondale, Grand Hogback, and southern Danforth Hills coal fields, eastern Piceance basin, Colorado: Quarterly of the Colorado School of Mines, v. 71, no. 1, 138 p.

Cumella, Stephen P. and Ostby, Douglas B, 2003, Geology of the Basin-Centered Gas Accumulation. In Piceance Basin Guidebook :Rocky Mountain Association of Geologists. p. 29.

Foster, Renee M., 2010, Sequence Stratigraphy of the Upper Cretaceous Middle Williams Fork Formation, Piceance Basin, Northwestern Colorado: Implications for Reservoir Sandstones: MS thesis, University of Colorado, Boulder, CO. 263 p.

Grose, L. T., 1972, Tectonics: Geologic Atlas of the Rocky Mountain Region: RMAG, p. 35-44.

Hettinger, R.D., and Kirschbaum, M.A., 1998, Stratigraphy and depositional environments of the Late Campanian coal-bearing Neslen/Mount Garfield Formations, eastern Book Cliffs, Utah and Colorado: U.S. Geological Survey Open-File Report 98-43, 1 sheet.

Hettinger, R.D., and M.A. Kirschbaum, 2002, Stratigraphy of the Upper Cretaceous Mancos Shale (upper part) and Mesaverde Group in the southern part of the Uinta and Piceance basins, Utah and Colorado: Report I-2764, 21 p.

Hettinger, R.D., M.A. Kirschbaum, and U. S. Geological Survey, Uinta- Piceance Assessment Team, United States, compiler (USA), 2003, Stratigraphy of the Upper Cretaceous Mancos Shale (upper part) and Mesaverde Group in the southern part of the Uinta and Piceance Basins, Utah and Colorado; Petroleum systems and geologic assessment of oil and gas in the Uinta-Piceance Province, Utah and Colorado: Report DDS-0069-B, 21 p.

Hettinger, R.D., L.N.R. Roberts, and T.A. Gognat, 2000, Investigations of the distribution and resources of coal in the southern part of the Piceance Basin, Colorado, Chapter O of Kirschbaum, M.A., Roberts, L.N.R., and Biewick, L.R.H., eds., Geologic assessment of coal in the Colorado Plateau—Arizona, Colorado, New Mexico, and Utah: U.S. Geological Survey Professional Paper 1625–B, 61 p.

Hewlett, Alicia C., 2010, Fluvial Architecture and Static Connectivity of the Williams Fork Formation, Central Mamm Creek Field, Piceance Basin, Colorado: MS thesis, University of Colorado. 228 p.

Hoak, T.E. & Klawitter, A.L, 1997, Prediction of fractured reservoir production trends and compartmentalization using an integrated analysis of basement structures in the Piceance basin, western Colorado. In: Hoak, T.E., Klawitter, A.L. & Blomquist, P.K. (eds) Fractured Reservoirs: Characterization and Modeling. Rocky Mountain Association of Geologists, Denver, CO, p. 67–102.

Johnson, R.C., 1989, Geological History and Hydrocarbon Potential of Late Cretaceous-Age, Low-permeability Reservoirs, Piceance Basin, Western Colorado (29A Economic Geology, Geology of Energy Sources; 06A Sedimentary Petrology; 12 Stratigraphy No. B 1787-E). United States Geological Survey, Reston, VA.

Johnson, R.C. & Flores, R.M., 2003, History of the Piceance Basin from latest Cretaceous through early Eocene and the characterization of lower Tertiary sandstone reservoirs. In: Peterson, K.M., Olson, T.M. & Anderson, D.S. (eds) Piceance Basin 2003 Guidebook. Rocky Mountain Association of Geologists, Denver, CO, 21–61.

Johnson, R.C. & May, F., 1980, A study of the Cretaceous-Tertiary unconformity in the Piceance Basin, Colorado – The underlying Ohio Creek Formation (Upper Cretaceous) redefined as a member of the Hunter Canyon or Mesaverde Formation. United States Geological Survey Bulletin, 1482–B.

Johnson, R. C., and S. B. Roberts, 2003, The Mesaverde total petroleum system, Uinta-Piceance province, Utah and Colorado (Chapter 7), in Petroleum Systems and geologic assessment of oil and gas in the Uinta-Piceance province, Utah and Colorado: USGS Digital Data Series DDS-69-B, 68 p.

Keeton, G. I., M. J. Pranter, R. D. Cole, and E. R. Gustason, 2015, Stratigraphic architecture of fluvial deposits from borehole images, spectral-gamma-ray response, and outcrop analogs, Piceance Basin, Colorado, AAPG Bulletin, vol. 99, no. 10, p. 1929-1956.

Kuuskraa, V.A., D. Decker, and H.B. Lynn, 1997 Optimizing technologies for detecting natural fractures in the tight sands of the Rulison Field, Piceance Basin: Proceedings of the Natural Gas Conference Emerging Technologies for the Natural Gas Industry, paper NG6-3, 29 p. 24

Kuuskraa, V. A., D. Campagna, and D. Decker, 1997, Application of high fold, multi-azimuth 3-D P-wave seismic to characterize natural fractures in the Rulison Field, Piceance Basin. In E. B. Coalson, J. C. Osmond & E. T. Williams (Eds.), Innovative applications of petroleum technology in the rocky mountain area (). United States (USA): Rocky Mountain Association of Geologists, Denver, CO, United States (USA).

Lorenz, J.C., 1983, Reservoir sedimentology in Mesaverde rocks at the multiwall site: Sandia National Laboratories report SAND83-1078, 38 p.

Lorenz, J.C., 2003, Fracture systems in the Piceance Basin, overview and comparison with fractures in the San Juan and Green River basins, in K.M. Peterson, T.M. Olsen, and D.S. Anderson, eds., Piceance Basin 2003 guidebook: Rocky Mountain Association of Geologist, p. 75-94.

Lorenz, J. C. and S. J. Finley, 1989, Differences in fracture characteristics and related production; Mesaverde Formation, northwestern Colorado, SPE Formation Evaluation, vol. 4, no. 1, p. 11-16.

Lorenz, J.C., N.R. Warpinski, P. Branagan, and A.R. Sattler, 1989, Fracture characteristics and reservoir behavior of stress-sensitive fracture systems in flat-lying lenticular formations: Journal of Petroleum Technology, v.4, no. 1, p. 11-16.

Patterson, P.E., Kronmueller, K. & Davies, T.D, 2003, Sequence stratigraphy of the Mesaverde Group and Ohio Creek Conglomerate, northern Piceance Basin, Colorado. In: Peterson, K.M., Olson, T.M. & Anderson, D.S. (eds) Piceance Basin 2003 Guidebook. Rocky Mountain Association of Geologists, Denver, CO, p. 115–129.

Pranter, M.J., A. I. Ellison, R.D. Cole, and P.E. Patterson, 2007, Analysis and modeling of intermediate-scale reservoir heterogeneity based on a fluvial point-bar outcrop analog, Williams Fork Formation, Piceance Basin, Colorado: AAPG Bulletin, v. 91, p. 1025-1051.

Pranter, M.J., M.F. Vargas, and T.L. Davis, 2008, Characterization and 3-D reservoir modeling of fluvial sandstones of the Williams Fork Formation, Rulison Field, Piceance Basin, Colorado: Journal of Geophysics and Engineering 5, p. 158-172.

Pranter, M. J., R. D. Cole, H. Panjaitan, and N. K. Sommer, 2009, Sandstone-body dimensions in a lower coastal-plain depositional setting; lower Williams Fork Formation, Coal Canyon, Piceance Basin, Colorado: AAPG Bulletin, vol. 93, no. 10, p. 1379-1401.

Pranter, M. J., *A. C. Hewlett, R. D. Cole, H. Wang, and J. R. Gilman, 2014, Fluvial architecture and connectivity of the Williams Fork Formation: use of outcrop analogues for stratigraphic characterization and reservoir modelling, in T. Good, J. Howell, A. W. Martinius, eds., Sediment-body geometry and heterogeneity: analogue studies for modelling the subsurface, The Geological Society of London, Special Publication, vol. 387, 308 p.

Pranter, M.J. and N. K. Sommer, 2011, Static connectivity of fluvial sandstones in a lower coastal-plain setting: An example from the Upper Cretaceous lower Williams Fork Formation, Piceance Basin, Colorado, AAPG Bulletin, vol. 95, p. 899–923.

Satter, Abdus, and Iqbal, Ghulam M., 2016, Reservoir Rock Properties: Reservoir Engineering, 3, 51 p.

Shaak, R. V., 2010, Stratigraphic architecture of shallow-marine to coastal-plain parasequences: lower Williams Fork Formation, southeastern Piceance Basin, Colorado: M.S. thesis, University of Colorado, Boulder, 163 p.

Stephens, D. B., Hsu, K. C., Prieksat, M. A., Ankeny, M. D., Blandford, N., Roth, T. L., & Whitworth, J. R. (1998). A comparison of estimated and calculated effective porosity. Hydrogeology Journal, 6, p. 156–165.

Tyler, R., and R. McMurray, 1995, Genetic stratigraphy, coal occurrence, and regional cross section of the Williams Fork Formation, Mesaverde Group, Piceance Basin, northwestern Colorado: Colorado Geological Survey Open File Report 95-2, 42 p.

APPENDICES

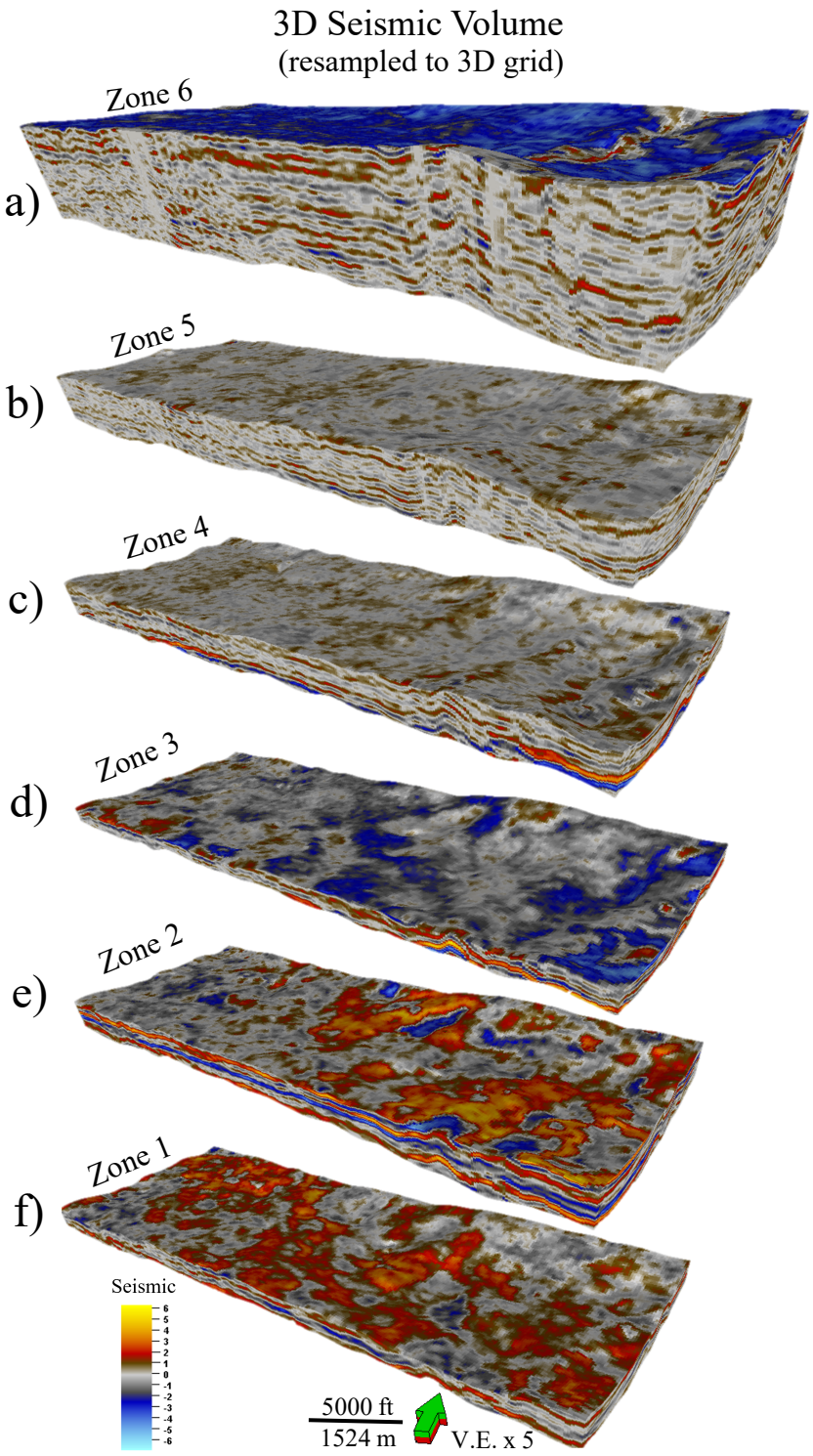

Appendix A: *3D Seismic Volume*: Depiction of the depth-converted 3D seismic volume associated with this study. For visual simplicity, the seismic volume has been resampled the 3D grid and is partitioned into the six zones referenced throughout this study.

Appendix B

Establishing a Relationship Between Lithology, Total porosity, and Sweetness

Initially, a general relationship was observed between total porosity (logs) and lithology (logs) at every well point. However, to constrain the lateral facies distribution within the 3D lithology model, an additional relationship needed to be established in between each well point. To accomplish this, various attributes were run on the seismic volume and individually cross plotted against total porosity with lithology set as the z-factor. Since the goal was to capture a relationship associated with lithology, I ran amplitude-based attributes on the seismic depth volume rather than geometric attributes. Of all the amplitude-based attributes that were applied, (such as RMS amplitude, sweetness, chaos, GLCM, and average energy), sweetness helped best capture the lithological relationship when cross plotted against total porosity.

Appendix C

Cross-Plot Generation

Once each amplitude-based attribute was run on the depth-converted seismic volume (Appendix A), they were resampled to the 3D grid associated with the 3D models in this study. In a cross-plot, I then set each resampled attribute as the x-variable, set the upscaled total porosity logs (Appendix E) as the y-variable, and set the upscaled lithology logs as the z-factor. Cross-plots were then generated for each individual amplitude-based attribute (RMS amplitude, sweetness, chaos, GLCM, and average energy) to pinpoint which combination revealed the strongest lithological relationship. The cross-plot combination that revealed the strongest lithological relationship was sweetness (3D attribute volume) (Appendix D) vs total porosity (upscaled logs) (Appendix E). Since resampling the seismic attributes to the 3D grid allows each voxel within the grid to be assigned to a specific value associated with the attribute, lithological relationships

present at each well point can then be propagated throughout the rest of the 3D volume beyond well points. Although the sweetness attribute volume was in 3D (Appendix D), to fully capture the lithological relationship in 3D, it needed to be cross plotted against total porosity in 3D as well. To accomplish this and justified because of the high well coverage within the study area, an initial 3D total porosity model (Appendix F) not constrained to lithology was generated. As a result of the 3D model cross plot, the lithological sweetness vs total-porosity relationships established at each well point were then assigned and propagated throughout the rest of the 3D sweetness volume. Once the lithological relationship was propagated in 3D, the resulting 3D proportions of sandstone and coal were used to generate sandstone and coal thickness probability maps per zone. These sandstone and coal thickness probability maps were used as lateral lithology constraints during the 3D lithology modeling process. Appendix G acts as a visual representation of the transition from 1) 3D sandstone and coal proportions to 2) thickness probability maps used to 3) constrain the lateral distribution of sandstone and coal in the 3D lithology model. Although Appendix G only depicts “zone 1”, this process was applied to all six zones.

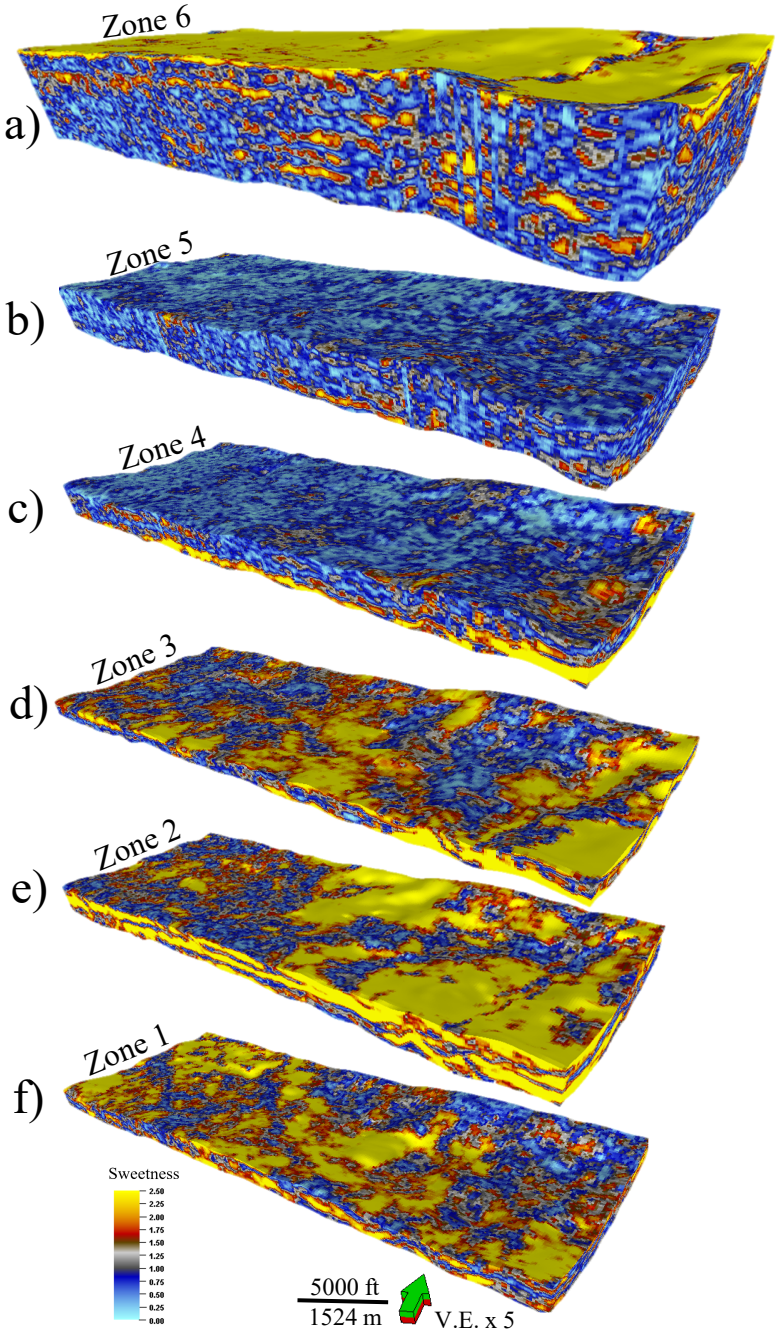

Appendix D: *3D Sweetness Attribute Volume*: Depiction of the 3D sweetness attribute volume used to establish a lithological relationship when cross plotted against total porosity. To maintain uniformity throughout the cross-plotting process, each of the plotting components (including the 3D sweetness attribute volume) were resampled to the 3D grid as depicted in **(a-f)**. For visual simplicity, the 3D sweetness attribute volume (resampled to the 3D grid) is partitioned into the six zones referenced throughout this study.

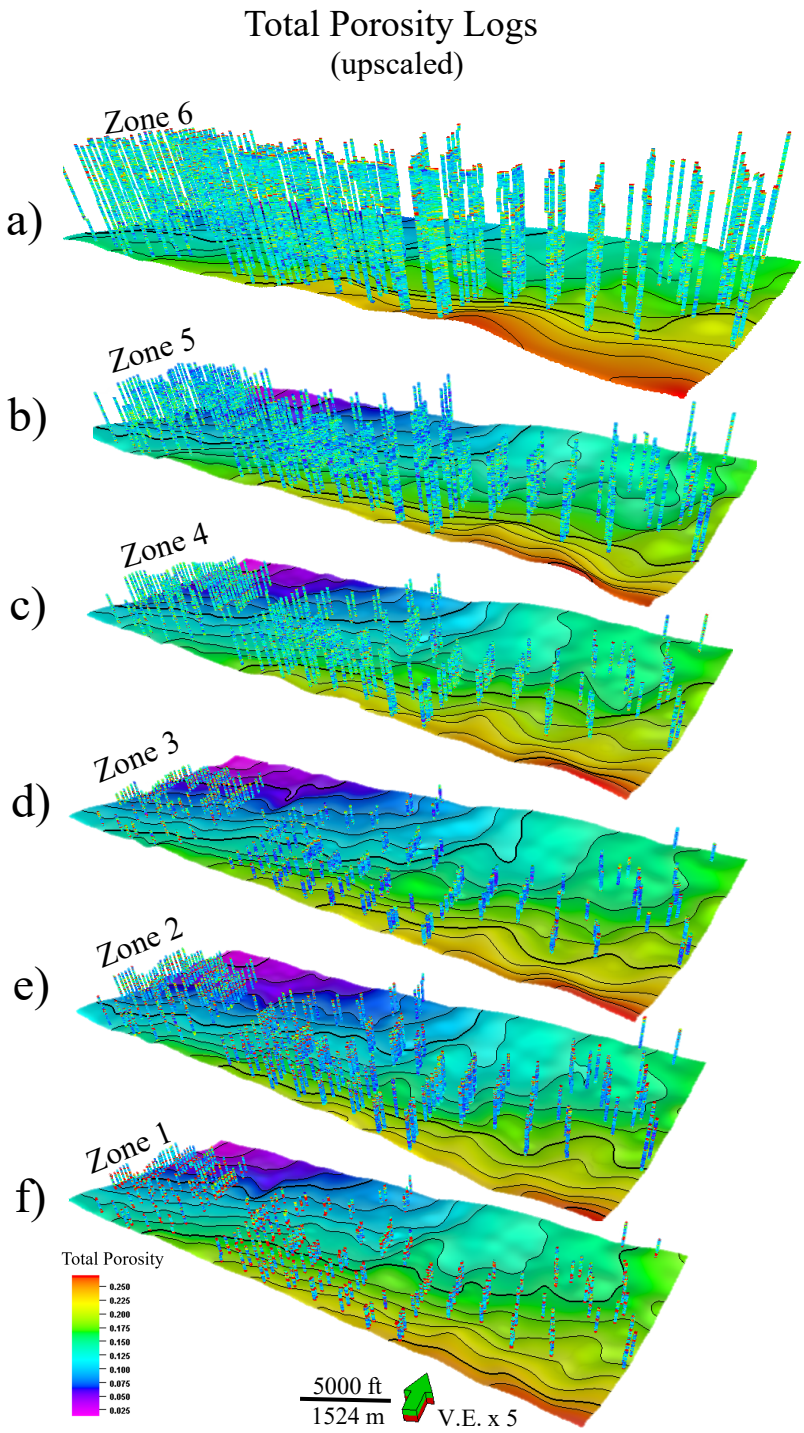

Appendix E: *Total Porosity Logs (upscaled)*: Depiction of the upscaled total porosity logs used to establish a lithological relationship (at each well location) when cross plotted against the 3D sweetness attribute volume. To maintain uniformity throughout the cross-plotting process, each of the plotting components (including the total porosity logs) were, in this case, upscaled to the 3D grid as depicted in **(a-f)**. For visual simplicity, the upscaled total porosity logs are displayed per zone (partitioned into the six zones referenced throughout this study).

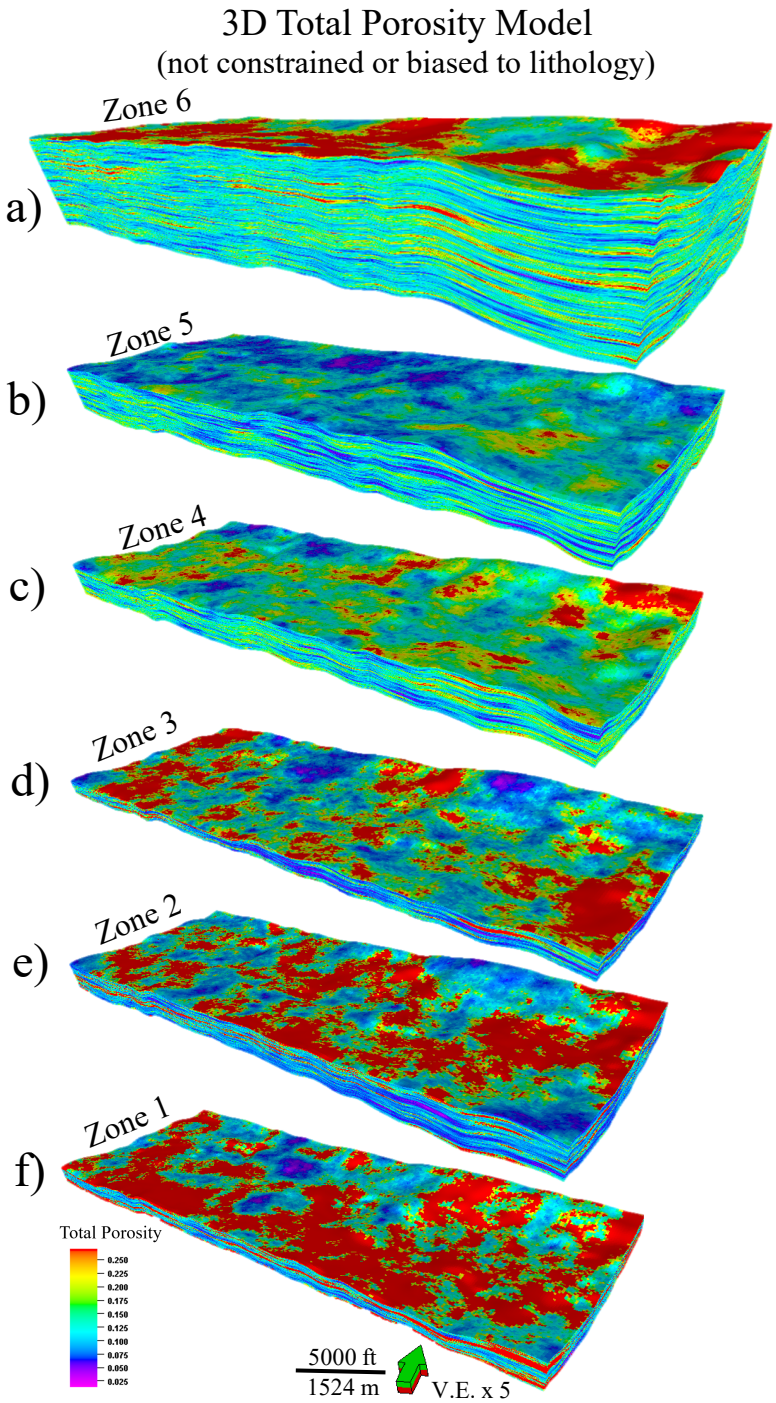

Appendix F: *3D Total Porosity Model (not constrained or biased to lithology)*: Depiction of the 3D total porosity model (not constrained or biased to lithology) used to establish a lithological relationship (in 3D) when cross plotted against the 3D sweetness attribute volume. To maintain uniformity throughout the cross-plotting process, each of the plotting components (including the 3D total porosity model) were resampled to the 3D grid as depicted in **(a-f)**. For visual simplicity, the 3D total porosity model (resampled to the 3D grid) is partitioned into the six zones referenced throughout this study.

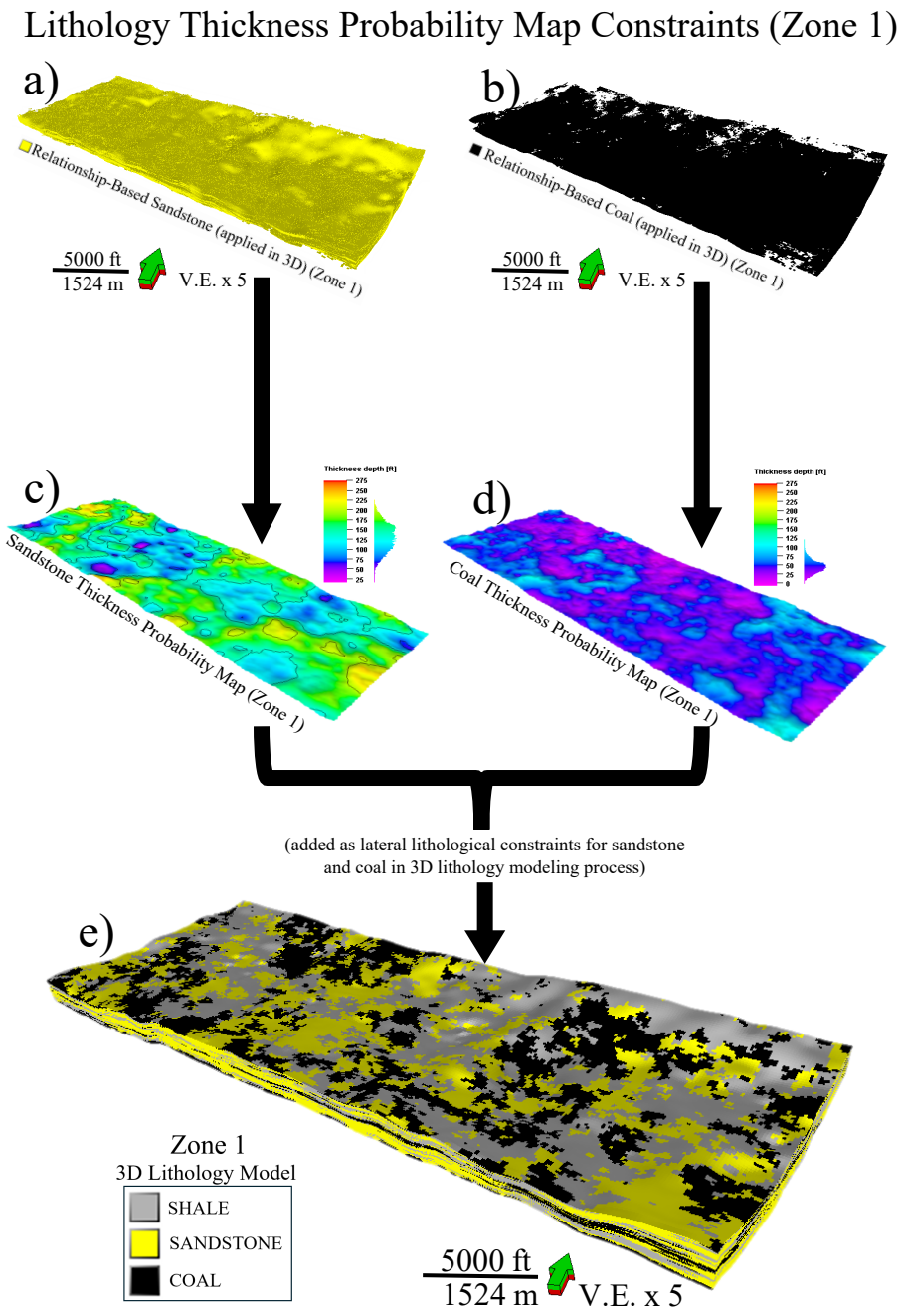

Appendix G: *Lithology Thickness Probability Map Constraints (Zone 1)*: Once the lithological relationship (formed between the 3D sweetness attribute volume and 3D total porosity model (not constrained or biased to lithology)) was propagated in 3D, the resulting 3D proportions of **a)** sandstone and **b)** coal were used to generate **c)** sandstone and **d)** coal thickness probability maps per zone. These sandstone and coal thickness probability maps were used as lateral lithology constraints during the **e)** 3D lithology modeling process. The transition from 1) 3D sandstone and coal proportions to 2) thickness probability maps used to 3) constrain the lateral distribution of sandstone and coal in the 3D lithology model is depicted in **(a-e)**. Although Appendix G only depicts "zone 1", this process was applied to all six zones.

Appendix H

Selection of Lithology Thickness Probability Maps Produced Per Zone

Throughout the lithology modeling process, shale was defined as the background lithology. As a result, no lithology thickness probability maps were created for shale. In addition to this caveat, coal thickness probability maps were only generated for zones 1 and 2. Before thickness probability maps were generated, the lithology distribution was analyzed for each zone. This was done using histograms (Appendix I) that compared the percentage of sandstone, shale, and coal present within the original well logs, calculated lithology logs, and upscaled logs per zone. Zones 3-6 have a very low percentage of coal content (Appendix I(a-d)). Therefore, to avoid overestimation of coal throughout the modeling process, rather than making coal thickness probability maps, coal content within these zones was added later stochastically. Coal presence in zone 1 and 2 was substantial enough (Appendix I(e-f)) to justify generating and applying coal thickness probability maps as lateral constraints. Sandstone was high in percentage in each zone (Appendix I(a-f)), so sandstone thickness probability maps were therefore generated in all 6 zones.

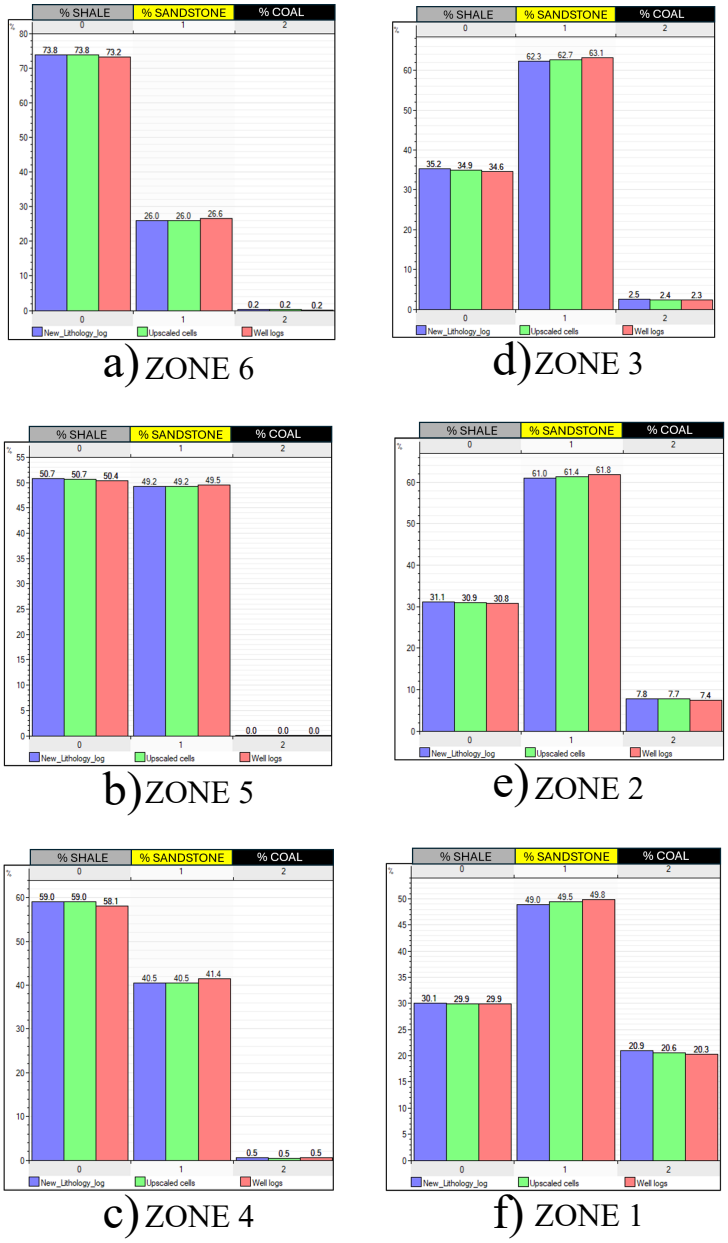

Appendix I: *Histograms Displaying Lithologic (upscaled lithology log) Distribution Per Zone*: Prior to creating lithology thickness probability maps (used as lateral lithology constraints in the 3D lithology modeling process) histograms **(a-f)** that compare the percentage of sandstone (yellow), shale (gray), and coal (black) present within the original well logs (red), calculated lithology logs (blue), and upscaled logs (green) were analyzed per zone. Depicted in **(a-d)**, zones 3-6 have a very low percentage of coal content. Therefore, to avoid overestimation of coal throughout the modeling process, rather than making coal thickness probability maps, coal content within these zones was added later stochastically. Coal presence in zone 1 and 2 was substantial enough **(e-f)** to justify generating and applying coal thickness probability maps as lateral constraints. Sandstone was high in percentage in each zone **(a-f),** so sandstone thickness probability maps were therefore generated in all 6 zones.

Variogram Parameters

a)

3D Total Porosity Model (not constrained or biased to lithology) Variogram Parameters						
Direction	**Zone 6**	**Zone 5**	**Zone 4**	**Zone 3**	**Zone 2**	**Zone 1**
Major	3000 ft	3000 ft	3000 ft	3000 ft	3000 ft	3000 ft
Minor	3000 ft	3000 ft	3000 ft	3000 ft	3000 ft	3000 ft
Vertical	19.0 ft	29.4 ft	26.1 ft	26.8 ft	32.3 ft	30.1 ft

b)

3D Lithology Model Variogram Parameters							
Lithology	**Direction**	**Zone 6**	**Zone 5**	**Zone 4**	**Zone 3**	**Zone 2**	**Zone 1**
SHALE	Major	3000 ft	3000 ft	3000 ft	3000 ft	3000 ft	3000 ft
	Minor	3000 ft	3000 ft	3000 ft	3000 ft	3000 ft	3000 ft
	Vertical	24.7 ft	23.2 ft	24.3 ft	34.6 ft	28.9 ft	33.5 ft
SANDSTONE	Major	3000 ft	3000 ft	3000 ft	3000 ft	3000 ft	3000 ft
	Minor	3000 ft	3000 ft	3000 ft	3000 ft	3000 ft	3000 ft
	Vertical	24.3 ft	31.2 ft	27.7 ft	36.6 ft	27.7 ft	30.0 ft
COAL	Major	3000 ft	3000 ft	3000 ft	3000 ft	3000 ft	3000 ft
	Minor	3000 ft	3000 ft	3000 ft	3000 ft	3000 ft	3000 ft
	Vertical	30.0 ft	27.8 ft	27.8 ft	31.4 ft	24.9 ft	34.3 ft

c)

3D Total Porosity Model (constrained / biased to lithology) Variogram Parameters							
Lithology	**Direction**	**Zone 6**	**Zone 5**	**Zone 4**	**Zone 3**	**Zone 2**	**Zone 1**
SANDSTONE	Major	2000 ft	2000 ft	2000 ft	2000 ft	2000 ft	2000 ft
	Minor	2000 ft	2000 ft	2000 ft	2000 ft	2000 ft	2000 ft
	Vertical	22 ft	29 ft	25 ft	34 ft	25 ft	28 ft

d)

3D Effective Porosity Model (constrained / biased to lithology) Variogram Parameters							
Lithology	**Direction**	**Zone 6**	**Zone 5**	**Zone 4**	**Zone 3**	**Zone 2**	**Zone 1**
SANDSTONE	Major	2000 ft	2000 ft	2000 ft	2000 ft	2000 ft	2000 ft
	Minor	2000 ft	2000 ft	2000 ft	2000 ft	2000 ft	2000 ft
	Vertical	22 ft	29 ft	25 ft	34 ft	25 ft	28 ft

e)

3D Permeability Model (constrained / biased to lithology) Variogram Parameters							
Lithology	**Direction**	**Zone 6**	**Zone 5**	**Zone 4**	**Zone 3**	**Zone 2**	**Zone 1**
SANDSTONE	Major	2000 ft	2000 ft	2000 ft	2000 ft	2000 ft	2000 ft
	Minor	2000 ft	2000 ft	2000 ft	2000 ft	2000 ft	2000 ft
	Vertical	22 ft	29 ft	25 ft	34 ft	25 ft	31 ft

f)

3D Water Saturation Model (constrained / biased to lithology) Variogram Parameters							
Lithology	**Direction**	**Zone 6**	**Zone 5**	**Zone 4**	**Zone 3**	**Zone 2**	**Zone 1**
SANDSTONE	Major	2000 ft	2000 ft	2000 ft	2000 ft	2000 ft	2000 ft
	Minor	2000 ft	2000 ft	2000 ft	2000 ft	2000 ft	2000 ft
	Vertical	22 ft	29 ft	25 ft	34 ft	25 ft	28 ft

Appendix J: *Table of Variogram Parameters*: The variogram parameters applied to each of the models in this study are listed in **(a-f)**. Listed parameters correspond to: **a)** the 3D total porosity model (not constrained or biased to lithology) used to establish a lithologic relationship with the 3D sweetness attribute volume and generate lateral lithologic constraints via lithology thickness probability maps per zone, **b)** the 3D lithology model, **c)** sandstone within the 3D total porosity model (constrained/biased to lithology), **d)** sandstone within the 3D effective porosity model (constrained/biased to lithology), **e)** sandstone within the 3D permeability model (constrained/biased to lithology), and **f)** sandstone within the 3D water saturation model (constrained/biased to lithology). The azimuth was set to zero for all six zones in all models. Variogram parameters were only applied to sandstone in **(c-f)** because the corresponding models were generated to characterize reservoir pay (as shale and coal are not reservoir pay). Variogram parameters are not listed for the 3D bulk volume water or reservoir pay models because they were calculated and generated from other 3D models (*see methods section*) and therefore did not have individual variogram inputs.

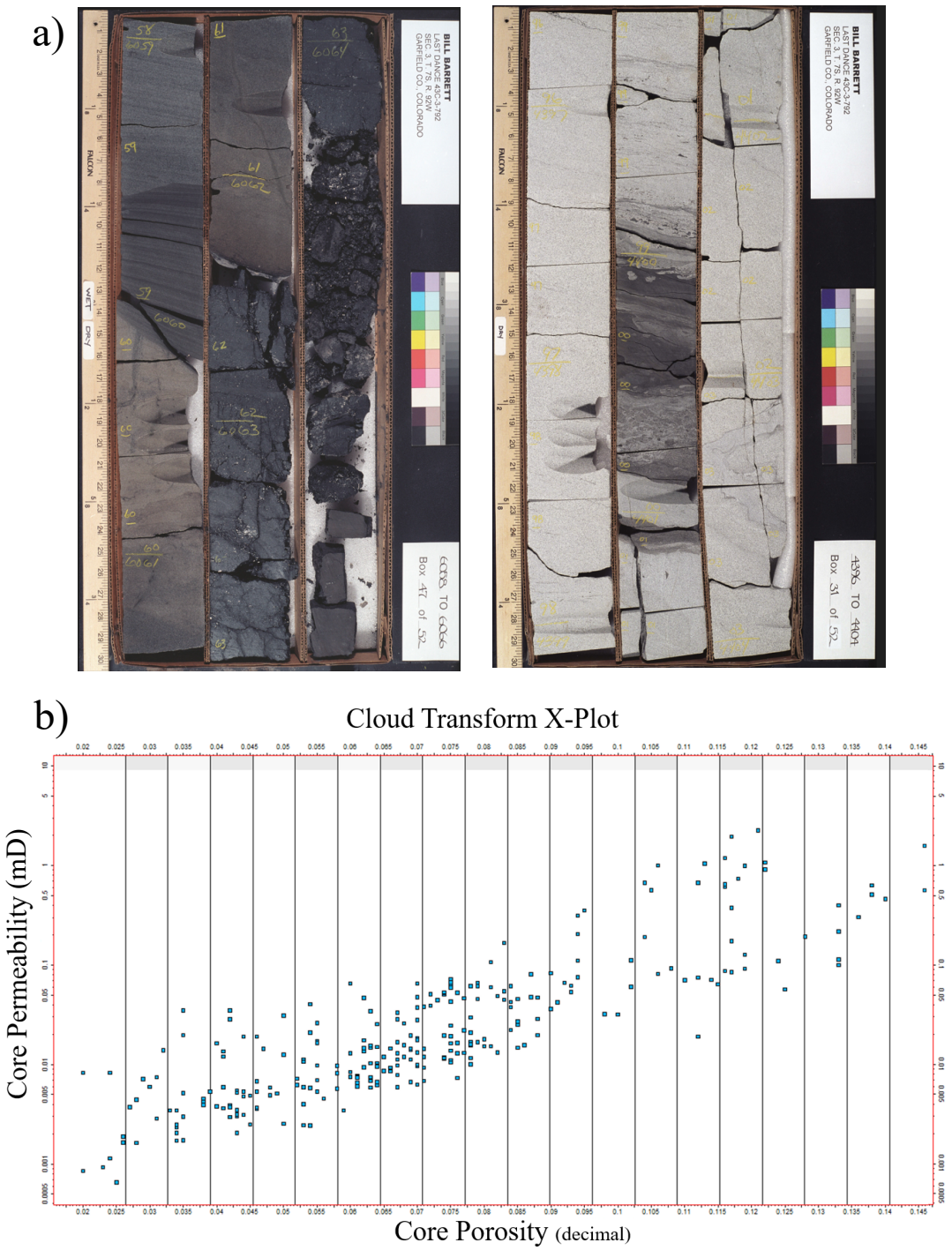

Appendix K: *Core and Cloud Transform Cross Plot:* Before producing a 3D permeability model, core permeability and porosity data associated with the **a)** Last-Dance 43C-3-792 cored-well were **b)** cross-plotted. The cross-plot correlation was then applied to all wells as a **b)** cloud transform with twenty equally spaced bins. Williams Fork Formation shale, coal, and sandstone are depicted in the **a)** Last-Dance 43C-3-792 cored-well pictures. See (Figure 2) for the approximate location of the Last-Dance 43C-3-792 cored-well.

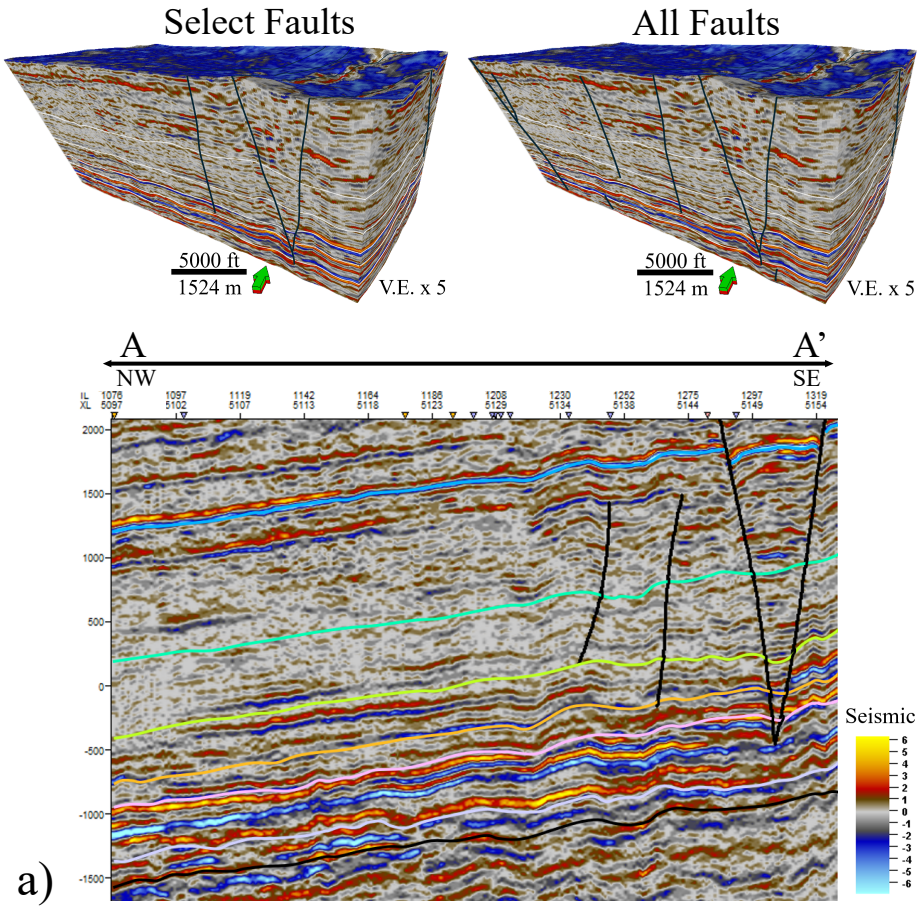
Select Faults
All Faults
5000 ft
1524 m
V.E. x 5
5000 ft
1524 m
V.E. x 5
A
A'
NW
SE
Seismic
a)
Select Faults
Seismic
b)
All Faults

Appendix L: *Faults Applied in this Study (select vs. all)*: Faults interpreted previously by Baytok (2010) were applied in this study to the 3D permeability model as conduits to flow. Two different fault-enhanced permeability models were generated including 1) a "select-faults" fault-enhanced 3D permeability model, and 2) an "all-faults" fault-enhanced 3D permeability model. The select group of faults used to produce the "select-faults" fault-enhanced permeability model (interpreted by Baytok (2010) and quality checked in this study) are depicted in the upper left 3D faulted seismic volume and in **a)** the seismic arbitrary line along cross section A-A'. The entire group of faults used to produce the "all-faults" fault-enhanced permeability model (interpreted by Baytok (2010)) are depicted in the upper right 3D faulted seismic volume and in **b)** the seismic arbitrary line along cross section A-A'. See (Figure 8b) for approximate location of A-A'.

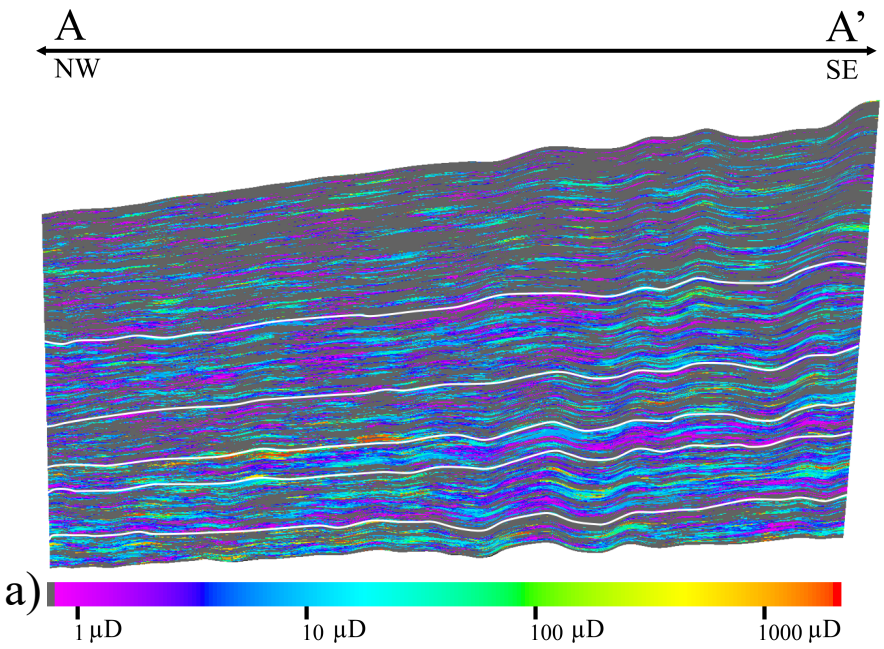

Williams Fork Formation Permeability
(No Faults)

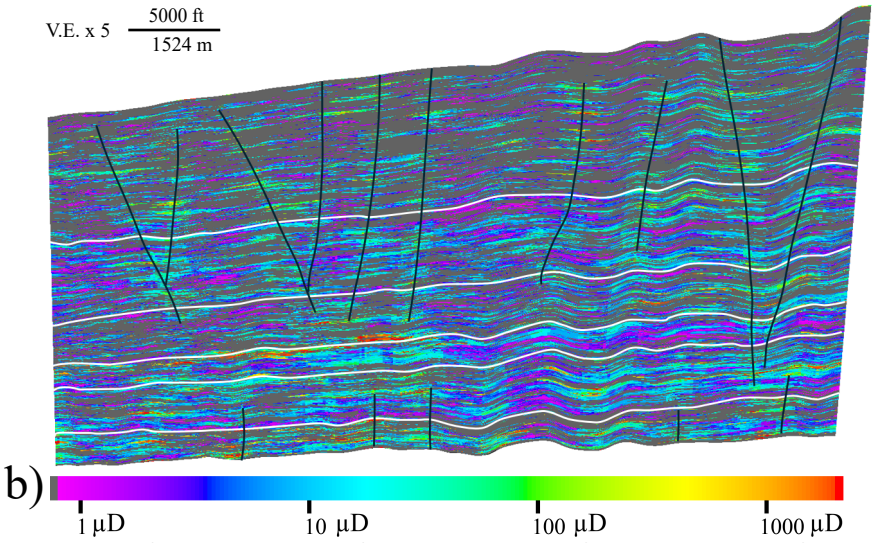

Williams Fork Formation Fault-Enhanced Permeability
(All Faults)

Appendix M: *Fault-Enhanced Permeability (all faults) along A-A'*: A comparison of the **a)** original Williams Fork Formation 3D permeability model (no faults incorporated) and **b)** fault-enhanced 3D permeability model (incorporating all faults interpreted by Baytok (2010)) in cross-sectional view along A-A'. See (Figure 8b) for approximate location of A-A'. Increasing permeability along faults, in some cases as high as ~550 µD, faults within the study area positively correlate with areas of highest reservoir quality.

a) No Faults

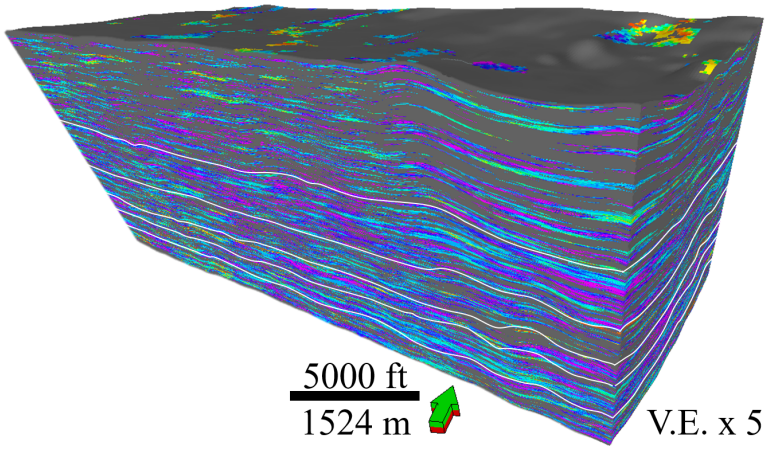

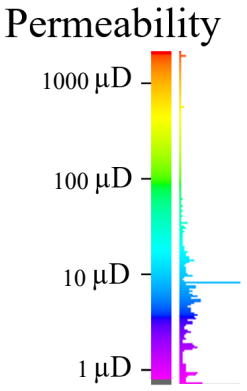

b) Select Faults

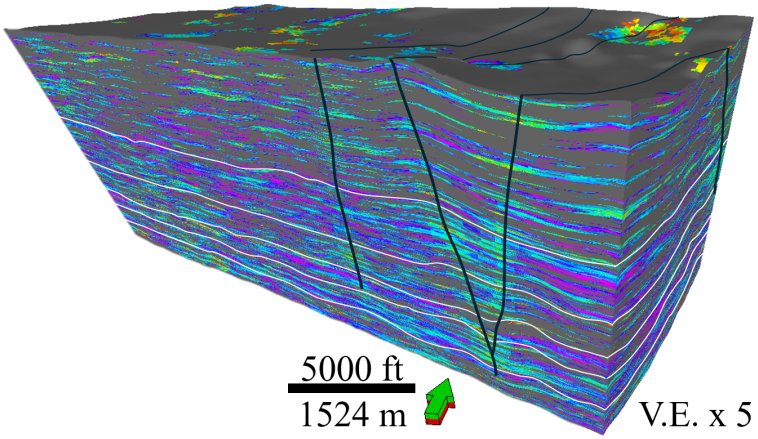

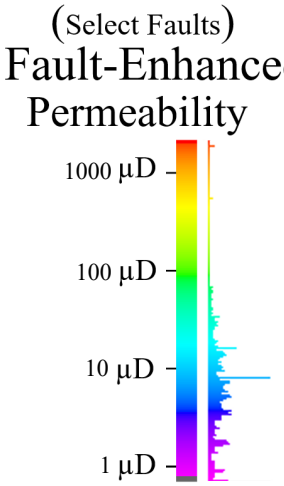

c) All Faults

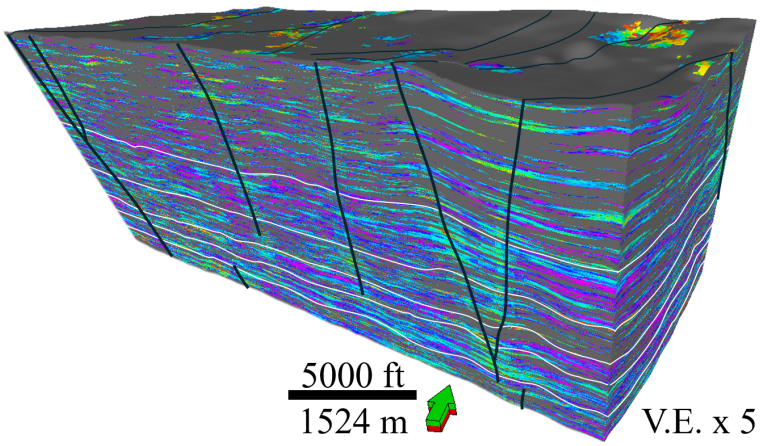

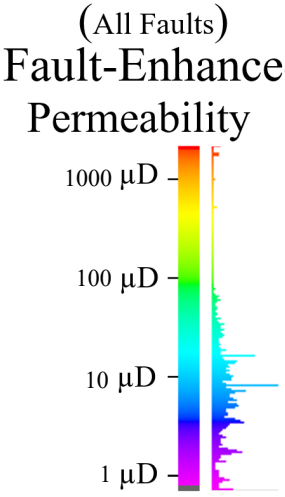

Appendix N: *Permeability Models with and without Faulting*: A comparison of the **a)** original Williams Fork Formation 3D permeability model (no faults incorporated), **b)** fault-enhanced 3D permeability model (incorporating a select group of quality-checked faults interpreted by Baytok (2010)), and **c)** fault-enhanced 3D permeability model (incorporating all faults interpreted by Baytok (2010)). Depicted in the histograms to the right of each color bar, the average permeability remains 7 µD regardless of the inclusion of faults. The inclusion of faults does however increase the approximate range of permeability values from (~0.7-10 µD) (within the original 3D permeability model) to (~2-60 µD) (within both fault-enhanced permeability models). Although the "all faults" fault-enhanced permeability model displayed in **(c)** factors in more faults than the "select faults" fault-enhanced permeability model displayed in **(b)**, the permeability values generally remained the same, increasing only in quantity in accordance with an increase in faults. Increasing permeability along faults, in some cases as high as ~550 µD, faults within the study area positively correlate with areas of highest reservoir quality.

Bulk and Pore Volume Per Zone

	Bulk Volume (*10^6 ft^3)	**Pore Volume** (*10^6 ft^3)
Zone 6	337131	3843
Pay	73290	2231
Non-pay	263841	1612
Zone 5	188074	3541
Pay	78505	2620
Non-pay	109570	921
Zone 4	126349	2495
Pay	40081	1420
Non-pay	86268	1074
Zone 3	70331	2034
Pay	34382	1087
Non-pay	35949	948
Zone 2	135322	3977
Pay	60054	2078
Non-pay	75268	1900
Zone 1	85387	2491
Pay	28178	1023
Non-pay	57209	1468
Total	942594	18381
Pay	314490	10459
Non-pay	628104	7923

Appendix O: *Table of Bulk and Pore Volume Per Zone of Reservoir Pay and Non-pay*: Listed per zone, the values displayed in the table represent 1) total bulk volume, 2) total pore volume, and 3) bulk and pore volumes of reservoir pay and non-pay. Of all six zones, zone 5 has the highest reservoir pay pore volume (2620 $*10^6$ ft^3), zone 6 has the second highest reservoir pay pore volume (2231 $*10^6$ ft^3), and zone 2 has the third highest reservoir pay pore volume (2078 $*10^6$ ft^3). Although zone 2 contains the third highest reservoir pay pore volume, when considering its size relative to zones 5 and 6, its reservoir pay pore volume is notably significant. For example, zone 2 is ~400 ft (121 m) thick, which is ~ 25% thinner than zone 5 (~550 ft (167 m) thick) and ~60% thinner than zone 6 (~1000 ft (304 m) thick). Despite this, zone 2's reservoir pay pore volume of (2078 $*10^6$ ft^3) is only slightly less than that of zone 5 (2620 $*10^6$ ft^3) and zone 6 (2231 $*10^6$ ft^3). Within the study area, the entire Williams Fork Formation is composed of ~10459$*10^6$ $ft^3$of reservoir pay.